



EXPERIMENTAL STUDY OF THERMAL CONDUCTIVITY OF NEW MIXTURES FOR ABSORPTION CYCLES AND THE EFFECT OF THE NANOPARTICLES ADDITION

Yolanda Cuenca Martínez

Dipòsit Legal: T.1561-2013

ADVERTIMENT. L'accés als continguts d'aquesta tesi doctoral i la seva utilització ha de respectar els drets de la persona autora. Pot ser utilitzada per a consulta o estudi personal, així com en activitats o materials d'investigació i docència en els termes establerts a l'art. 32 del Text Refós de la Llei de Propietat Intel·lectual (RDL 1/1996). Per altres utilitzacions es requereix l'autorització prèvia i expressa de la persona autora. En qualsevol cas, en la utilització dels seus continguts caldrà indicar de forma clara el nom i cognoms de la persona autora i el títol de la tesi doctoral. No s'autoritza la seva reproducció o altres formes d'explotació efectuades amb finalitats de lucre ni la seva comunicació pública des d'un lloc aliè al servei TDX. Tampoc s'autoritza la presentació del seu contingut en una finestra o marc aliè a TDX (framing). Aquesta reserva de drets afecta tant als continguts de la tesi com als seus resums i índexs.

ADVERTENCIA. El acceso a los contenidos de esta tesis doctoral y su utilización debe respetar los derechos de la persona autora. Puede ser utilizada para consulta o estudio personal, así como en actividades o materiales de investigación y docencia en los términos establecidos en el art. 32 del Texto Refundido de la Ley de Propiedad Intelectual (RDL 1/1996). Para otros usos se requiere la autorización previa y expresa de la persona autora. En cualquier caso, en la utilización de sus contenidos se deberá indicar de forma clara el nombre y apellidos de la persona autora y el título de la tesis doctoral. No se autoriza su reproducción u otras formas de explotación efectuadas con fines lucrativos ni su comunicación pública desde un sitio ajeno al servicio TDR. Tampoco se autoriza la presentación de su contenido en una ventana o marco ajeno a TDR (framing). Esta reserva de derechos afecta tanto al contenido de la tesis como a sus resúmenes e índices.

WARNING. Access to the contents of this doctoral thesis and its use must respect the rights of the author. It can be used for reference or private study, as well as research and learning activities or materials in the terms established by the 32nd article of the Spanish Consolidated Copyright Act (RDL 1/1996). Express and previous authorization of the author is required for any other uses. In any case, when using its content, full name of the author and title of the thesis must be clearly indicated. Reproduction or other forms of for profit use or public communication from outside TDX service is not allowed. Presentation of its content in a window or frame external to TDX (framing) is not authorized either. These rights affect both the content of the thesis and its abstracts and indexes.

Doctoral Thesis

Yolanda Cuenca Martínez

EXPERIMENTAL STUDY OF THERMAL CONDUCTIVITY OF NEW MIXTURES FOR ABSORPTION CYCLES AND THE EFFECT OF THE NANOPARTICLES ADDITION

Department of Mechanical Engineering



UNIVERSITAT ROVIRA I VIRGILI

UNIVERSITAT ROVIRA I VIRGILI
EXPERIMENTAL STUDY OF THERMAL CONDUCTIVITY OF NEW MIXTURES FOR ABSORPTION CYCLES AND THE EFFECT OF
THE NANOPARTICLES ADDITION
Yolanda Cuenca Martínez
Dipòsit Legal: T.1561-2013

Yolanda Cuenca Martínez

EXPERIMENTAL STUDY OF THERMAL
CONDUCTIVITY OF NEW MIXTURES FOR
ABSORPTION CYCLES AND THE EFFECT
OF THE NANOPARTICLES ADDITION

Doctoral Thesis

Supervised by:
Dr. Manel Vallès
Dr. Anton Vernet

Department of Mechanical Engineering



UNIVERSITAT ROVIRA I VIRGILI

Tarragona, September 2013

UNIVERSITAT ROVIRA I VIRGILI
EXPERIMENTAL STUDY OF THERMAL CONDUCTIVITY OF NEW MIXTURES FOR ABSORPTION CYCLES AND THE EFFECT OF
THE NANOPARTICLES ADDITION
Yolanda Cuenca Martínez
Dipòsit Legal: T.1561-2013



UNIVERSITAT
ROVIRA I VIRGILI

DEPARTAMENT D'ENGINYERIA MECÀNICA

Escola Tècnica Superior d'Enginyeria Química (ETSEQ).
Av. Països Catalans 26. 43007 Tarragona (Spain)

Dr. Manel Vallès and Dr. Anton Vernet, Professors in the Mechanical Engineering
Department of Universitat Rovira i Virgili,

CERTIFY:

That the present study, entitled:

*Experimental Study of Thermal Conductivity of New Mixtures for Absorption Cycles and the
Effect of the Nanoparticles Addition*

presented by Mrs Yolanda Cuenca Martínez for the award of the degree of Doctor, has been
developed under our supervision at the Department of Mechanical Engineering of this
university and it is fully adequate in scope and quality as a dissertation for the degree of
Doctor of Philosophy with the International Mention.

And, to inform you of that and in order for it to have the needed effects, we sign this
certification.

Tarragona, September 2013

Dr. Manel Vallès

Dr. Anton Vernet

UNIVERSITAT ROVIRA I VIRGILI
EXPERIMENTAL STUDY OF THERMAL CONDUCTIVITY OF NEW MIXTURES FOR ABSORPTION CYCLES AND THE EFFECT OF
THE NANOPARTICLES ADDITION
Yolanda Cuenca Martínez
Dipòsit Legal: T.1561-2013

*To my lovely husband Adrián,
who encouraged me to take up my studies again
and gave me emotional support during these years*

“A friend in need is a friend indeed”

Abstract

This study investigates the thermal conductivity of working fluids for absorption refrigeration cycles activated by solar thermal energy or waste heat. Absorption refrigeration is receiving increasing attention as an alternative to vapour compression cycles because of the rising cost of energy and concerns about the environmental impact of the working fluids employed in vapour compression systems. Nowadays, commercial refrigeration plants use absorption chillers with $\text{NH}_3 + \text{H}_2\text{O}$ or $\text{H}_2\text{O} + \text{LiBr}$ mixtures as working fluids. Accurate thermodynamic and transport properties such as thermal conductivity are needed for adequate design, analysis and evaluation of such systems. Available data in the literature for this property, especially for the $\text{NH}_3 + \text{H}_2\text{O}$, is scanty mainly at high temperatures and concentrations. Furthermore, most of the data are very old and shows remarkable disagreements. Unfortunately, the high vapour pressure of the mixture, the electrical conductivity of the liquid and the corrosive nature, combine to make the experimental measurement of thermal conductivity difficult. In order to solve these discrepancies between the reported experimental data and to extend the range of available data on high ammonia concentrations, the thermal conductivity of $\text{NH}_3 + \text{H}_2\text{O}$ mixtures containing 0.1 to 0.5 mass fraction ammonia has been measured at temperature between 293.15 and 313.15 K. On the other hand, for the $\text{H}_2\text{O} + \text{LiBr}$ mixture the available experimental data in the literature were measured in a wide range of temperature and concentrations with good agreement, moreover some reported data were correlated with an average deviation of 0.6%. Then, one composition of $\text{H}_2\text{O} + \text{LiBr}$ solution was measured at 0.4 mass fraction LiBr in the temperature range from 298.15 to 428.15 K in order to validate these available data with our system.

However, these commercial working fluids have some drawbacks such as; crystallization, corrosion problems and low pressure operation for the $\text{H}_2\text{O} + \text{LiBr}$ mixture, and the need of rectification of the refrigerant vapour at the desorber outlet for the $\text{NH}_3 + \text{H}_2\text{O}$ mixture. Efforts are being made to search for better working fluid in order to overcome these limitations. A promising mixture for solar activated refrigeration systems is $\text{NH}_3 + \text{LiNO}_3$. Some properties of this mixture such as, vapour-liquid equilibrium, density, viscosity and heat capacity have been presented in earlier works, but no previous experimental data have been found for thermal conductivity. Therefore, this property has been measured with ammonia mass fraction range from 0.3 to 0.6 and temperatures between 303.15 and 353.15 K. Results show lower values in thermal conductivity than those for $\text{NH}_3 + \text{H}_2\text{O}$ and $\text{H}_2\text{O} + \text{LiBr}$, and it is known that low thermal conductivity is a primary limitation in the development of energy-efficient heat transfer fluids that are required in these systems. To overcome this limitation, the addition of water or carbon nanotubes (CNTs) to the binary

mixture ($\text{NH}_3 + \text{LiNO}_3$) was proposed. Therefore, in order to evaluate the advantages of these additions, thermal conductivity of the ternary mixtures $\text{NH}_3 + \text{LiNO}_3 + \text{H}_2\text{O}$ and $\text{NH}_3 + \text{LiNO}_3 + \text{CNTs}$ has been analyzed in the ammonia mass fraction range from 0.3 to 0.6, H_2O range from 0.2 to 0.25, CNTs from 0.005 to 0.2 % and temperatures between 303.15 and 353.15 K. The addition of a third component in the binary mixture indicates an enhancement in the effective thermal conductivity in both cases. These results also suggest that the thermal conductivity enhancement with CNTs is less than the thermal conductivity enhancement with water addition.

Thermal conductivity measurements were carried on with the transient hot wire technique. Two different devices were designed and built in this work. The first one, consist in the typical platinum wire coated by Teflon capable to measure the thermal conductivity of fluids. The second one was a new technique developed, allowing measurements of electrically conducting fluids at elevated temperature and being more readily fabricated. This technique is based on a variation of the transient hot wire method, where the platinum wire was replaced with a glass capillary filled with liquid metal (mercury) in the present work. The apparatus and method were validated by comparing the measured values of the thermal conductivity of pure water, toluene, dimethyl phthalate, ethylene glycol and water + lithium nitrate with published values. Uncertainty in the measurements was estimated to be less than $0.017 \text{ W}\cdot\text{m}^{-1}\cdot\text{K}^{-1}$ for the platinum wire device and $0.025 \text{ W}\cdot\text{m}^{-1}\cdot\text{K}^{-1}$ for the liquid metal device.

A comprehensive model based in the local composition concept has been used for predicting the thermal conductivity of $\text{NH}_3 + \text{H}_2\text{O}$, $\text{NH}_3 + \text{LiNO}_3$ and $\text{NH}_3 + \text{LiNO}_3 + \text{H}_2\text{O}$ at various temperatures and ammonia concentrations. The model incorporates the surface area parameter, the local area fraction and thermal conductivities of pure components in conjunction with a single binary parameter per solvent mixtures. Also, the effect of electrolytes is modelled by accounting for a contribution of individual ions and interactions between pairs of species.

Finally, finite element transient thermal analysis with ANSYS has been used in order to exactly represent the geometry of the liquid metal capillary. Good agreement between predicted and experimental results was obtained. Also, the coating effect was analyzed by solving the heat equation for the line source case.

Resumen

En esta tesis doctoral se estudia la conductividad térmica de fluidos de trabajo para ciclos de refrigeración por absorción activados mediante energía solar térmica o calor residual. Los sistemas de refrigeración por absorción están recibiendo cada vez más atención como alternativa a los ciclos de compresión de vapor, debido al incremento del precio en energías primarias así como el interés en proteger el medio ambiente. Hoy en día, las mezclas de trabajo más utilizadas comercialmente son el $\text{H}_2\text{O} + \text{LiBr}$ y el $\text{NH}_3 + \text{H}_2\text{O}$. El conocimiento de las propiedades termofísicas, tales como la conductividad térmica del fluido de trabajo utilizado en los ciclos de refrigeración por absorción, es necesario para que estos sistemas puedan ser apropiadamente evaluados y diseñados. Los datos disponibles en la literatura para esta propiedad, especialmente para el $\text{NH}_3 + \text{H}_2\text{O}$ son escasos, sobre todo a altas temperaturas y concentraciones. Además, la mayoría de los datos son muy antiguos y muestran una gran discrepancia entre ellos. Desafortunadamente, la alta presión de vapor de la mezcla, la conductividad eléctrica del líquido, y la naturaleza corrosiva de la solución se combinan dificultando así la medición experimental de la conductividad térmica para estas mezclas de trabajo. Con el fin de resolver las discrepancias entre los datos experimentales reportados y ampliar el rango de datos disponibles a altas concentraciones de amoníaco, la conductividad térmica de la mezcla $\text{NH}_3 + \text{H}_2\text{O}$ con fracciones máxicas entre 0.1 y 0.5 de amoníaco han sido medidas a temperaturas entre 293.15 y 313.15 K. En el caso de la mezcla $\text{H}_2\text{O} + \text{LiBr}$ los datos experimentales disponibles en la literatura se midieron en un amplio rango de concentraciones y temperatura mostrando una buena conformidad entre ellos, además algunos de los datos se correlacionaron con una desviación media del 0.6 %. Así, en este estudio la mezcla de trabajo $\text{H}_2\text{O} + \text{LiBr}$ se midió con una fracción máxica del 0.4 LiBr y un rango de temperaturas entre 298.15 y 428.15 K con el fin de validar los datos disponibles en la bibliografía con nuestro sistema.

Sin embargo, las mezclas de trabajo comerciales presentan ciertos inconvenientes, tales como; cristalización, problemas de corrosión y problemas de presión de operación para la mezcla $\text{H}_2\text{O} + \text{LiBr}$, y la necesidad del uso de un rectificador de vapor a la salida del generador para la mezcla $\text{NH}_3 + \text{H}_2\text{O}$. Por ello, se están buscando nuevos fluidos de trabajo con el fin de mejorar dichas limitaciones. Una mezcla prometedor para sistemas de refrigeración activados mediante energía solar es el $\text{NH}_3 + \text{LiNO}_3$. Algunas propiedades de esta mezcla, tales como; equilibrio líquido-vapor, densidad, viscosidad y capacidad calorífica han sido presentadas en trabajos anteriores, pero desafortunadamente no se han encontrado datos experimentales con anterioridad para la conductividad térmica. Por lo tanto, se midió ésta propiedad para la mezcla $\text{NH}_3 + \text{LiNO}_3$ en un rango de 0.3 a 0.6 de fracción máxica de amoníaco y temperaturas entre 303.15 y 353.15 K. Los resultados mostraron valores de

conductividad térmica más bajos que aquellos obtenidos para el $\text{NH}_3 + \text{H}_2\text{O}$ y el $\text{H}_2\text{O} + \text{LiBr}$. Los valores bajos de conductividad térmica son una de las principales limitaciones en el desarrollo de fluidos de transferencia de calor requeridos en estos sistemas. Para superar esta limitación, se propuso la adición de agua o nanotubos de carbono (CNT) en la mezcla binaria ($\text{NH}_3 + \text{LiNO}_3$). Por lo tanto, con el fin de evaluar las ventajas, la conductividad térmica de las mezclas ternarias de $\text{NH}_3 + \text{LiNO}_3 + \text{H}_2\text{O}$ y $\text{NH}_3 + \text{LiNO}_3 + \text{CNTs}$ se ha analizado en un rango de 0.3 a 0.6 de fracción de másica de amoníaco, entre 0.20 y 0.25 de H_2O y 0.005 a 0.2 % de CNTs, a temperaturas entre 303.15 y 353.15 K. La adición de un tercer componente en la mezcla binaria indicó una mejora en la conductividad térmica para ambos casos. Estos resultados también mostraron que la mejora de la conductividad térmica con nanotubos de carbono es menor que la obtenida con agua.

Las medidas de conductividad térmica se realizaron mediante la técnica transitoria del hilo caliente. Dos equipos experimentales fueron diseñados y construidos en este trabajo. El primero, consiste en el típico montaje basado en un hilo de platino recubierto de Teflón desarrollado para medir conductividad térmica de fluidos. El segundo, fue una nueva técnica desarrollada que permite medir fluidos eléctricamente conductores a elevadas temperaturas y presión. Ésta técnica se basa en la variación del método del hilo caliente, donde el hilo de platino ha sido reemplazado por un capilar de vidrio relleno de un metal líquido (mercurio). El equipo y el método se validaron con la medición de la conductividad térmica en fluidos de referencia como el agua, el tolueno, el dimetil ftalato y el etilenglicol. Además se midió el agua nitrato de litio como fluido conductor eléctrico y con características similares a las mezclas de trabajo. La incertidumbre de la medida se estimó por debajo de $0.017 \text{ W}\cdot\text{m}^{-1}\cdot\text{K}^{-1}$ para el hilo de platino y $0.025 \text{ W}\cdot\text{m}^{-1}\cdot\text{K}^{-1}$ para el capilar de vidrio.

Un modelo exhaustivo basado en el concepto de composición local ha sido utilizado para la predicción de la conductividad térmica de las mezclas $\text{NH}_3 + \text{H}_2\text{O}$, $\text{NH}_3 + \text{LiNO}_3$ y $\text{NH}_3 + \text{LiNO}_3 + \text{H}_2\text{O}$ a diversas temperaturas y composiciones de amoníaco. El modelo incorpora el área superficial molecular, la fracción de área local y las conductividades térmicas de los componentes puros, junto con un único parámetro binario por mezcla de solventes. Además, el efecto de los electrolitos se tiene en cuenta mediante la contribución de iones individuales y las interacciones entre pares de especies.

Por último, se realizó un análisis térmico transitorio con ANSYS mediante elementos finitos con el fin de representar exactamente la geometría del capilar de vidrio utilizado en las medidas experimentales. Se obtuvo una buena relación entre los resultados numéricos y los experimentales. Además, se analizó el efecto del grosor de aislante mediante la resolución de la ecuación de transferencia de calor.

Acknowledgments

I would like to acknowledge financial support of this research which was supported by the Spanish Ministry of Science and Technology through projects ENE2008-00863 and DPI2010-17212. Also, the Government of Catalonia is acknowledged for financial assistance through 2011FI_B 01018 scholarship.

A special thanks to Manel Vallès and Anton Vernet without whom this work would not have been possible. Thank you very much for your unconditional help, for spending countless hours teaching me with your useful advices, and because you always took the time to listen me. I am honoured to have you as supervisors.

I will never forget the time spent in Georgia Tech (Atlanta) and especially the opportunity to work with Professor Aryn S. Teja who provided me with useful advices during my stage. I also happily acknowledge the contribution of Carole Teja who gave me moral support and lots of laughs. I want to personally thank all the other members of the Teja's research group, Pramod Warriar, Mohamad Kassae and Zahid Hossain, I could not have done without your help and support.

I am also very grateful to Carlos Nieto de Castro for his collaboration with the thermal conductivity measurements and João França for his unconditional help during my short stage at the Faculty of Science University of Lisbon (Portugal).

I also acknowledge the whole Department of Mechanical Engineering at URV for their assistance, especially to M^a José Duran, Samuel Garcia, Vicenç Puig and José Rodriguez, for your unconditional kindness and support, even when you don't had to do it.

Of course, many thanks go to all my Colleagues from CREVER and ECOMMFIT Group, who sheared the good and the bad times with me during these years. Thank you very much for the good mood!!!!!!

I am forever grateful to my parents, grandmother and Argentina's family. I couldn't have come this without your support and love.

I need to further thank all my best friends forever; Tamara, Dani, Olga, Jaime, Ainhoa and Jordi, who have helped me, supported me and encouraged me during stressful times. They deserve a special thanks because they have been like a second family to me. Thank you so much for understanding me.

I don't want to forget the three wonderful boys who share my heart: Lisan, Aleix and Héctor, I love you so much!!!!

Last but definitely not least, Adrián and Kira, the best family I could have ever chosen.

List of Publications and Conferences

Publications in Journal Papers

Y.Cuenca, D. Salavera, A. Vernet, M. Vallès. “Thermal Conductivity of Ammonia + Water Mixtures Over a Wide Range of Concentrations” *Int. J. of Refrigeration*, 2013, 36(3), 998-1003.

Y.Cuenca, D.Salavera, A.Vernet, A. S.Teja, M.Vallès “Thermal conductivity of Ammonia + Lithium Nitrate and Ammonia + Lithium Nitrate + Water Solutions over a Wide Range of Concentrations and Temperatures”. In press in *Int. J. of Refrigeration*.

DOI: <http://dx.doi.org/10.1016/j.ijrefrig.2013.08.010>

Y.Cuenca, A.Vernet, M.Vallès “Thermal Conductivity enhancement of the binary mixture ($\text{NH}_3 + \text{LiNO}_3$) by the addition of CNTs” *Int. J. of Refrigeration* (Submitted September 2013 Ref. IJIR-D-13-00441)

Y.Cuenca, A.Vernet, M.Vallès “Modelling of the thermal conductivity for working fluids in absorption refrigeration cycles” (In preparation)

Contribution to Conferences

Y.Cuenca, A.Vernet, M.Vallès, “Experimental study of thermal conductivity of new mixtures for absorption cycles and the effect of the CNTs addition” Poster Presentation, 8th doctoral day poster exhibition, Tarragona (Spain), April 2010.

Y.Cuenca, A.Vernet, M.Vallès., “Thermal conductivity of ammonia + lithium nitrate” Oral Presentation, International Congress of Sorption Heat Pump Conference, Padua (Italy), April 2011.

Y.Cuenca, A.Vernet, M.Vallès., “Thermal conductivity of ammonia + water” Oral Presentation, International Congress of Ammonia Refrigeration Technology, Ohrid (Republic of Macedonia), April 2011.

Y.Cuenca, A.Vernet, M.Vallès., “Conductividad Térmica de la Mezcla Amoníaco + Nitrato de litio + Agua” Oral Presentation, VII Congreso Nacional de Ingeniería Termodinámica, Bilbao (Spain), June 2011.

Y.Cuenca, A.Vernet, M.Vallès., “Conductividad Térmica del Amoníaco + Nitrato de Litio y Amoníaco + Nitrato de Litio + Agua en un amplio intervalo de concentraciones y temperaturas” Oral Presentation, XXXIV Reunión Bienal de la Real Sociedad Española de Física y 23º Encuentro Ibérico de Enseñanza de la Física Bienal Física, Valencia (Spain), July 2013.

Y.Cuenca, A.Vernet, M.Vallès., “Enhanced Thermal Conductivity of New Working Fluid (NH₃ + LiNO₃) Using CNTs Binary Nanofluid” Oral Presentation, International Workshop on New Working Fluids for Absorption Heat Pumps and Refrigeration Systems, Eurotherm, Tarragona (Spain), July 2013.

Internships

Georgia Institute of Technology (Atlanta, GA, US) _ International Mention

November 2011 and from January 2013 to April 2013

Advisor: Amyn S. Teja

Correlate and predict experimental data using different mathematical models.

Analyse experimental results with finite element simulation by using ANSYS software.

Faculty of Science University of Lisbon (Portugal)

October 2010

Advisor: C.A. Nieto de Castro

Experimental evaluation by using a commercial thermal properties analyser (KD2 Pro)

General Index

Abstract	iii
Resumen.....	v
Acknowledgments.....	vii
List of Publications and Conferences	ix
List of Tables	xiii
List of Figures	xv
List of Symbols	xix
1. Introduction	1
1.1 Background	8
1.2 Objectives.....	10
2. State of the Art	13
2.1 Methodology	18
2.1.1 Techniques to Measure Thermal Conductivity.....	18
2.1.2 The Transient Hot Wire Method (THW):Principle of Measurement	20
2.1.3 Mathematical Model.....	21
2.2 Literature Review of Working Fluids	27
2.2.1 H ₂ O + LiBr Binary Mixture.....	27
2.2.2 NH ₃ + H ₂ O Binary Mixture	29
2.2.3 NH ₃ + LiNO ₃ Binary Mixture.....	31
2.2.4 NH ₃ + LiNO ₃ + H ₂ O Ternary Mixture.....	32
2.2.5 NH ₃ + LiNO ₃ + CNTs Ternary Mixture	33
3. Experimental Setup	37
3.1 Experimental Apparatus.....	37

3.1.1	Coated Platinum Wire Device	38
3.1.2	Glass Capillary Device Filled with Mercury	42
3.2	Data Acquisition System.....	45
3.3	Sample Preparation	48
3.4	Carbon Nanotubes (CNTs).....	51
3.4.1	Chemical Treatment of Carbon Nanotubes and Stability Study	53
3.5	Calibration Procedure.....	56
3.6	Experimental Procedure	61
3.7	Uncertainty estimation	62
4.	Results and Discussion.....	69
4.1	Thermal Conductivity of $\text{NH}_3 + \text{H}_2\text{O}$	69
4.2	Thermal Conductivity of $\text{H}_2\text{O} + \text{LiBr}$	72
4.3	Thermal Conductivity of $\text{NH}_3 + \text{LiNO}_3$	73
4.4	Thermal Conductivity of $\text{NH}_3 + \text{LiNO}_3 + \text{H}_2\text{O}$	76
4.5	Thermal Conductivity of $\text{NH}_3 + \text{LiNO}_3 + \text{CNTs}$	79
4.6	Summary	84
5.	Modelling Thermal Conductivity.....	87
6.	Hot Wire Numerical Studies	103
7.	Conclusions	113
	References.....	117
	Appendix A: Computer Programs	I
	Appendix B: Uncertainty	V

List of Tables

Table 3.1: Source and purity of materials.....	51
Table 3.2: Specifications of commercial multi wall carbon nanotubes.....	52
Table 3.3: Calibration constants obtained from the thermal conductivity of water.....	57
Table 3.4: Deviations of the ammonia/lithium nitrate measured thermal conductivities from their literature values [93].....	58
Table 3.5: Effective length of ten experiments at three temperatures.....	59
Table 3.6: Thermal conductivity of reference fluids measured with the mercury filled glass capillary.....	59
Table 3.7: Calibration parameters for platinum wire and glass capillary devices.....	60
Table 3.8: Expanded uncertainty values ($K=2$).....	67
Table 4.1: Thermal conductivity for $\text{NH}_3+\text{H}_2\text{O}$ at several temperatures and compositions....	70
Table 4.2: Thermal conductivity of $\text{H}_2\text{O} + \text{LiBr}$ and comparison with literature data.....	72
Table 4.3: Thermal conductivity for NH_3 (1) + LiNO_3 (2) at several temperatures and ammonia mass fractions.....	74
Table 4.4: Thermal conductivity for NH_3 (1) + LiNO_3 (2) + H_2O (3) at several temperatures and 0.2 in water mass fraction in the absorbent solution.....	77
Table 4.5: Thermal conductivity for NH_3 (1) + LiNO_3 (2) + H_2O (3) at several temperatures and 0.25 in water mass fraction in the absorbent solution.....	77
Table 4.6: Effective thermal conductivity of CNTs nanofluids with $\text{NH}_3 + \text{LiNO}_3$ (40 wt.%) as the base fluid.....	80
Table 4.7: Effective thermal conductivity of CNTs nanofluids with $\text{NH}_3 + \text{LiNO}_3$ (30 wt.%) as the base fluid.....	81
Table 4.8: Effective thermal conductivity of CNTs nanofluids with $\text{NH}_3 + \text{LiNO}_3$ (50 wt.%) as the base fluid.....	82
Table 5.1: Adjustable parameters in the Filippov and Bohne equation with $\text{NH}_3 + \text{H}_2\text{O}$	91
Table 5.2: Adjustable parameters in Filippov and Bohne equations with $\text{NH}_3 + \text{LiNO}_3$	93
Table 5.3: Coefficients used in equation (5.20) for selected Ions.....	99
Table 5.4: Interaction parameters used in equation (5.26) for each studied mixture.....	99

Table 5.5: Correlations and models used in this work for each mixture	102
Table 5.6: Root Mean Square Error for all the measured systems with Wang&Anderko model	102
Table 6.1: Thermophysical properties for ANSYS.....	104
Table 6.2: Comparison between slope values for reference fluids.	108
Table 6.3: Comparison between thermal conductivity values ($W \cdot m^{-1} \cdot K^{-1}$)	109
Table 6.4: Simulation analysis for the coating effect	111

List of Figures

Figure 1.1: Total consumption (%) according to energy sources in residential buildings in Spain, 2011 (IDAE).	1
Figure 1.2: Total consumption (%) according to services in residential buildings in Spain, 2011 (IDAE).	2
Figure 1.3: Absorption refrigeration cycle activated by solar energy	3
Figure 2.1: Schleiermacher's hot wire instrument [31]	15
Figure 2.2: Hot-wire instrument proposed by Weber [31]	16
Figure 2.3: Example of transient hot-wire instrument for fluids [31].	17
Figure 2.4: Parallel plate instrument.	19
Figure 2.5: Transient hot wire instrument.	20
Figure 2.6: The coordinate system of an insulated wire immersed in a liquid. Region 1 is the bare metallic wire, region 2 is the electrical insulation layer, and region 3 is the surrounding fluid.	22
Figure 2.7: Comparison between literature data for H ₂ O + LiBr mixtures	28
Figure 2.8: Comparison between literature data for NH ₃ + H ₂ O mixtures.	30
Figure 2.9: Calculated data proposed by Ferreira (1984) for NH ₃ + LiNO ₃ mixtures.	32
Figure 3.1: Transient hot-wire apparatus. (A) stainless-steel vessel, (B) coated wire,	38
Figure 3.2: Schematic of the experimental setup. (A) 1 liter expansion vessel, (B) coiled tubing, (C) thermostatic bath, (D) data acquisition system, (E) computer	40
Figure 3.3: Welded weight.	41
Figure 3.4: Study of the maximum work temperature without a welded weight	42
Figure 3.5: Liquid metal transient hot-wire apparatus. (A) stainless-steel vessel, (B) mercury filled glass capillary, (C) gaskets, (D) vessel tap, (E) connections.	44
Figure 3.6: Microscope image of glass capillary in two different sections	45
Figure 3.7: Data acquisition system A) current source Keithley 6221 B) current source Keithley 2601A C) nanovoltmeter Keithley 2182A	46
Figure 3.8: System connections for PC control	47
Figure 3.9: Schematic of electrical circuit	47

Figure 3.10: Sample introduced by syringe	48
Figure 3.11: Sample preparation cells. A) ammonia cylinder B) mixing cell	49
Figure 3.12: Sample transport setup. A) high pressure nitrogen cylinder B) solution	50
Figure 3.13: TEM image of multi-walled carbon nanotubes.....	52
Figure 3.14: Ultrasonic water bath.....	54
Figure 3.15: Comparison of the visualization of CNTs 0.01 wt.% binary nanofluid without (A) and with (B) oxidation treatment after 1 day.	54
Figure 3.16: Visualization of distribution stability of CNTs suspension in NH ₃ + LiNO ₃ mixture (A) 0.005 wt.% (B) 0.01 wt.% (C) 0.02 wt.% and (D) 0.2 wt.%.	55
Figure 3.17: Resistance - Temperature relation for the A) Platinum B) Mercury.....	56
Figure 3.18: Fish-bone diagram of the uncertainty contributors	63
Figure 4.1: Thermal conductivity for NH ₃ +H ₂ O at several temperatures and compositions .	70
Figure 4.2: Thermal conductivity comparison between our experimental values and the literature data for NH ₃ + H ₂ O mixtures.....	71
Figure 4.3: Thermal conductivity comparison between our experimental values and the literature data for H ₂ O + LiBr mixtures.....	73
Figure 4.4: Thermal conductivity of NH ₃ + LiNO ₃ at several temperatures and compositions	74
Figure 4.5: Thermal conductivity comparison between our experimental values and the calculated data proposed by Infante Ferreira (1984) for NH ₃ + LiNO ₃ mixtures.....	75
Figure 4.6: Thermal conductivity for NH ₃ + LiNO ₃ + H ₂ O at several temperatures and compositions. A) 0.2 water mass fraction B) 0.25 water mass fraction	78
Figure 4.7: Effect of water addition to the binary mixture NH ₃ + LiNO ₃ : (A) 0.3 mass fraction ammonia, (B) 0.4 mass fraction ammonia, (C) 0.5 mass fraction ammonia and (D) 0.6 mass fraction ammonia.	79
Figure 4.8: Thermal conductivity comparison of CNTs concentrations with NH ₃ + LiNO ₃ (40 wt.%) as the base fluid.....	82
Figure 4.9: Thermal conductivity ratio comparison of NH ₃ concentrations with 0.01 wt% of CNTs.....	83
Figure 5.1: Comparison of some predictive methods with the experimental data of NH ₃ + H ₂ O at 293 K.....	90

Figure 5.2: Comparison of Filippov and Bohne equation using the new fitting parameters with the experimental data of $\text{NH}_3 + \text{H}_2\text{O}$ at different temperatures.....	91
Figure 5.3: Comparison of Filippov equation with the experimental data of $\text{NH}_3 + \text{LiNO}_3$ at different temperatures	92
Figure 5.4: Comparison of Bohne equation with the experimental data of $\text{NH}_3 + \text{LiNO}_3$ at different temperatures	93
Figure 5.5: Comparison between calculated values by Wang and Anderko (2008) model and experimental data of $\text{NH}_3 + \text{H}_2\text{O}$ at different temperatures.....	96
Figure 5.6: Comparison between calculated values by Wang and Anderko (2008) model and experimental data of $\text{NH}_3 + \text{LiNO}_3$ at different temperatures.	100
Figure 5.7: Comparison between predicted values by Wang and Anderko (2008) model and experimental data of $\text{NH}_3 + \text{LiNO}_3 + \text{H}_2\text{O}$ (20%) at different temperatures.	101
Figure 6.1: 2D-Axisymmetric geometry used in the numerical simulations.....	104
Figure 6.2: Example of mesh independence study for dimethyl phthalate.....	105
Figure 6.3: 2D-Axysymmetric geometry meshed and the temperature profile for Toluene at 343 K.....	106
Figure 6.4: Temperature rise comparison between numerical and experimental data for....	107
Figure 6.5: Slope selection for ANSYS data with Toluene	108
Figure 6.6: Temperature increase comparison between numerical and experimental data for A) $\text{NH}_3 + \text{LiNO}_3$ (40%) and B) $\text{NH}_3 + \text{LiNO}_3 + \text{H}_2\text{O}$ (20%)	109
Figure 6.7: Temperature profiles for Toluene at 343 K with coating and without coating ..	110

List of Symbols

A	area (m^2)
C_p	specific heat capacity ($\text{J}\cdot\text{kg}^{-1}\cdot\text{K}^{-1}$)
c	calibration constant
D	thermal diffusivity ($\text{m}^2\cdot\text{s}$)
d	distance (m)
I	electrical current (A)
k	thermal conductivity ($\text{W}\cdot\text{m}^{-1}\cdot\text{K}^{-1}$)
l	length (m)
L_{eff}	effective capillary length (m)
M	molecular mass ($\text{g}\cdot\text{mol}^{-1}$)
Q	surface area parameter
q	heat generation per unit of length ($\text{W}\cdot\text{m}^{-1}$)
\dot{q}	heat flux per unit of volume ($\text{W}\cdot\text{m}^{-3}$)
R	resistance (Ω)
r	radius (m)
T	temperature (K)
t	time (s)
V	voltage (V)
w_i	mass fraction of the component i
X	adjustable parameter
x_i	mole fraction of the component i
ρ	density ($\text{kg}\cdot\text{m}^{-3}$)
α	temperature coefficient of resistance (K^{-1})
φ	increase ratio
θ	local area fraction.

Subscripts:

m mixture, 1 ammonia, 2 lithium nitrate, 3 water

Chapter 1

1. Introduction

The rapidly growing consumption world energy has already raised concerns over supply difficulties, exhaustion of energy resources and heavy environmental impacts such as ozone layer depletion, global warming, climate change, etc. The electrical energy consumption in the residential sector has soared over the years; the global contribution from buildings towards energy consumption is 40 % in the EU and has exceeded the other major sectors: industrial and transportation [1]. This is largely due to the growing in population, the increasing demand for building services and comfort levels together with the rise in time spent inside buildings, and it seems the upward trend in energy demand will continue in the future. For this reason, energy efficiency in buildings is today a prime objective for energy policy at regional, national and international levels. Among buildings services, the growth in HVAC (heating, ventilation, and air conditioning) systems energy use is particularly significant (around 50 % of building consumption) [2]. A review of energy consumption on residential buildings in Spain demonstrates, in terms of final energy, an estimated annual consumption of 17 % [3].

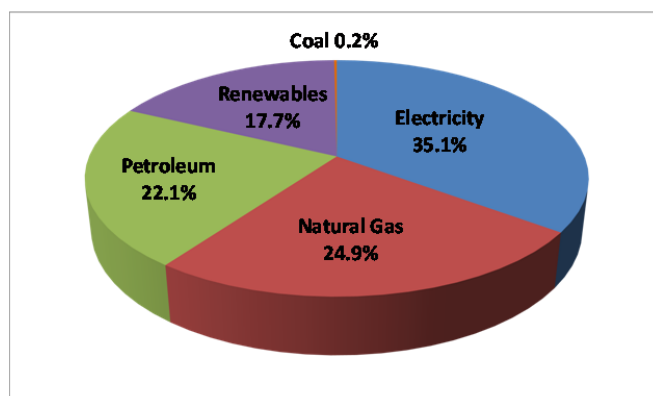


Figure 1.1: Total consumption (%) according to energy sources in residential buildings in Spain, 2011 (IDAE).

Chapter 1: Introduction

More in detail, Figure 1.1 shows the total consumption in terms of electricity which is about 35 % of total demand. Also, heating and cooling are the services with the main end use with a total weight close to 66 %, appliances follows with 19.4 % and cooking with 7.4 % (See Figure 1.2)

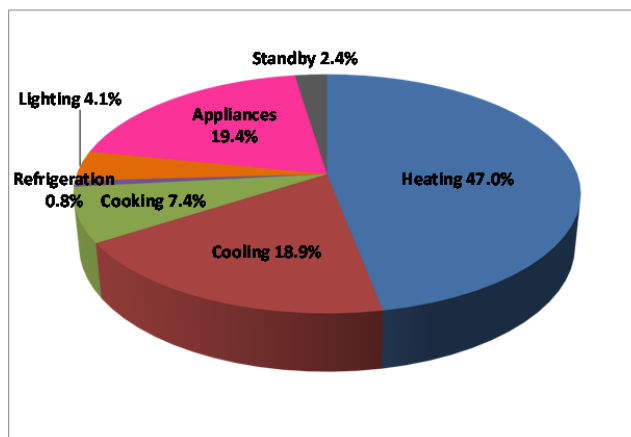


Figure 1.2: Total consumption (%) according to services in residential buildings in Spain, 2011 (IDAE).

In terms of environmental impacts, the building sector contributes up to 30 % of global annual greenhouse gas emissions and if nothing is done, greenhouse gas emissions from buildings will more than double in the next 20 years [4]. Reduce energy consumption, increased use of renewable energy sources and satisfy the Kyoto Protocol could achieve the three objectives for 2020 based on [1]:

- 20 % reduction in total emissions of greenhouse gases
- 20 % increase in energy efficiency
- 20 % of the total consumption of energy from renewable sources

Other target from January 1, 2010; the use of Virgin HCFCs (hydrochlorofluorocarbon) are forbidden in the maintenance or revision of air conditioners and can only be used recycled or reclaimed HCFCs (Montreal Protocol).

Accordingly with the previous review, during the last decade research efforts have been intensified in order to develop new solar low capacity absorption equipment for air-conditioning in residential buildings. The increasing price of primary energy and

environmental concerns such as global warming and ozone layer depletion, make the absorption refrigeration technology an alternative to the vapour compression system.

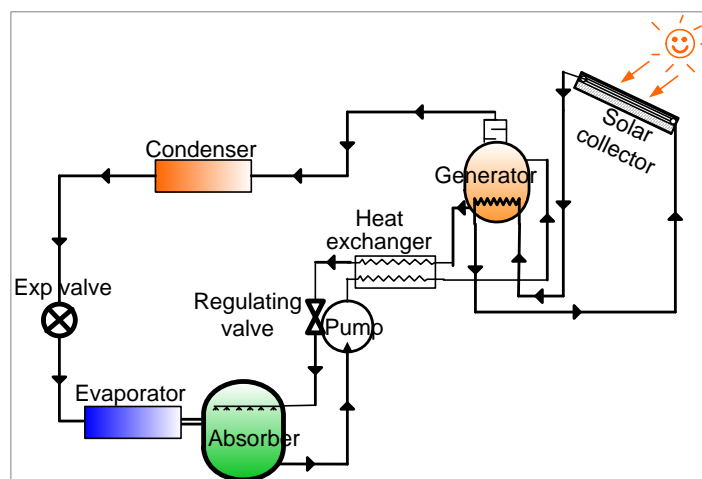


Figure 1.3: Absorption refrigeration cycle activated by solar energy

Figure 1.3 shows the schematic diagram of absorption refrigeration cycle. It is a way to produce cold water via the evaporation and condensation of a refrigerant at different pressures within the machine, just as the compression cycle, where the main difference between these two systems is the compression method of the refrigerant in the cycle. More in detail, the operation of a simple absorption cycle is based on evaporate the liquid refrigerant entering in the evaporator in a low pressure environment by extracting heat from its surroundings. The next step, in the absorber, the vapour refrigerant is absorbed-dissolved into the liquid absorbent. The working mixture (refrigerant-absorbent) is pumped to the generator where the heat is applied to the solution in order to distil the refrigerant from de absorbent. Finally the pure refrigerant enters the condenser. In this heat exchanger, the hot vapour refrigerant is cooled and condenses to a liquid. With an expansion valve the pressure of the refrigerant is reduced allowing the cycle to restart. The absorbent is recycled back to the absorber by another expansion valve.

In the compression system, the compressor sucks the refrigerant from the evaporator and compresses it to the high pressure. In the absorption system, the process of compression is carried out by two different devices called absorber and generator. Thus the absorber and the generator replace the compressor in the absorption cycle usually working with mixtures

Chapter 1: Introduction

of two components, where one is the refrigerant and another is used as the absorption of the refrigerant, and is physically based on the ability of some liquid substances to absorb other substances in the vapour phase. Another major difference between compression and absorption cycle is the method in which the energy input is given to the system. In the compression cycle the input energy is in the form of the mechanical work run by the electricity. On the other hand, in the absorption cycles the energy input is given in the form of the heat, either waste heat or renewable energy such as solar energy.

Some advantages of absorption cycles in front of compression systems are described followed:

- The use of solar energy for driving the cycle instead of electrical energy. Thus, running cost of the absorption cycle is much lesser than the compression cycle if waste heat or solar energy is used.
- The compressor operates at very high speeds and it makes lots of vibrations and noise, while the absorption refrigeration systems operate silently.
- Typical refrigerants used in the absorption cycles are available cheaply and easily. In case of the compression system halocarbons are used as the refrigerants, which are very expensive and produce greenhouse effect.

In contrast, the cycle efficiency of absorption cycles is lower than the efficiency achieved by the compression method and its initial capital cost is much higher. Comparing the typical coefficient of performance (COP), which is the ratio of cooling effect to the amount of energy input, for absorption cycle is around 0.5-1.5 and the COP for compression system is around 4.5-5.5 [5].

Hence, absorption refrigeration technology is a good alternative to the vapour compression system where electricity is unreliable, costly, or unavailable, where noise from the compressor is problematic, where surplus heat is available, or where lesser releasing of CO₂ emissions is needed.

Performance of an absorption refrigeration system is critically dependent on the chemical and thermodynamic properties of the working fluid. The working fluid consists in a binary solution formed by the refrigerant and the absorbent. There are fundamental features required in the refrigerant-absorbent pair [6]:

- A fundamental requirement is the affinity between the absorbent and refrigerant under working conditions and must have a margin of miscibility within the operating temperature range of the cycle in the liquid phase.
- The refrigerant must be much more volatile than the absorbent, thus it can be easily separated in the generator. For the same reason, the mixture must have different boiling points at the same pressure.
- The operating pressures, established by the physical properties of the refrigerant, should be moderate.
- Refrigerant should have high heat of vaporization in order to maintain low circulation rate between the generator and the absorber.
- Transport properties such as, viscosity, surface tension, thermal conductivity and diffusion coefficient, that influence heat and mass transfer should be favourable.
- The mixture should also be chemically stable, non-toxic, and non-explosive.

Even there are around 40 refrigerant and 200 absorbent compounds suggested in literature [7]. However nowadays, most absorption heat pumps and chillers use $\text{NH}_3 + \text{H}_2\text{O}$ and $\text{H}_2\text{O} + \text{LiBr}$ mixtures as working fluids. The first mixture, $\text{NH}_3 + \text{H}_2\text{O}$ is widely used due to its high stability for a wide range of operating temperature and pressure. Also, the use of NH_3 as a refrigerant allows applications at temperatures below 0°C , and provides efficient performance of the system due to the high latent heat of evaporation. But, the main drawback of this mixture is the water volatility; the cycle requires a rectifier after the generator to remove the water that normally evaporates with NH_3 reducing the system

Chapter 1: Introduction

performance. There are other handicaps such as its toxicity, high pressure and corrosive action to copper. However, the mixture is environmental friendly and low-cost. On the other hand $\text{H}_2\text{O} + \text{LiBr}$, has two major advantages; the non-volatility of the absorbent (LiBr) without the necessity of rectification, and the use of H_2O as a refrigerant with extremely high heat of vaporization. Nevertheless, using H_2O as a refrigerant limits the low temperature application (above 0°C) and the system must be operated under vacuum conditions. Also, the mixture is corrosive, expensive and present crystallization problems at high concentrations.

Even though $\text{NH}_3 + \text{H}_2\text{O}$ and $\text{H}_2\text{O} + \text{LiBr}$ are the typical commercial mixtures commonly used for many years and their properties are well known, relevant activities in this topic are focused on the research of new working fluids in order to overcome these limitations, improve the cycle efficiency and reduce the driving temperature. The use of solar energy requires systems operating at low temperatures, ideally from 80 to 90 $^\circ\text{C}$. A promising mixture for solar activated refrigeration systems is $\text{NH}_3 + \text{LiNO}_3$, identified in the literature as a potentially suitable mixture for low temperature applications, allowing the use of flat solar collectors to obtain the input energy [8], [9], [10], [11], [12]. Some outstanding features of the $\text{NH}_3 + \text{LiNO}_3$ mixture are important in front of the conventional working fluids $\text{NH}_3 + \text{H}_2\text{O}$ and $\text{H}_2\text{O} + \text{LiBr}$, for example: no rectification is needed, the absorption cycle can operate at lower driven temperature and no crystallization problems at high heat sink temperature [13]. However, experimental studies of absorption cycles operating with this mixture have shown low rates of heat and mass transfer in the absorber limited by the poor transport properties of the salt solution [14], [15], [16]. In this work, in order to overcome this limitation, the addition of water or carbon nanotubes (CNTs) to the binary mixture ($\text{NH}_3 + \text{LiNO}_3$) has been proposed. More detailed information about previous studies and the effect of this addition can be seen in sections 2.2.4 and 2.2.5.

Although absorption equipments have been in use since the 19th century, the knowledge of the thermophysical properties for the absorbent-refrigerant pair are scanty. In order to compare and appropriately design and evaluate the efficiency of absorption refrigeration cycles operating with different working fluids, it is necessary to obtain the thermodynamic and transport properties of these mixtures, especially for the absorber because it is the most

critical component in the cycle. In particular, it is essential to determine the thermal conductivity of the mixture as a function of its composition and temperature to obtain heat transfer coefficients. For the commercial working fluid $\text{H}_2\text{O} + \text{LiBr}$, thermal conductivity values are well known in a wide range of temperatures and concentrations. Several experimental data can be found in the literature [17], [18], [19], [20], [21]. Hence, one composition of $\text{H}_2\text{O} + \text{LiBr}$ solution was measured at 40 wt. % of LiBr in the temperature range from 298.15 to 428.15 K and a constant pressure of 1.5 MPa in order to confirm these available data with our system. Other typical commercial mixture commonly used is $\text{NH}_3 + \text{H}_2\text{O}$. Unfortunately, few experimental data on the thermal conductivity are available in the literature. Besides, the currently available data cover only very limited temperature, pressure, and concentration ranges. Most reported data are very old and shows remarkably discrepancies. In order to resolve these disagreements and to extend the range of available data on high ammonia concentrations, the thermal conductivity of $\text{NH}_3 + \text{H}_2\text{O}$ mixtures containing 0.1 to 0.5 mass fraction ammonia has been measured at temperature between 293.15 and 313.15 K. On the other hand, for the promising mixture $\text{NH}_3 + \text{LiNO}_3$, no previous experimental studies on the thermal conductivity have been found in the literature. For this reason and to complete the existing thermophysical properties database for the mixture [11], [12], the thermal conductivity from 0.3 to 0.6 in ammonia mass fraction and temperatures between 303.15 K and 353.15 K has been measured and new data has been provided to the literature. Results show lower performance in thermal conductivity. Therefore, in order to evaluate the advantages of the addition of water or CNTs to the binary mixture, its effect on the heat transfer and in particular on the thermal conductivity has been analysed with ammonia mass fraction range from 0.3 to 0.6, H_2O range from 0.20 to 0.25 and CNTs range from 0.005 to 0.2 %, at temperatures between 303.15 and 353.15 K. These results indicate an enhancement in the effective thermal conductivity and also suggest that the thermal conductivity enhancement with CNTs is less than the thermal conductivity enhancement with water addition. For more detailed literature review of these mixtures see section 2.2.

Chapter 1: Introduction

1.1 Background

To carry out this study we have in account that thermal conductivity of heat transfer fluids plays a vital role in the development of high performance absorber devices. It is known low thermal conductivity is a primary limitation in the development of energy-efficient heat transfer fluids that are required in these systems. Especially in the absorber because it is the most critical component of the absorption machines; it has simultaneous heat and mass transfer process. The high price of absorption machines is related with the complexity of the system and the size of the heat exchangers [22]. The absorber usually is the largest element of absorption machines due to its low heat and mass transfer coefficients, and this determines the final design of the whole system.

In recent decades, several new working fluids have been proposed as alternatives to develop high-efficiency systems. The promising mixture reflected in this work for solar activated refrigeration systems is $\text{NH}_3 + \text{LiNO}_3$. The new mixture displays higher COP values and lower driven temperature comparing with $\text{NH}_3 + \text{H}_2\text{O}$ systems. However, when the mixture was charged in an absorption machine designed for $\text{NH}_3 + \text{H}_2\text{O}$, some authors note the high viscosity of the salt solution, and results show poor transport properties that limited the performance of the system [14], [15], [16]. Thus, thermophysical properties must be known in order to appropriately design an equipment fully for this mixture.

The first target was to measure the thermal conductivity of the proposed mixture since no experimental data were found in the literature. The only previous data available is the correlation proposed by Ferreira in 1984 [8] giving extremely higher values of thermal conductivity. Even though the main objective of this work is the experimental study of thermal conductivity in new mixtures, searching this property in the literature for typical commercial working fluids it was observed a significant lack of data for the $\text{NH}_3 + \text{H}_2\text{O}$ mixture. In this sense, the next step was to measure experimentally the thermal conductivity of the commercial working fluid $\text{NH}_3 + \text{H}_2\text{O}$, providing new data to the literature.

Recently, has emerged a new line of research based on the addition of nanoparticles to enhance heat and mass transfer coefficients [23]. Fluids in which nanoparticles, below 100 nm in diameter, are suspended evenly and stable in the base fluid are called nanofluids [24]. It is known that heat transfer by conduction through solid is orders of magnitude larger than that by convection/conduction through a fluid. Then, is expected than fluids containing suspended solid particles, display higher thermal conductivity than the base fluids. But, nanofluids not only increase the thermal performance of base fluid. The small particle diameter and the small volume fraction of the particle needed for heat transfer enhancement also solve problems such as sedimentation, erosion, cohesion and corrosion which happen conventionally with the use of micro-sized particles [25]. However, not only nanoparticles can enhance thermal conductivity of conventional fluids. In the past few years numerous investigations have been carried out seeking to develop novel methods for enhancing the thermal performance or heat transfer fluids, and many studies have been conducted to the absorption area actively. For example, it was found that the addition of a third component in the binary mixture $\text{NH}_3 + \text{LiNO}_3$, with high affinity for ammonia such as water, not only improve the thermal conductivity of the solution, it can also decrease the viscosity of the mixture [26], [27]. Despite all this review, no experimental works focused in the measurement of thermal conductivity with the binary mixture ($\text{NH}_3 + \text{LiNO}_3$) containing water or CNTs have been found. Consequently, the ternary mixtures $\text{NH}_3 + \text{LiNO}_3 + \text{H}_2\text{O}$ and $\text{NH}_3 + \text{LiNO}_3 + \text{CNTs}$ have been measured and in both cases the results indicate an enhancement in the effective thermal conductivity.

As mentioned above, thermal conductivity is the property measured in this work. A number of different techniques to determine thermal conductivity can be found in the literature. Each of these techniques is suitable for a limited type of materials, depending on the thermal properties and the medium temperature. First division can be made between steady-state technique, where the material is analysed in complete temperature equilibrium taking usually long time periods, and transient-state technique, in this case the thermal conductivity of a medium is determined by the temperature rise and response to heating is fast. Transient hot-wire method is the most widely used and well documented technique in literature. One of the biggest advantages of this method is the almost complete elimination

Chapter 1: Introduction

of natural convection due to the short measurement time [28], [29]. The hot-wire technique entails measuring the temperature/time response of a wire by passing a constant electrical current. The wire is used as both heater and thermometer.

1.2 Objectives

The overall project objective is to intensify heat and mass transfer processes in the absorber machine and to find the optimal conditions to design a highly effective absorption system for $\text{NH}_3 + \text{LiNO}_3$ mixture. *REF: ENE2008-00863*

The main objective of this study is to measure the thermal conductivity of the new mixture $\text{NH}_3 + \text{LiNO}_3$ because no data were found in the literature, and for the commercial working fluid $\text{NH}_3 + \text{H}_2\text{O}$ since available literature data are scanty and limited to low temperatures and concentrations.

On the other hand, the main research goal is to analyse the effect of carbon nanotubes or water addition on the new working fluid ($\text{NH}_3 + \text{LiNO}_3$) by the enhancement of thermal conductivity and consequently improve heat transfer in coolants.

More specifically, some important tasks that will be carried out during the project are recounted below:

- Design and setup the experimental equipment based in a transient hot wire system to measure the thermal conductivity of electrically conducting fluids at high pressures (2.0 MPa) and temperatures (353.15 K).
- Develop a program in commercial software (Agilent VEE) for automated measurement and data logging.
- Analyse the effect of the insulating layer thickness of the wire when electrically conducting fluids are measured.

- Validate the apparatus and methodology by comparing measurements with the values of references fluids such as water, toluene, dimethyl phthalate and ethylene glycol. Also with water + lithium nitrate as an electrolyte solution with similar characteristics than the target mixtures.
- Comprehensive study of uncertainties in the experimental measurements.
- Develop a methodology for sample preparation in order to work and measure under pressure.
- Thermal conductivity measurements of the three binary working mixtures $\text{NH}_3 + \text{H}_2\text{O}$, $\text{H}_2\text{O} + \text{LiBr}$ and $\text{NH}_3 + \text{LiNO}_3$ at different concentrations and temperatures.
- Study and analysis of some important parameters in the use of carbon nanotubes such as; concentration, stable suspensions, influence of dispersant and chemical treatments.
- Carry out a chemical treatment by surface modification of CNTs through oxidation in order to get an stable and homogeneous distribution in the base fluid.
- Prepare and characterize the new working fluid ($\text{NH}_3 + \text{LiNO}_3$) having nanoparticles or water.
- Measure the thermal conductivity of the binary nanofluid formed by $\text{NH}_3 + \text{LiNO}_3 + \text{CNTs}$ and the ternary mixture formed by $\text{NH}_3 + \text{LiNO}_3 + \text{H}_2\text{O}$.
- Modeling thermal conductivity of $\text{NH}_3 + \text{H}_2\text{O}$, $\text{NH}_3 + \text{LiNO}_3$ and $\text{NH}_3 + \text{LiNO}_3 + \text{H}_2\text{O}$ mixtures as function of ammonia mass fraction and temperature.
- Numerical simulations, using a finite element program ANSYS, for the THW method in order to exactly represent the geometry of the measurement sensor and to analyse the coating effect of the wire.

Chapter 2

2. State of the Art

Heat transfer plays a vital role in many fields such as power generation, air conditioning, transportation, and microelectronics due to the heating and cooling processes involved. It is important to say that one of the major parameters in heat transfer is the thermal conductivity of the working fluid. Thermal conductivity (k) is the intrinsic property of a material which relates its ability to conduct heat. It is defined by the law of heat conduction as the coefficient of proportionality between the rate of heat flux (q) and the temperature gradient (dT/dx) given by the Fourier's law, using the one-dimensional form in the x direction, where x is the distance of the gradient (2.1).

$$q_x = -k \cdot \frac{dT}{dx} \quad (2.1)$$

Knowledge of this property values are needed in process design calculations involving the sizing of heat exchangers, the calculation of unsteady state heating or cooling times, and the calculation of temperature profiles in a body exposed to heat or cold. Consequently, the measurement of thermal conductivity has received much attention in the literature. There are a number of different techniques in order to measure the thermal conductivity of a solids, liquids or gases. Each of these techniques is suitable for a limited range of materials, depending on the thermal properties and the medium temperature. A quick overview of some methods to measure thermal conductivity can be found [30]:

- **Steady-State Method:** where a temperature difference across a sample is measured in response to an applied amount of heating power.

Chapter 2: State of the Art

- Comparative Technique: this method uses the known thermal conductivity of a standard which is put in series between the heater and the sample as the reference material for heat-flow measurements.
- Radial Flow Method: heat is applied internally to the sample and creates an angularly uniform distribution of temperature.
- Laser-Flash Diffusivity: in this technique one face of a sample is irradiated by a short laser pulse, there is an IR detector monitor temperature rise of the opposite side of the sample, and the thermal diffusivity is calculated from the temperature rise versus time profile, finally the thermal conductivity (k) is related to the thermal diffusivity (D) by the density (ρ) and the heat capacity (Cp) [$D = k \cdot \rho^{-1} \cdot Cp^{-1}$].
- Pulse-Power Method: it is basically the same as in steady-state measurements except the heating current which is a pulsed with a square wave of constant current.
- Transient Techniques: measurements are performed during the process of heating up a wire probe. This technique is the most widely used and well documented technique in the literature to determine the thermal conductivity of liquids over a wide range of conditions.

This work is focused on the transient hot wire method in order to carry out the experimental measurements. The review in the historical evolution of the transient hot wire technique, starting from the first experiments in 1780, is presented followed in order to have a better insight into the development of this technique [31]. This analysis is divided into three main periods in which a brief selection of instruments evolution is presented:

The initial stages: from 1780 to 1888

In 1780 Joseph Priestley [32] was probably the first one to carry out experiments in conduction during the discussions of whether gases could conduct heat. During this period the discussion about conduction in gases was still going on. But, was in 1848 (W. R. Grove) [33] and some years after in 1861 (G. Magnus) [34], [35] and 1863 (J. Tyndall) [36] when

experiments with heated wires in gases started to become common in this era. Nevertheless, the debate about conduction in gases had not seen its end with these experimental works. Was between 1860 (J. C. Maxwell) [37], [38] and 1862 (R. J. E. Clausius) [39], [40] when the gas conduction debate ended in essence with the wide acceptance on the dynamic theory of gases and his calculation of a theoretical value of the thermal conductivity of a gas. Finally in 1888, Schleiermacher [41] measured the thermal conductivity of gases by using a platinum hot wire (probably first real application of hot wire instrument). Figure 2.1 shows the instrument, composed of a horizontal platinum wire of 0.4 mm diameter and 32 cm length, placed in the center of a glass cylinder of 2.4 cm diameter and kept taut by a metallic spring. Potential leads were soldered at points A and B.



Figure 2.1: Schleiermacher's hot wire instrument [31]

Then, during the first period from 1781 to 1888, the thermal conductivity measurements were only conducted for gases.

Develop of the transient hot wire technique: from 1888 to 1971

In the second period, from 1888 to 1971, the transient hot wire instrument was developed for measuring the thermal conductivity of fluids and solids. In 1917 Weber [42] proposed a modified apparatus which significantly reduce the errors resulting from convection, involved in the determination of the thermal conductivity of gases by the method of Schleiermacher [41]. The apparatus shown in Figure 2.2 was placed vertically, probably for the first time, and consist in a platinum wire of 0.4 mm diameter and 54.5 cm length placed inside a 2.3 cm diameter glass tube. The wire was employed as a four-terminal resistance bridge, and was kept taut by a spring at the bottom of the vessel. However, was Stålhane and Pyk in 1931 [43] who measured the thermal conductivity of solids and powders (and some liquids) with the first "transient" hot-wire instrument. They further investigated the relationship between

Chapter 2: State of the Art

the time and temperature rise, for a fine straight wire subjected to a step change in the heat input to the wire.

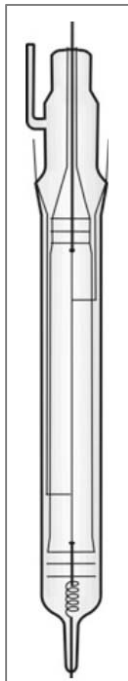


Figure 2.2: Hot-wire instrument proposed by Weber [31]

Progress on the transient hot wire instruments was still going on during these years, improvements in order to measure at low temperatures, reduce the uncertainties of the equipment, and optimize times recorded between others. But the most important change was in 1971 with the work of Haarman [44]. His equipment allowed measuring the resistance of two identical wires except for their length by using an automatic Wheatstone bridge equipped with an electronic potential comparator. Therefore, the elimination of end effects of the wire, and the reduction in the duration of the experimental time, eliminated completely the convection errors and reduced greatly other time dependent errors.

Last period: from 1971 until Today

The pioneering work of Haarman [44] using two wires, faster electronic bridge and experimental time of seconds, was the start of a new series of transient hot wire instruments developed after 1971. Figure 2.3 shows an example of some characteristic changes that the transient hot wire has experienced since 1971.

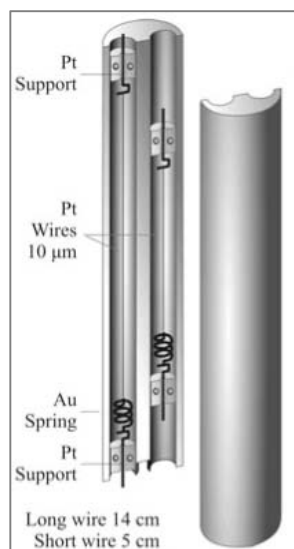


Figure 2.3: Example of transient hot-wire instrument for fluids [31]

Other major event during this period was the paper published by Healy in 1976 [45], which summarized the theory of the transient hot wire method and the most important corrections needed during the measurements such as eliminate convection effects, assume a finite diameter and length of the wire and eliminate end effects. Finally, the use of cheap, accurate, and reliable data acquisition systems together with a fully theory exists, enables higher precision measurements and much lower uncertainties.

However, despite of the successful application of the transient hot-wire technique in the measurement of the thermal conductivity of gases, liquids, melts, nanofluids, and solids, over very wide ranges of temperature and pressure, there are still some areas where the technique cannot be applied [31]. For example; in fluids near of the critical regions because physical properties changes are too large with temperature and the technique requires a temperature rise of a few kelvins. Also with thin films, in this case since the thickness of the sensor is similar to the thickness of the sample heat losses can take place and then the technique is not suitable.

Nowadays the use of finite elements in the measurements procedure of thermal conductivity is being developed. The finite element solution is used in order to represent exactly the geometry of the measurements sensors and to improve accuracy in the measurements.

Chapter 2: State of the Art

2.1 Methodology

2.1.1 Techniques to Measure Thermal Conductivity

The different experimental techniques found in the literature for determining thermal conductivity of liquids can be divided in two major groups: steady-state methods and transient methods. These two methods are capable of isolating the contributions due to heat conduction from those resulting from convection and radiation.

The steady-state methods typically use simpler equipment but require long time period to reach up the sample equilibrium. The measurement is performed when the temperature of the material measured does not change with time. The disadvantages are that heat lost is difficult to quantify and may give considerable inaccuracy, and natural convection may set in, which gives higher apparent values of conductivity. In general, steady-state techniques confine the fluid between two surfaces maintained at different temperatures. There are several instruments but measurements of the thermal conductivity of fluids and solids using steady-state methods employ usually the geometry of parallel plate.

Figure 2.4 shows a schematic diagram of the parallel plate instrument, where the fluid occupies a thin gap between the two horizontally aligned plates (upper and lower). A small amount of heat is generated electrically in the upper plated and is transported through the sample to the lower plate. With the known heat flux (q) and temperatures at the surfaces of the upper and lower plates (ΔT), the thermal conductivity of the fluid can be calculated from the Fourier's law (2.2):

$$k = \frac{q \cdot d}{A \cdot \Delta T} \quad (2.2)$$

Where, A is the area of the plates and d is the distance between the plates.

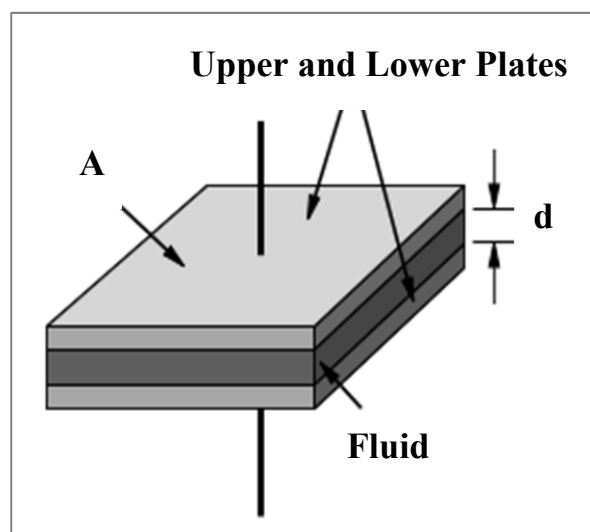


Figure 2.4: Parallel plate instrument

The problematic with these methods is in the careful design and construction of the cell. The two plates should be perfectly aligned on a horizontal axis to minimize convection errors, and the gap between the plates has to be small as possible. In addition, applying this technique requires special attention for radiation emissivity of the plates and other heat losses.

Whereas, the transient state techniques are often faster, lasts only a few seconds, and not involve the careful preparation of the sample. The main advantage is the almost complete elimination of natural convection and radiation losses that greatly simplifies experimental procedures. The disadvantages are that the mathematical analysis of the data is in general more difficult and also requires precision instrumentation. The most widely used and well documented technique in the literature is the transient hot wire method [28], [29]. This technique employs a wire suspended in a liquid to measure the thermal conductivity. A constant current is passed through the wire and its temperature increases due to the power dissipation by Joule heating after a time period. Finally, the thermal conductivity of the surrounding liquid is determined by measuring the temperature change of the wire respect to time. It is particularly simple to use because the wire can be modelled as a line with simple geometry and therefore, heat conduction equation can be solved. Consequently, to measure thermal conductivity accurately it is best to use transient methods.

Chapter 2: State of the Art

2.1.2 The Transient Hot Wire Method (THW): Principle of Measurement

The transient hot wire technique is known to be a fast and accurate method for fluid thermal conductivity measurements. The principle of this technique is based on a constant electrical current passing through a thin wire, usually made of platinum, submerged in the liquid whose thermal conductivity is to be measured (See Figure 2.5). The wire is heated by sending current through it and its temperature increases, due to the power dissipation by Joule heating, with time is measured. The temperature variation induced by the heating of the wire is obtained by measuring the voltage rise, with precision data acquisition system, and then determining the resistance change. This voltage measurement must be done quickly, for a maximum of 4-6 seconds, to avoid natural convection effects. The resistance values can be used to calculate the temperature change since the resistivity of the wire material shows a highly linear temperature dependence. Finally, the thermal conductivity of the surrounding liquid is determined by measuring the temperature change of the wire respect to time. The higher the thermal conductivity of the surrounding liquid, the lower will be the temperature rise of the wire. In this method the wire is used as both, heater and thermometer.

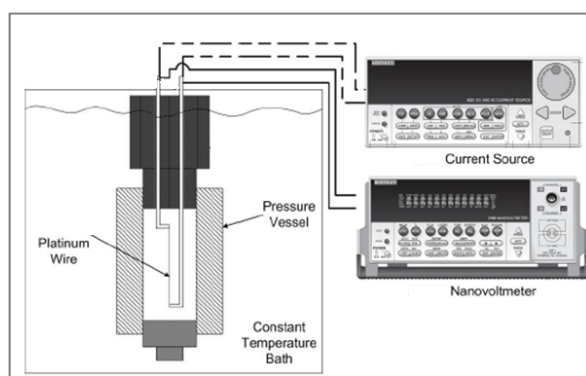


Figure 2.5: Transient hot wire instrument

However, for electrically conducting fluids this method is not usable with bare metal wire because it could lead to ambiguous results in the measurements. The resulting thermal conductivity is not accurately determined due to the leakage of current, polarization of the fluid at surface of the wire, and distortion of output voltage signal due to influence of the conducting liquid [28]. As alternative an insulated wire can be used [28], [21], [46]. The

effects of the insulating layer's thickness have been analyzed [28], [47], [48] and appropriate corrections to the temperature change that this insulation cause have been determined (See section 2.1.3).

The thermal conductivity relationship is obtained by using the following equation (2.3) (for more detailed analysis see section 2.1.3).

$$k = c \cdot \frac{q}{4 \cdot \pi \cdot \left(\frac{d\Delta T}{d \ln t} \right)} \quad (2.3)$$

Where k is the thermal conductivity of the liquid in $\text{W}\cdot\text{m}^{-1}\cdot\text{K}^{-1}$, ΔT is the temperature difference between the local temperature in the coated wire at any time and the initial temperature of the medium, q is the heat generation per unit of length of the wire in $\text{W}\cdot\text{m}^{-1}$, t is time in seconds, and c is a calibration constant related to the finite length of the wire and the coating effect. The value of c is determined experimentally via measurements on reference fluids with available thermal conductivity values (See section 3.5 for more detail).

2.1.3 Mathematical Model

The mathematical model for the transient hot wire method, proposed by Nagasaka and Nagashima in 1981 [28], is developed here for a general cases of an insulated wire to determine the thermal conductivity of the liquid. The model takes into account the effect on temperature distribution due to thin insulation coating and is based on several assumptions such as:

- The wire is infinitely long and thin and is surrounded by an infinite medium.
- The wire is a perfect thermal conductor so that the temperature distribution within the wire can be treated as uniform.

Chapter 2: State of the Art

- The wire loses heat radially only by conduction to the surrounding medium.

Figure 2.6 shows the three regions of conduction heat transfer from the wire to the surrounding fluid:

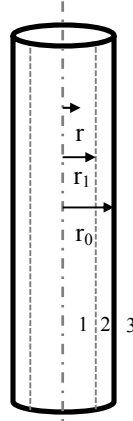


Figure 2.6: The coordinate system of an insulated wire immersed in a liquid. Region 1 is the bare metallic wire, region 2 is the electrical insulation layer, and region 3 is the surrounding fluid.

The basis of the mathematical model is the heat transfer in a cylindrical coordinates given in equation (2.4).

$$\rho \cdot C_p \cdot \frac{\partial T}{\partial t} = \frac{1}{r} \cdot \frac{\partial}{\partial r} \cdot \left(k \cdot r \cdot \frac{\partial T}{\partial r} \right) + \frac{1}{r^2} \cdot \frac{\partial}{\partial \phi} \cdot \left(k \cdot \frac{\partial T}{\partial \phi} \right) + \frac{\partial}{\partial z} \cdot \left(k \cdot \frac{\partial T}{\partial z} \right) + \dot{q} \quad (2.4)$$

Assuming one-dimensional heat conduction with a line heat source at the axis of the cylindrical domain, then the terms (2.5) and (2.6) for the other two dimensions can be set equal 0:

$$\frac{1}{r^2} \cdot \frac{\partial}{\partial \phi} \cdot \left(k \cdot \frac{\partial T}{\partial \phi} \right) = 0 \quad (2.5)$$

$$\frac{\partial}{\partial z} \cdot \left(k \cdot \frac{\partial T}{\partial z} \right) = 0 \quad (2.6)$$

Also, if the physical properties are considered constants, then the working equation (2.4) is based on a specific solution of Fourier's law governing in each of these three regions:

$$\frac{\partial^2 \Delta T_1}{\partial r^2} + \frac{1}{r} \cdot \frac{\partial \Delta T_1}{\partial r} - \frac{1}{D_1} \cdot \frac{\partial \Delta T_1}{\partial t} = -\frac{q}{\pi \cdot r_1^2 \cdot k_1} \quad 0 \leq r \leq r_1 \quad (2.7)$$

$$\frac{\partial^2 \Delta T_2}{\partial r^2} + \frac{1}{r} \cdot \frac{\partial \Delta T_2}{\partial r} - \frac{1}{D_2} \cdot \frac{\partial \Delta T_2}{\partial t} = 0 \quad r_1 \leq r \leq r_0 \quad (2.8)$$

$$\frac{\partial^2 \Delta T_3}{\partial r^2} + \frac{1}{r} \cdot \frac{\partial \Delta T_3}{\partial r} - \frac{1}{D_3} \cdot \frac{\partial \Delta T_3}{\partial t} = 0 \quad r_0 \leq r \quad (2.9)$$

Where r is the radial coordinate measured from the center of the wire, r_1 is the radius of metallic wire, r_0 is the overall radius of coated wire, D is the thermal diffusivity, k is the thermal conductivity, q is the heat generation per unit length of wire and ΔT is the temperature difference between the local temperature in the wire or in the Teflon at any time and the initial temperature of the medium. The suffixes denote each region according to Figure 2.6. Since there is no current passing through region 2 and 3, these two regions don't have the heat generation term in their corresponding Fourier equations (2.8) and (2.9).

The imposed initial and boundary conditions are:

$$\Delta T_1 = \Delta T_2 = \Delta T_3 = 0 \quad t \leq 0 \quad (2.10)$$

$$k_1 \cdot \frac{\partial \Delta T_1}{\partial r} = k_2 \cdot \frac{\partial \Delta T_2}{\partial r} \quad r = r_1 \quad (2.11)$$

$$\Delta T_1 = \Delta T_2 \quad r = r_1 \quad (2.12)$$

$$k_2 \cdot \frac{\partial \Delta T_2}{\partial r} = k_3 \cdot \frac{\partial \Delta T_3}{\partial r} \quad r = r_0 \quad (2.13)$$

$$\Delta T_2 = \Delta T_3 \quad r = r_0 \quad (2.14)$$

$$\Delta T_3 = 0 \quad r \rightarrow \infty \quad (2.15)$$

The solution for the problem, using the expansion method outlined by Carslaw and Jaeger [49], is expressed as:

Chapter 2: State of the Art

$$\begin{aligned}
 \Delta T_1(r, t) = \frac{q}{4\pi k_3} & \left[\ln \frac{4D_3 t}{r_0^2 C} + \frac{2k_3}{k_2} \ln \frac{r_0}{r_1} - \frac{k_3(r^2 - r_1^2)}{r_1^2 k_1} \right. \\
 & + \frac{1}{t} \left\{ \frac{r^2 - r_1^2}{4k_1} \left[(k_2 - k_3) \left(\frac{1}{D_1} - \frac{1}{D_2} \right) + \frac{k_1}{D_1} \right] \right. \\
 & + \frac{r_1^2}{2} \left(\frac{1}{D_2} - \frac{1}{4D_1} \right) + \frac{r_0^2}{2} \left(\frac{1}{D_3} - \frac{1}{D_2} \right) \\
 & + \frac{r_1^2}{k_2} \left(\frac{k_2}{D_2} - \frac{k_1}{D_1} \right) \ln \frac{r_0}{r_1} + \frac{1}{2k_3} \left[r_1^2 \left(\frac{k_2}{D_2} - \frac{k_1}{D_1} \right) \right. \\
 & \left. \left. + r_0^2 \left(\frac{k_3}{D_3} - \frac{k_2}{D_2} \right) \right] \ln \frac{4D_3 t}{r_0^2 C} \right] \quad (2.16)
 \end{aligned}$$

$$\begin{aligned}
 \Delta T_2(r, t) = \frac{q}{4\pi k_3} & \left[\ln \frac{4D_3 t}{r_0^2 C} + \frac{2k_3}{k_2} \ln \frac{r_0}{r} \right. \\
 & + \frac{1}{t} \left\{ \frac{r_1^2}{4} \left(\frac{1}{D_2} - \frac{1}{2k_1} \right) + \frac{r_0^2}{4} \left(\frac{2}{D_3} - \frac{2}{D_2} + \frac{r_2}{D_2 r_0^2} \right) \right. \\
 & + \frac{r_1^2}{2k_2} \left(\frac{k_2}{D_2} - \frac{k_1}{D_1} \right) \ln \frac{r_0}{r_1 r} + \frac{1}{2k_3} \\
 & \left. \left. \times \left[r_1^2 \left(\frac{k_2}{D_2} - \frac{k_1}{D_1} \right) + r_0^2 \left(\frac{k_3}{D_3} - \frac{k_2}{D_2} \right) \right] \ln \frac{4D_3 t}{r_0^2 C} \right] \right] \quad (2.17)
 \end{aligned}$$

Where $C = \exp^\gamma = 1.781$ and γ is Euler's constant. The above approximate solution is valid for large values of $\frac{D_3 t}{r^2}$.

The intensity is applied directly to the wire and assuming uniform temperature distribution over the wire, then the temperature rise ΔT_1 of the hot wire is given as;

$$\begin{aligned}
 \Delta T_1 &= \int_0^{r_1} \Delta T_1 \frac{2r}{r_1^2} dr \\
 &= \frac{q}{4\pi k_3} \left[\ln \frac{4D_3 t}{r_0^2 C} + \frac{2k_3}{k_2} \ln \frac{r_0}{r_1} + \frac{k_3}{2k_1} \right. \\
 &\quad \left. + \frac{1}{t} \left\{ \frac{r_1^2}{8} \left[\left(\frac{k_3 - k_2}{k_1} \right) \left(\frac{1}{D_1} - \frac{1}{D_2} \right) + \frac{4}{D_2} - \frac{2}{D_1} \right] \right. \right. \\
 &\quad \left. \left. + \frac{r_0^2}{2} \left(\frac{1}{D_3} - \frac{1}{D_2} \right) + \frac{r_1^2}{k_2} \left(\frac{k_2}{D_2} - \frac{k_1}{D_1} \right) \ln \frac{r_0}{r_1} \right. \right. \\
 &\quad \left. \left. + \frac{1}{2k_3} \left[r_1^2 \left(\frac{k_2}{D_2} - \frac{k_1}{D_1} \right) + r_0^2 \left(\frac{k_3}{D_3} - \frac{k_2}{D_2} \right) \ln \frac{4D_3 t}{r_0^2 C} \right] \right\} \right] \quad (2.18)
 \end{aligned}$$

The above equation is rewritten using the constant terms A, B and C, which are involving the insulation and geometry of the wire, the thermal diffusivity and the thermal conductivity.

$$\Delta T_1 = \frac{q}{4 \cdot \pi \cdot k_3} \left[\ln t + A + \frac{1}{t} (B \cdot \ln t + C) \right] \quad (2.19)$$

The terms A, B and C are defined as follows:

$$A = \ln \left(\frac{4D_3}{r_0^2 C} \right) + \frac{2k_3}{k_2} \ln \frac{r_0}{r_1} + \frac{k_3}{2k_1} \quad (2.20)$$

$$B = \frac{1}{2k_3} \left[r_1^2 \left(\frac{k_2}{D_2} - \frac{k_1}{D_1} \right) + r_0^2 \left(\frac{k_3}{D_3} - \frac{k_2}{D_2} \right) \right] \quad (2.21)$$

$$\begin{aligned}
 C &= \frac{r_1^2}{8} \left[\left(\frac{k_3 - k_2}{k_1} \right) \left(\frac{1}{D_1} - \frac{1}{D_2} \right) + \frac{4}{D_2} - \frac{2}{D_1} \right] \\
 &\quad + \frac{r_0^2}{2} \left(\frac{1}{D_3} - \frac{1}{D_2} \right) + \frac{r_1^2}{k_2} \left(\frac{k_2}{D_2} - \frac{k_1}{D_1} \right) \ln \left(\frac{r_0}{r_1} \right) \\
 &\quad + \frac{1}{2k_3} \left[r_1^2 \left(\frac{k_2}{D_2} - \frac{k_1}{D_1} \right) + r_0^2 \left(\frac{k_3}{D_3} - \frac{k_2}{D_2} \right) \right] \ln \frac{4D_3}{r_0^2 C} \quad (2.22)
 \end{aligned}$$

Chapter 2: State of the Art

If the term $\frac{1}{t}(B \cdot \ln t + C)$ in equation (2.19) is small enough than the term $\ln t + A$, which is the case for a wire diameter in microscale, there exist a linear relationship between ΔT_1 and $\ln t$. The constant term A just shifts the ΔT_1 against $\ln t$ relationship without changing the slope from which thermal conductivity k_3 is calculated. Therefore, the thermal conductivity of a fluid is given by equation (2.23).

$$k_3 = \frac{q}{4 \cdot \pi \cdot \left(\frac{d \Delta T_1}{d \ln t} \right)} \quad (2.23)$$

Where k_3 is the thermal conductivity of the liquid in $\text{W} \cdot \text{m}^{-1} \cdot \text{K}^{-1}$, ΔT_1 is the temperature difference between the local temperature in the coated wire at any time and the initial temperature of the medium, q is the heat generation per unit of length of the wire in $\text{W} \cdot \text{m}^{-1}$, t is time in seconds.

Another effect that we should take into account is the finite length of the wire. It is no possible to predict the error due to the finite length of the wire analytically [28]. The short and long wire method is typically used to avoid the extreme errors, but due the technically difficulty in the design of the cell to work at high pressure and temperature this error is determined experimentally. A calibration constant (c) related to the length of the wire and the coated effect is determined with measurements on pure water with well-known thermal conductivity values and validated with water-lithium nitrate as an electrolyte solution. A detailed analysis explaining this point is described in the calibration section 3.5. Then, the thermal conductivity of the surrounding liquid is determined by the following equation (2.24).

$$k = c \cdot \frac{q}{4 \cdot \pi \cdot \left(\frac{d \Delta T}{d \ln t} \right)} \quad (2.24)$$

2.2 Literature Review of Working Fluids

This section presents a review of thermal conductivity in comercial working fluids ($\text{H}_2\text{O} + \text{LiBr}$ and $\text{NH}_3 + \text{H}_2\text{O}$), as well as in the new potential mixture ($\text{NH}_3 + \text{LiNO}_3$) for absorption cycles activated by solar energy. Also, an analysis of H_2O and CNTs influences in the last binary mixture is presented.

The review is based on previous studies and available data of thermal conductivity in the literature for each mixture.

2.2.1 $\text{H}_2\text{O} + \text{LiBr}$ Binary Mixture

The application of $\text{H}_2\text{O} + \text{LiBr}$ as working pair has been used in absorption cycles since 1950s. Is the most widely used mixture in air conditioning systems. The disadvantages of this working fluid include the limited operation range of these cycles, due to the water freezing point in the evaporator and crystallization problems of the salt at high temperatures in the absorber. These systems operate under high vacuum pressures and consequently vacuum pumps are necessary to maintain the vacuum inside the equipment and to eliminate unwanted gases. Also the lithium bromide solution is corrosive to some metals used for construction of absorption equipment. Despite of these drawbacks the systems have good performance, volatility ratio, affinity, stability, latent heat and the mixture is no toxic and no dangerous for the environment. Moreover, there are different methods to overcome the drawbacks of this mixture listed before. For example, the addition of lithium iodide (LiI) to improve the solubility of the salt and reduce the crystallization risks [50], [51]. Also, it is possible to reduce the corrosive effect with the addition of lithium nitrate (LiNO_3) [52].

The design of refrigeration and heat pump systems which use aqueous lithium bromide solutions requires accurate thermal conductivity data. Most literature data, however, are

Chapter 2: State of the Art

limited to low temperatures and limited range of lithium bromide concentrations. Riedel in 1951 [17] measured the mixture with 40 wt. % of LiBr at 293 K. In 1963 Uemura and Hasaba [18] reported the data from 26 to 60 wt. % of LiBr between 293 K and 353 K. Alloush *et al.* [19] in 1982 measured between 41 to 54 wt. % and the temperature range from 297 K to 357 K. Kawamata *et al.* [20] in 1988 shows the results from 30 to 57 wt. % of LiBr and from 302 K to 373.5 K of temperature. However was in 1990 when DiGuilio *et al.* [21] measured in the range of 30 to 65 wt. % of LiBr and temperatures between 293 K and 463 K. Figure 2.7 shows a direct comparison between literature data in order to demonstrate the agreement among authors. Results with comparable concentrations and temperatures have very similar values of thermal conductivity following the same trend, where thermal conductivity increases slightly first with temperature and then decreases at higher temperatures. The data plotted in Figure 2.7 also show how thermal conductivity decreases with concentration of LiBr.

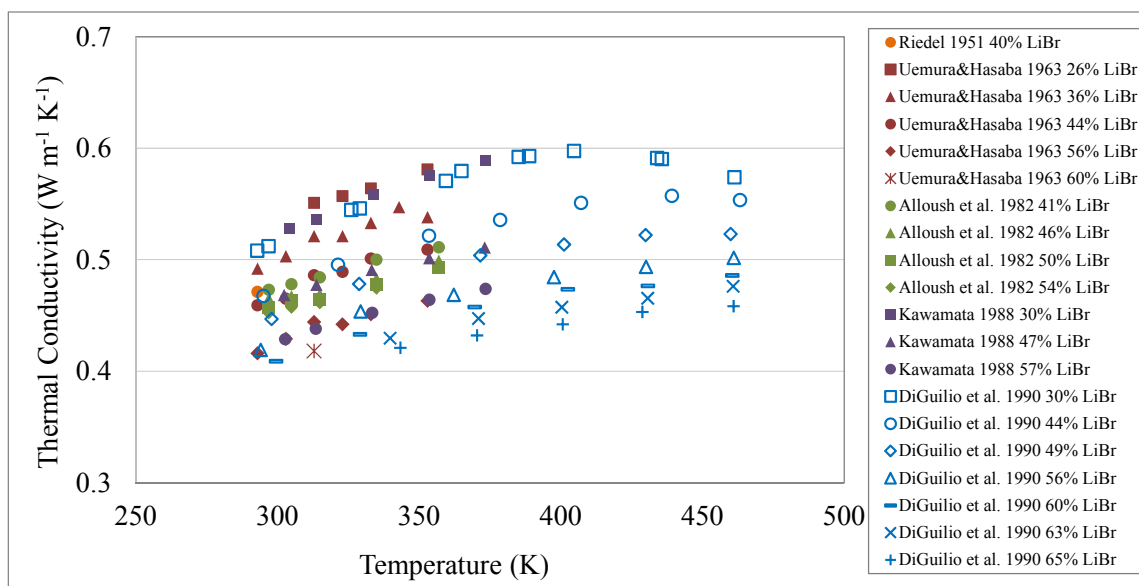


Figure 2.7: Comparison between literature data for H₂O + LiBr mixtures

Also, the data of DiGuilio *et al.*, [21] were correlated as a function of temperature and weight percent lithium bromide with an average deviation of 0.6 % [21]. Then, all the data range is covered in order to appropriately evaluate and design these cycles.

2.2.2 NH₃ + H₂O Binary Mixture

Absorption cycles working with NH₃ + H₂O mixtures have been in use since the 18th century. They are often used to cover the thermal demands in the temperature range below 0 °C where H₂O + LiBr units are not operational. Also, to decrease environmental impact, natural working fluids such as NH₃ + H₂O have been considered as alternative refrigerants to replace chlorofluorocarbons (CFC) in some refrigeration applications since this mixture does not affect the atmospheric ozone layer nor does it contribute to the greenhouse effect.

Although this mixture has been used in absorption machines and others industrial processes since long time, it is essential have knowledge of NH₃ + H₂O thermal conductivity in function of its composition and temperature; unfortunately few experimental data are available in the literature. Furthermore, most of the data are very old and is therefore not considered useful for comparison with new data since electronics as well as creating high-purity components and mixtures was much more difficult. However, in order to make clear the paucity of the data available in the literature and to understand its discrepancies, it was decided to compare all of the available data. The primary reasons for the scarcity of data are experimental difficulties related to the fact that this system is corrosive, toxic, potentially flammable, and has a high vapour pressure. The currently available data are at atmospheric pressure and cover only very limited temperature and concentration ranges. Thus, most of the data reported were measured at near ambient temperatures and with ammonia mass fractions below 30 %. For example, Lees in 1898 [53] measured the thermal conductivity of this system at 293.15 K and ammonia concentration of 15 - 30 wt. %, whereas Braune (1937) [54] reached 302.15 K but with only 8 wt. % of ammonia, and also measured at 293.15 K and with ammonia concentrations of 5 - 10 wt. %. Riedel (1951) [17] reported the data from Lees (1898) [53] and Braune (1937) [54] together. Chernen'kaya *et al.* (1972) [55] measured thermal conductivities at 298.15 K and ammonia concentrations between 4 - 26 wt. %, and also at 323.15 K with 7 - 15 wt. % of ammonia. The most extensive data were reported by Baranov (1997) [56], who covered ammonia concentrations in the range of 20 to 100 wt. %,

Chapter 2: State of the Art

at temperatures between 303.15 K and 375.15 K, but these data are presented graphically and were never published.

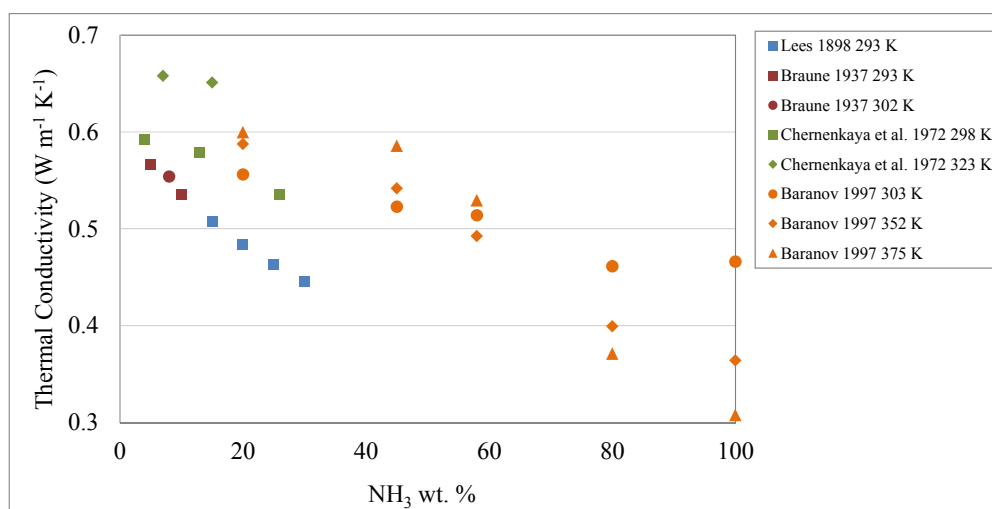


Figure 2.8: Comparison between literature data for NH₃ + H₂O mixtures

Literature data are plotted together in Figure 2.8 showing remarkable inconsistencies and the scanty available data. The data of Lees [53] and Braune [54] seems to yield each other but the measurement range of temperature and concentration are very limited. Unfortunately, the data of Baranov (1997) [56] and Chernenkaya *et al.* (1972) [55] do not agree with each other or with the rest of the published data. It is difficult to provide reasons for these discrepancies since the authors did not give enough information about their techniques, methodologies, purity of the mixtures, etc. It is known that some of the authors [55], [56] used different techniques than the hot wire method. These discrepancies have been also noted by Conde (2006) [57], who attempted to correlate the thermophysical properties of NH₃ + H₂O mixtures using the equations proposed by Filippov (1955) [58] and Jamieson *et al.* (1975) [59]. The author found that neither of these equations was able to precisely fit all the published data.

Therefore, accurate thermal conductivity data are essential and needed to the development of a reference correlation equation in order to cover all the temperature and concentration range. Then, an objective behind this study is the measurement of NH₃ + H₂O mixtures in a wide range of concentrations and temperatures.

2.2.3 NH₃ + LiNO₃ Binary Mixture

As was mentioned before, NH₃ + LiNO₃ is a promising mixture for solar activated refrigeration systems. The performance against various generator, evaporator, absorber and condenser temperatures is better than that for NH₃ + H₂O cycles, not only because of higher COP values, but also because no rectifiers are needed [16], [60].

Regarding the major advantages provided by these systems over the conventional working fluids include (a) lower generator temperatures, which allow operation with simple flat-plate solar collectors, (b) lower evaporation temperatures in comparison with the H₂O + LiBr system, and (c) higher coefficient of performance in comparison with the NH₃ + H₂O system. Nevertheless, the heat and mass transfer in the absorber are limited by the poor transport properties of the salt solution. To overcome this drawback some authors proposed the addition of H₂O or CNTs to the binary mixture (For more detail see section 2.2.4 and 2.2.5).

In order to appropriately design and evaluate the efficiency of absorption refrigeration cycles, the thermodynamic and transport properties of this mixture must be known. In previous works, Libotean *et al.*, in 2007 and 2008 [11], [12] presented the vapor-liquid equilibrium, density, viscosity and heat capacity of the binary mixture NH₃ + LiNO₃ at temperatures between (293.15 and 353.15) K and a fixed pressure of 1.8 MPa. Unfortunately, for the thermal conductivity the only previous available data in the literature is the correlation presented by Ferreria in 1984 [8], based in the data of Blytas and Daniels 1962 [61] reporting thermal conductivity values for solutions of NaSCN in ammonia and using the method proposed by Kok [62] to predict the thermal conductivity of the NH₃ + LiNO₃ system, resulting in the following equation (2.25).

$$k = 2.093 + 0.47E-8 \cdot T + (-1.5478 - 0.7612E-3 \cdot T - 0.15353E-4 \cdot T^2) \cdot w \quad (2.25)$$

Where T is in °C and w is the ammonia mass fraction.

Chapter 2: State of the Art

However, the obtained values using equation (2.25) are extremely higher than thermal conductivity values expected for liquids. Figure 2.9 shows an example of the obtained data using the correlation (2.25) for the mixture $\text{NH}_3 + \text{LiNO}_3$ between 303.15 and 353.15 K and from 30 to 60 NH_3 wt. %.

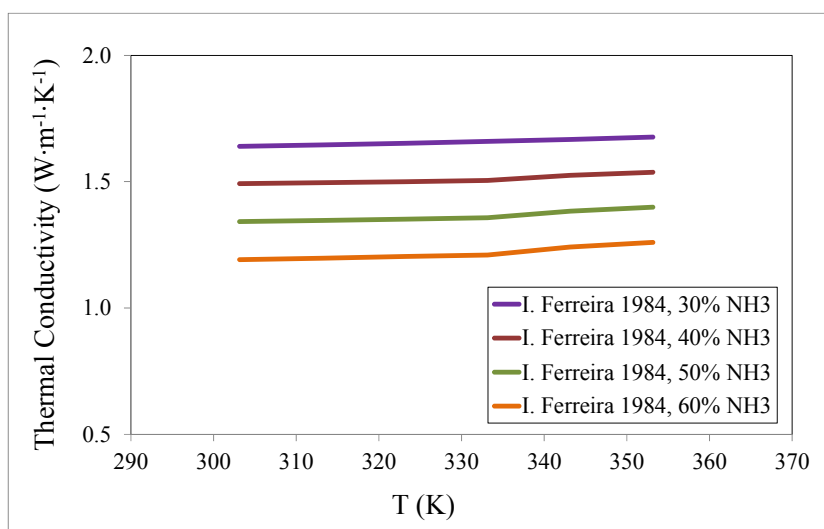


Figure 2.9: Calculated data proposed by Ferreira (1984) for $\text{NH}_3 + \text{LiNO}_3$ mixtures

It is difficult to provide reasons for these discrepancies since the author did not measure experimentally and there is no information about techniques, methodologies, purity of the mixtures, etc. Therefore, one of the main motivations behind this work is the absence of experimental data in the literature.

2.2.4 $\text{NH}_3 + \text{LiNO}_3 + \text{H}_2\text{O}$ Ternary Mixture

One of the main objectives in this work is the thermal conductivity enhancement of the binary mixture $\text{NH}_3 + \text{LiNO}_3$ getting an effective alternative working fluid. Regarding to the main disadvantage in the binary mixture, the addition of a third component with high affinity for ammonia, such as water, not only would improve the mixture solubility and decrease the viscosity; it would also enhance the thermal conductivity of the mixture. But, the idea of

using water as a method for augmenting heat and mass transfer processes is not a recent discovery. Ehmke *et al.* and Bokelmann [26], [27] proposed the addition of water to the binary mixture to be used in absorption heat pumps. Later, Reiner and Zaltash [63] proposed using the ternary mixture for solar-GAX systems as an alternative to the $\text{NH}_3 + \text{H}_2\text{O}$ systems. Furthermore, the effect of water on the solubility and viscosity of the ternary mixtures was studied and an optimal water mass fraction between 0.20 and 0.25 in the absorbent mixture ($\text{LiNO}_3 + \text{H}_2\text{O}$) was suggested [64]. Bokelmann [27] carried out experimental research concerning the performance of an absorption heat pump with the ternary mixture and results were reported [65]. Another significant improvement in the coefficient of performance (COP), comparing the use of the $\text{NH}_3 + \text{H}_2\text{O}$ and $\text{NH}_3 + \text{LiNO}_3 + \text{H}_2\text{O}$ mixtures as working fluids for heat pump applications, was reported [66]. Moreno-Quintanar *et al.* [67] compared the performance of a solar driven intermittent absorption refrigeration system when the working mixture was the binary or the ternary mixture. The results showed that the COP was up to 24 % higher for the ternary mixture. Oronel *et al.* [68] studied heat and mass transfer in a bubble plate absorber with the binary and the ternary mixture. The author found that the mass absorption flux and the solution heat transfer coefficient achieved with the ternary mixture were around 1.3-1.6 and 1.4 times higher, respectively, than those of the binary mixture under similar operating conditions.

Some authors measured thermodynamic and transport properties of this mixture such as, density, viscosity, heat capacity and vapor-liquid equilibrium [64], [9], [63], [11], [12]. But, no data of thermal conductivity was found in literature for the $\text{NH}_3 + \text{LiNO}_3 + \text{H}_2\text{O}$ mixture. Then, other objective of this work is to complete these transport properties by measuring the thermal conductivity and analyze the influence of the water addition.

2.2.5 $\text{NH}_3 + \text{LiNO}_3 + \text{CNTs}$ Ternary Mixture

In the past few years numerous investigations have been carried out seeking to develop novel methods for enhancing the thermal performance of heat transfer fluids. It seems that nanofluids, which are a fluid with nanoparticles below 100 nm in diameter suspended evenly

Chapter 2: State of the Art

and stable [24], have a huge potential of application to improve heat transfer. One of the methods to achieve this objective is to create mixtures by adding solid particles into the fluid. Since solid materials have thermal conductivities much higher than fluids, such an attempt obviously results in a thermal conductivity enhancement.

In the last decade, a significant amount of experimental and theoretical research was made to investigate the thermophysical behaviour of nanofluids. The discussion will begin with a review of existing work in the field of nanoparticle or carbon nanotubes for experimental studies on thermal conductivity enhancement. Choi, 1995 [24] reported that the enhancement of the thermal conductivity of water reached up to 40 % by adding low volume fraction, around 5 %, of nanoparticles and nanotubes. Eastman *et al.*, 2001 [69] found that the enhancement of the thermal conductivity for ethylene glycol based fluid increased up to 40 % with the addition of 0.3 % (v/v) Cu nanoparticles. Xie *et al.*, 2003 [70] reported the enhancement of thermal conductivity in water and ethylene glycol with the addition of multiwalled nanotubes (MWNT) without the need of surfactant and by using an oxidation treatment with concentrated nitric acid. Keblinski *et al.*, 2005 [71] informed that nanofluids containing only a small amount of nanoparticles, especially with carbon nanotubes (CNTs), its thermal conductivity can increase 38 % at 0.6 % (v/v). Hwang *et al.*, 2006 [72] investigated the thermal conductivity enhancement of MWNT, CuO and SiO₂ in water and CuO in ethylene glycol and reported that enhancement depends on thermal conductivity of both nanoparticles and fluids. Li and Peterson, 2006 [73] measured the thermal conductivity of CuO and Al₂O₃ nanoparticles with distilled water. The results indicate that the nanoparticles have a significant impact on the effective thermal conductivity, and 6 vol.% of CuO increase the effective thermal conductivity 1.52 times that of pure distilled water. And 10 vol.% of Al₂O₃ increased the effective thermal conductivity by a factor of 1.3. Pang *et al.*, 2013 [74] added Al₂O₃ nanoparticles in methanol and the highest obtained thermal conductivity enhancement was 6.34 % for 40 vol.% of methanol and 0.1 vol.% of Al₂O₃.

Nowadays, studies applying small quantities of CNTs or nanoparticles in the absorption working fluids to improve the thermal conductivity and consequently the absorber performance of absorption cycles have been carried out actively. Some authors have experimentally studied the increased thermal conductivity of this binary nanofluid respect to

the base fluid. Kim *et al.*, 2006 [75] defined the concept of binary nanofluid as the binary mixture in which nanoparticles are evenly distributed. Regarding to intensification of the absorption process with the addition of CNTs or nanoparticles in the working mixture to increase thermal conductivity, some studies are available in the literature. Xuehu *et al.*, 2007 [76] found that thermal conductivity of the $\text{NH}_3 + \text{H}_2\text{O}$ solution is 16 % higher with the addition of CNTs. And Jung *et al.*, 2011 [77] said that the thermal conductivity of the binary nanofluids ($\text{H}_2\text{O} + \text{LiBr}$ with Al_2O_3 nanoparticles) increases with the particle volume concentration and enhances by 2.2 % at 0.1 % (v/v). Even though many studies have been found the enhancement of thermal conductivity in the base fluid by the addition of CNTs or nanoparticles, the experimental results show that thermal conductivity enhancements in working fluids for absorption cycles are significantly smaller. No previous studies have been found in the literature for the binary nanofluid $\text{NH}_3 + \text{LiNO}_3 + \text{CNTs}$, consequently this is other target mixture behind this work.

In conclusion, the measurements in this study will be done by the transient hot wire technique. The mixture $\text{H}_2\text{O} + \text{LiBr}$ will be measured and compared with the correlation proposed by DiGiulio [21]. Due to the scarcity data available in the literature the $\text{NH}_3 + \text{H}_2\text{O}$ mixture will be also measured at different temperatures and compositions, and the data will be correlated in order to provide more data in a wide range of temperatures and composition. The new mixture $\text{NH}_3 + \text{LiNO}_3$ will be measured and a correlation will be developed since there are no experimental data available in the literature. Finally the thermal conductivity of the ternary mixtures $\text{NH}_3 + \text{LiNO}_3 + \text{H}_2\text{O}$ and $\text{NH}_3 + \text{LiNO}_3 + \text{CNTs}$ will be experimentally determined and the influence of this addition at different concentrations and temperatures will be studied.

Chapter 3

3. Experimental Setup

After the theoretical principle and the mathematical model have been presented, in this section the two experimental approaches used in this work are described. Also, the data acquisition system as well as the requirements in the sample preparation and the experimental procedure is discussed here.

3.1 Experimental Apparatus

The experimental setup described here has been designed based on the transient hot wire method in order to measure the thermal conductivity of electrically conducting liquids in gas state at normal conditions of temperature and pressure. Although the concrete design is addressed to measurements on working fluids and nanofluids, the system settings can be flexible adapted to measure any other fluids.

Two different approaches were used for thermal conductivity measurements: The first one is the common method using the platinum wire, and the other device is a variant of the classical method, using a single glass capillary filled with mercury as an isolated hot wire. Details in the parameters design are discussed later.

Chapter 3: Experimental Setup

3.1.1 Coated Platinum Wire Device

Figure 3.1 shows a schematic of the transient hot wire apparatus designed and built in this work together with pictures of the experimental system. The apparatus consists of a stainless-steel vessel (A) with an internal volume of 80 cm^3 that is filled with the liquid whose thermal conductivity is to be measured. A platinum wire coated with a Teflon layer (B) is placed along the axis of the cell, and fixed to two brass rods (C) that pass through the vessel tap (D) over two electrically isolated gaskets (E). There are two connections to fill the cell and to pressurize the system (F).

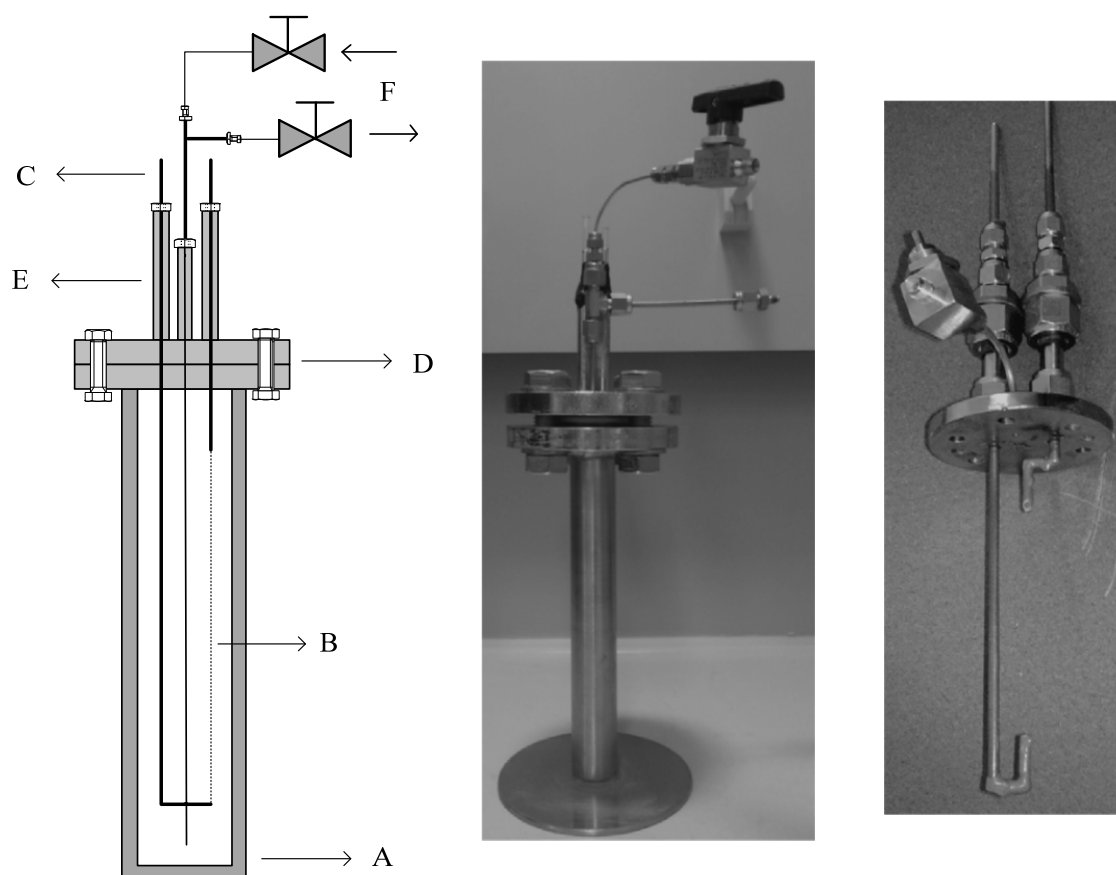


Figure 3.1: Transient hot-wire apparatus. (A) stainless-steel vessel, (B) coated wire, (C) brass rods, (D) vessel tap, (E) gaskets, (F) connection

Some of the important design parameters that were considered include:

- **Wire material.** Platinum was chosen because of its high electrical resistivity ($10.58 \mu\Omega\cdot\text{cm}$ at 293.15 K) combined with its high temperature coefficient of resistance (0.00392 K^{-1} from 273.15 K to 373.15 K) [78]. Platinum also exhibits linear variation of resistance over a large temperature range, which makes it an ideal material for temperature measurement.
- **Wire diameter.** $25 \mu\text{m}$ was chosen to ensure high resistance to current flow without sacrificing tensile strength.
- **Insulating material.** Teflon was chosen as the wire coating because it is highly resistant to stress-cracking at the working temperature, chemical reaction, and corrosion. The insulation thickness was $1 \mu\text{m}$ and care was taken to avoid any disruption of the coating during the apparatus construction. Also, the brass rods were coated with a ceramic compound (epoxy) for electrical insulation (Loctite Nordbak 7234).
- **Wire length.** $10\text{-}12 \text{ cm}$ was chosen in order to provide a large length to diameter ratio. The wire may therefore be considered to be of infinite length [79].

The cell is designed to work at pressures up to 2 MPa and temperatures up to 423.15 K . The cell also allows easy filling and removal of the liquid in the vessel which includes, for this purpose, two specific valves. Figure 3.2 shows a schematic of the experimental setup, including the pressure line and the data acquisition system. In order to avoid pressure fluctuations, a 1 liter expansion vessel (A) was installed in a line connecting the cell to a high pressure nitrogen cylinder. Nitrogen from the cylinder was used to introduce the sample into the cell and keep it in the liquid state. Additionally, 1 meter of small-diameter coiled tube (B) was used to connect the expanding volume with the sample cell, thus minimizing diffusion of N_2 into the cell. Therefore, no nitrogen was allowed to enter the cell. The cell was immersed in a bath filled with water (C), whose temperature was

Chapter 3: Experimental Setup

controlled by a thermostat (Selecta Digitem 100) and measured with a precision thermometer (Automatic System Laboratories F205 MKII using a PT100 probe). The data acquisition system (D) consisted of a current source (Keithley 6221), and a nanovoltmeter (Keithley 2182A) connected to a computer (E) that was used to control the two instruments. An Agilent VEE dataflow program specifically written for this application was used to control both instruments and for data logging.

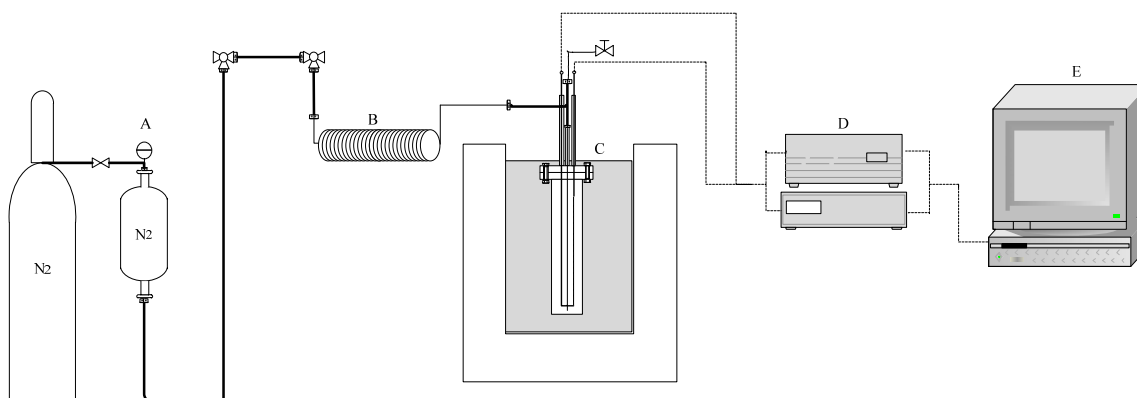


Figure 3.2: Schematic of the experimental setup. (A) 1 liter expansion vessel, (B) coiled tubing, (C) thermostatic bath, (D) data acquisition system, (E) computer

More in detail the platinum wire with 25 μm of diameter (A-M Systems, Inc.) was fixed with silver thermoplastic resin (Electrodag 1415M) at both ends of the brass rods. This resin has very high conductivity and maintains its low electrical resistance even after exposure to heat, cold, humidity and salt. Before, the Teflon layer in the wire extremes was removed by heat in order to allow electrical contact. The supporting leads are two brass rods to keep the wire straight and taut and to connect it to the electrical system, also allow

to keep the wire inside the cell in a vertical position and concentric in order to approximate the system to the ideal model. These rods were electrically insulated after the assembly. The length of the wire was 10.400 ± 0.034 cm as determined with a vernier calliper. The resistance of the wire for this diameter and length was on the order of 25Ω at room temperature.

Additional complexity with the insulated wire assembly is the use of a weight welded at the bottom of the wire, in order to minimize bending effect and ensuring that the wire returns to its initial state after suffering a change temperature.



Figure 3.3: Welded weight

Was in 1971 when McLaughlin and Pittman [80] proposed, probably for first time, the use of a weight attached at the bottom of the wire. Other authors follow this interesting application to allow the wire for thermal expansion over the range of operating temperatures [81]. Nowadays news instruments still using a weight keeping the wire under constant tension [82]. However, in previous assemblies we have tried to work with this weight welded at the bottom, but it was really difficult provide a good insulation and a good electrical contact in this moving part (See Figure 3.3).

In order to corroborate how the weight affects the thermal expansion of the wire in our operating range temperatures some previous experimental studies have been done. Results show that the limit maximum work temperature working without that weight is 323.15 K. After this temperature, the wire does not return to the initial state and the obtained values of thermal conductivities are higher. Figure 3.4 shows different measurements of thermal conductivity in water at 303 K obtained in different days. Every day the thermal

Chapter 3: Experimental Setup

conductivity of water was measured at 303 K and the sample was set at different temperatures. First day, the temperature was set at 303 K. Second day, the measurements were made at 303 K and after the equipment was set at 313 K. Third day, the measurements were made again at 303 K and the equipment was set at 323 K. Fourth day, measurements were repeated at 303 K and results show how thermal conductivity is remarkably higher than those for the first 3 days before the temperature rise at 323 K. Next two days measurements at 303 K were doing in order to study a possible recovery in thermal expansion. In conclusion, the limit temperature for our platinum wire device, to ensure repeatability in the measurements, is 323 K and after this temperature the wire does not return to the initial state.

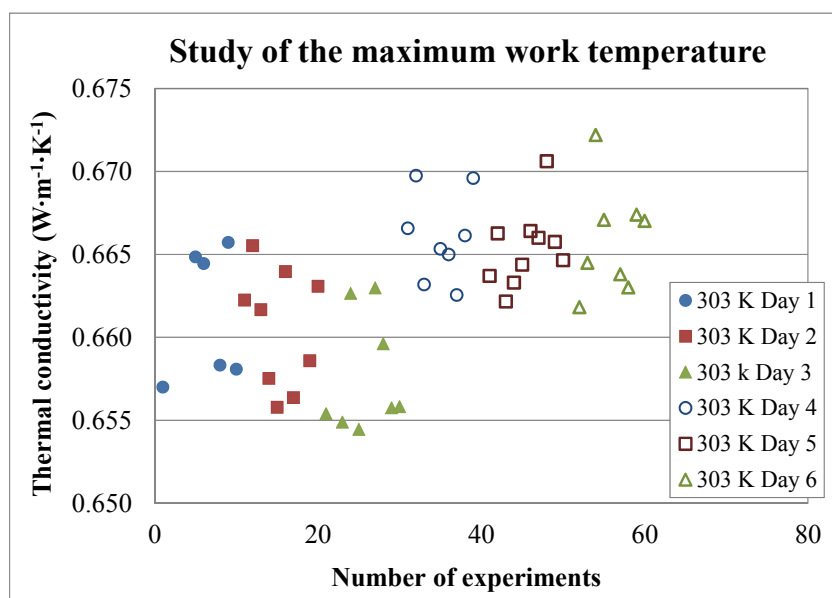


Figure 3.4: Study of the maximum work temperature without a welded weight

3.1.2 Glass Capillary Device Filled with Mercury

It was mentioned before the necessity of using an insulated wire in order to measure electrically conducting fluids with the transient hot wire technique (See section 2.1.2). Nevertheless, some authors demonstrated that the use of an insulated layer has temperature limitations. For example, in the use of a platinum wire with polyester layer, the coating

decomposed at temperatures above 423 K [28]. Another technique was the use of a tantalum wire anodized to have an oxide layer [19], in this case, the temperature limitation were found at 373 K, were the oxide layer cracked due to differences in thermal expansion between the oxide layer and the tantalum wire [20], [84]. Therefore, each coating technique has to be adapted to the wire and liquid types, and to the working temperature and pressure conditions.

In this work, the second device is based in the liquid metal probe concept pioneered by Hoshi, Omotani and Nagashima in 1981 [83], and was adapted for use with ammonia, salt solutions and nanofluids working at high temperature and pressure. Some drawbacks with the isolated platinum wire, working without a welded weight, are the temperature limitation at 323 K (See Figure 3.4). Also, the use of brass rods coated by a ceramic compound, this epoxy has a limited duration and after some experiments using ammonia the ceramic coating decomposes resulting in current leaks. Moreover, the calibration constant (c) could change after some experiments, due to coated degradation, and it is difficult to provide an accurate value of this variable. Therefore, our goal was to build an apparatus allowing measurements on electrically conducting liquids without current leaks, working at temperatures above 323 K without bending effects, and being more readily fabricated than a platinum wire coated by Teflon with a welded weight at the bottom. Additionally, the samples are in gas state at normal conditions of temperature and pressure. So, the entire equipment has to work under pressure ensuring liquid mixtures and no leaks during all the experiment. Then, in this study we also have chosen to use a relative transient hot wire apparatus with a mercury-filled glass capillary [84], [46] adapted for use with ammonia, salt solutions and nanofluids working at high temperature and pressure.

The apparatus and the experimental setup is the same as described before in section 3.1.1 with the exception of using a single glass capillary filled with mercury acting as the platinum wire. Figure 3.5 shows a schematic of the liquid metal transient hot wire apparatus designed and built in this work together with pictures of the experimental system. The apparatus consists of a stainless-steel vessel (A) with an internal volume of 80 cm³ which held the liquid to be measured. A glass capillary filled with mercury (B) is placed along the

Chapter 3: Experimental Setup

axis of the cell, and fixed to two gaskets (C) that pass through the vessel tap (D). There are two connections to fill the cell and to pressurize the system (E).

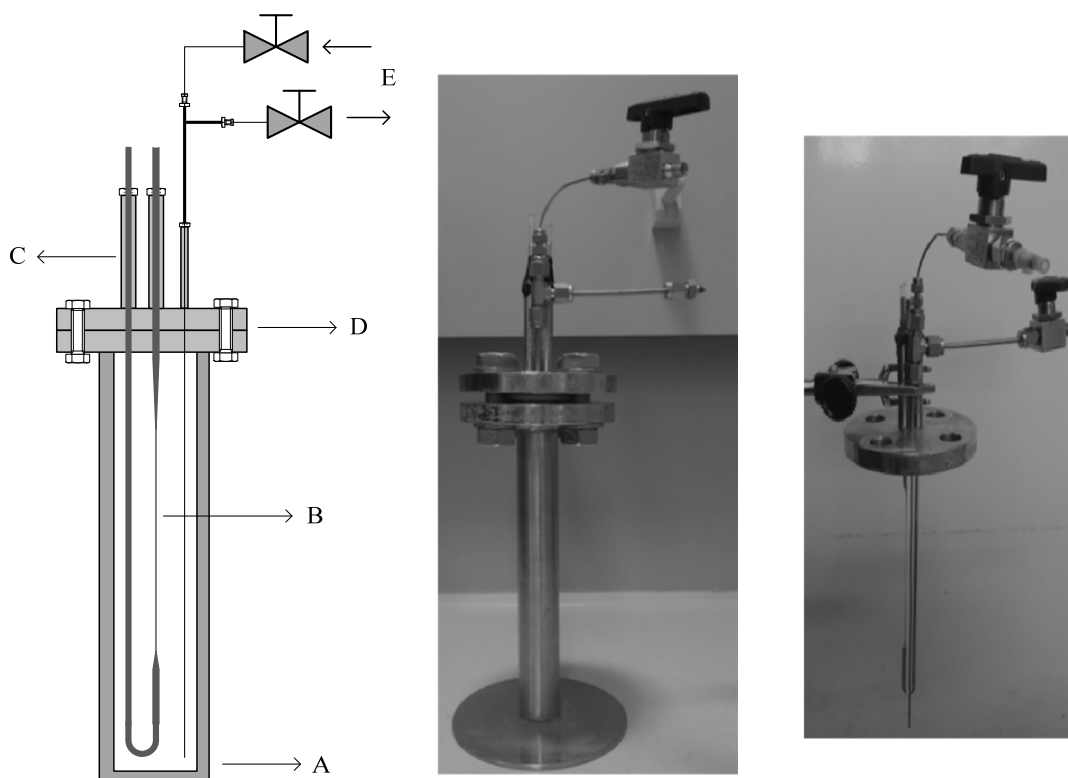


Figure 3.5: Liquid metal transient hot-wire apparatus. (A) stainless-steel vessel, (B) mercury filled glass capillary, (C) gaskets, (D) vessel tap, (E) connections.

The borosilicate glass capillary (Pyrex 7740 type 1) with 4 mm of outer diameter and 2 mm of inner diameter was built by forming a U tube and heating and stretching one leg of the tube to form the capillary. The diameter of the capillary was measured with a microscope (FEI QUANTA 600) resulting a nonuniform cross sectional area. The average outer and inner diameter across the capillary was 231 μm and 160 μm , respectively (See Figure 3.6).

After, the capillary was fixed to the vessel tap with an epoxy encapsulant (STYCAST 2850 FT) and filled with mercury using a vacuum pump. On the outside of the cell, platinum wires (0.3 mm o.d.) were submerged to each mercury leg and connected to the data acquisition system as the electrical contact. The effective length of the capillary (L_{eff}) in this

case, was obtained by calibration with water, and it was validated with toluene, dimethyl phthalate, ethylene glycol and water + lithium nitrate. The obtained average length used in this work was 9.61 ± 0.54 cm. The resistance of the glass capillary for this diameter and length was on the order of 5Ω at room temperature.

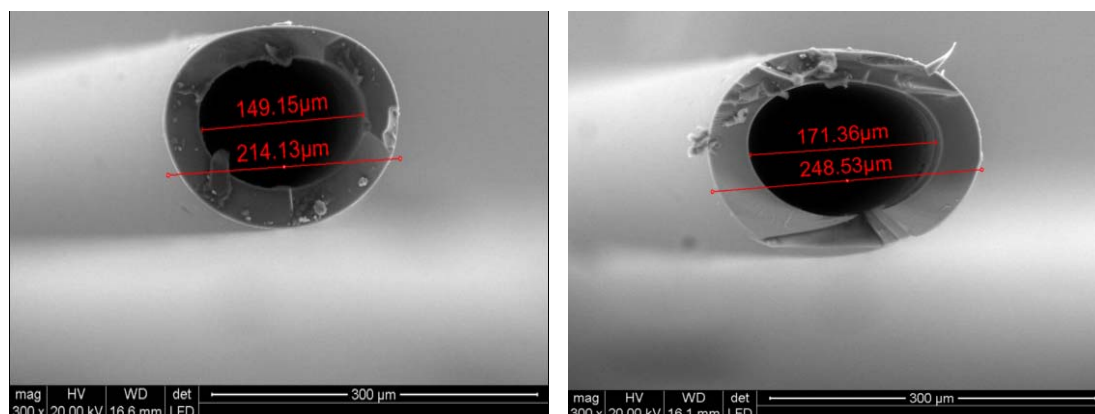


Figure 3.6: Microscope image of glass capillary in two different sections

3.2 Data Acquisition System

Although the principle of the method is apparently simple, its experimental implementation requires suitable automated control and data acquisition system, because of the short experimental times and large amounts of data involved in the measurement process. Then, one of the limiting factors to the accuracy of the transient hot wire method is the precision in recording the temperature rise of the wire. In this study this difficulty was overcome using a current source and nanovoltmeter with very high precision. The source-meter can supply and measure very precisely the voltage or current. It is extremely important to have a voltage meter with a high degree of sensitivity because the voltage variations of the wire are usually very small ($< \text{mV}$). Furthermore, the instrumentation allows the resistance to be directly measured without the need of a Wheatstone bridge circuit [85].

Chapter 3: Experimental Setup

The data acquisition system is composed by a current source (Keithley 6221) and a nanovoltmeter (Keithley 2182A) for the platinum wire technique. Nevertheless, the intensity limited for this current source is 100 mA, which is enough when the resistance of the wire is in the order of 25 Ω . But, in the case of the mercury-filled glass capillary where the resistance is much lower (5 Ω) it is necessary to apply higher intensity in order to heat the wire and get at least a ΔT between 1 to 3 $^{\circ}\text{C}$. Then, a current source (Keithley 2601A) with a maximum output of 1 A was used in this case. The precision of the current source (Keithley 6221) is 0.1 % of the reading + 50 μA and for (Keithley 2601A) is 0.05 % of the reading + 1.8 mA. In the case of the nanovoltmeter, the resolution is 1 μV and the precision is 25 ppm of reading + 2 ppm of range (See Figure 3.7).

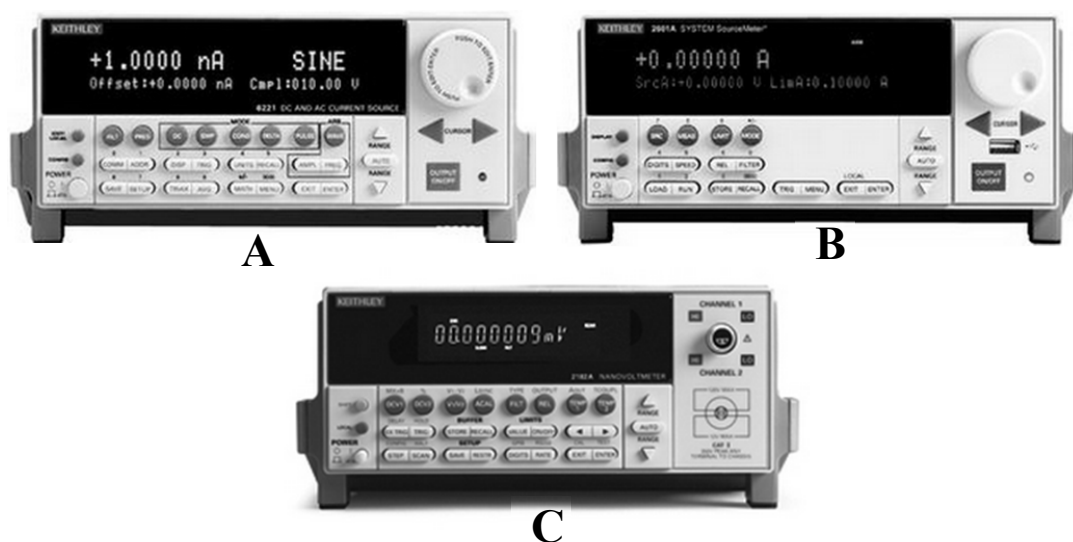


Figure 3.7: Data acquisition system A) current source Keithley 6221 B) current source Keithley 2601A C) nanovoltmeter Keithley 2182A

The current source is connected to the computer via Ethernet port and controlled utilizing an Agilent VEE dataflow program specifically written for this application. The acquired data are transmitted to the computer by means of the serial RS-232, and are stored and processed by Excel data files (See Figure 3.8). The Agilent code routines can be found in Appendix A.

The output current source is sending using a Triax connector in the rear panel. After 6 seconds, the current source is turned off and the collected data are transferred to the Nanovoltmeter using an input cable connected in the front panel. Figure 3.9 shows the wires configuration.

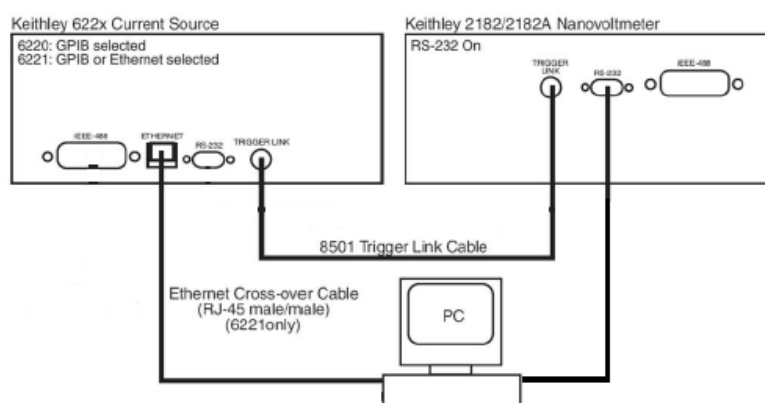


Figure 3.8: System connections for PC control

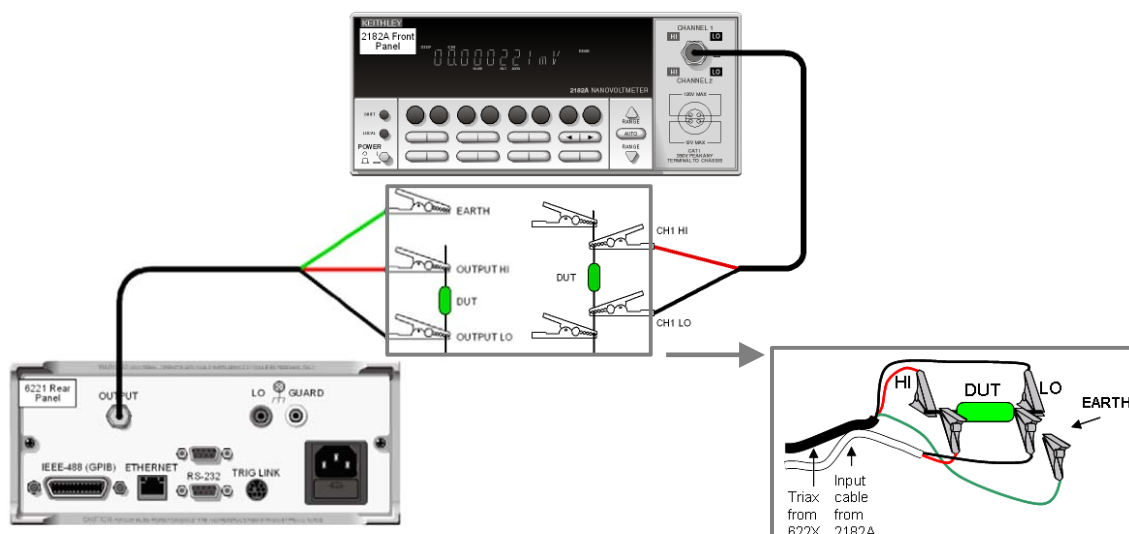


Figure 3.9: Schematic of electrical circuit

Other important factor is the speed of the data acquisition with the nanovoltmeter, it can vary depending on the choice of the integration time NPLC (number of power line cycles). In order to provide the best number of data in the experimental time, the NPLC value is always set at 0.1, which corresponds to an acquisition rate of about 17-20 ms. [85], [86].

Chapter 3: Experimental Setup

3.3 Sample Preparation

The sample preparation and its handling prior to the measurement is a very important step in the analytical technique. Also, sample preservation ensures that the sample retains its physical and chemical characteristics so that the analysis truly represents the object under study.

Most of the pure components in liquid state at room temperature such as water, toluene, dimethyl phthalate, and ethylene glycol, are ready for direct introduction into the measurement cell. Binary solutions such as water + lithium bromide or water + lithium nitrate were prepared gravimetrically based on weight percent. The suspension is dissolved and agitated with magnetic stirrer for few hours. These two types of samples were introduced into the measurement cell by the inlet valve with the help of a syringe. Once the cell has been filled, the sample is released by the outlet valve (See Figure 3.10).

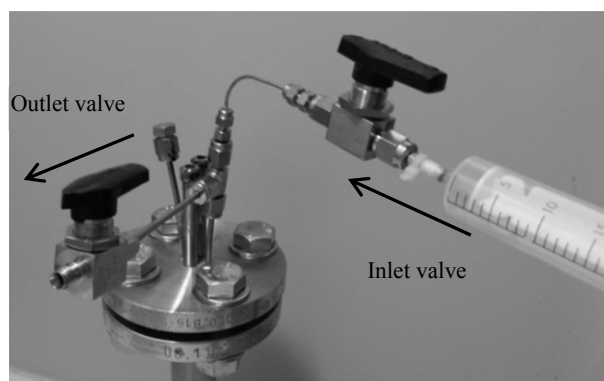
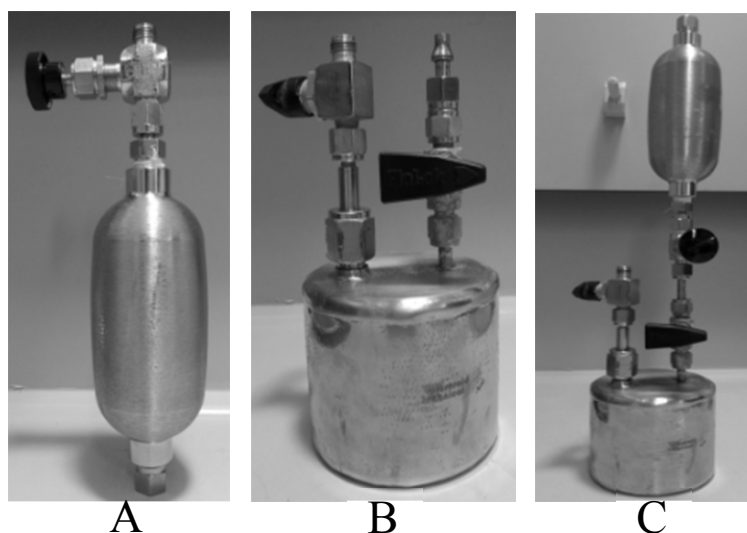


Figure 3.10: Sample introduced by syringe

However, the hardest part is the preparation of those samples which involve the use of ammonia. These mixtures are in gas state under normal conditions of temperature and pressure. Then, both preparation and transporting to the measurement cell should be made under pressure conditions in order to keep it in the liquid state. The sample is prepared gravimetrically based on weight percent for each component. The procedure is as follows:

- First, ammonia is collected in a pressure cylinder with an internal volume of 100 cm³ (See Figure 3.11A). The pressure line is around 0.4 MPa and the cylinder is cooled by liquid nitrogen to help for ammonia transporting. The ammonia cylinder is weighed until get the desired weight.
- After, the other components used for the mixture (H₂O and/or LiNO₃ and/or CNTs) are prepared by weight in the mixing cell with an internal volume of 300 cm³ (See Figure 3.11B).
- Then, ammonia is passed into the mixing cell (See Figure 3.11C). The ammonia cylinder is heated while the mixing cell is cooled in order to ease ammonia transport.



**Figure 3.11: Sample preparation cells. A) ammonia cylinder B) mixing cell
C) ammonia transport setup**

- The ammonia cylinder is weighed before and after the transport; the difference between the two masses gives the mass of ammonia. Also, the mixing cell is weighed before and after, to be sure there are no ammonia leaks.
- Once all the components are in the mixing cell, the solution is agitated with magnetic stirrer for few hours.

Chapter 3: Experimental Setup

- Previous the measurement cell is charged with the sample (See Figure 3.12 C) it is pressurized with nitrogen at the same initial pressure than vessel A in Figure 3.12.
- Finally, Figure 3.12 shows how the dissolved solution (B) is carefully passed under pressure of nitrogen (A) through tubes into the measurement cell (C). In order to check if the cell has been filled, the sample is released by the outlet valve (D)

Once the sample preparation and transport is completed, the measurement is carried out in the measurement cell with the experimental setup shown in Figure 3.2.

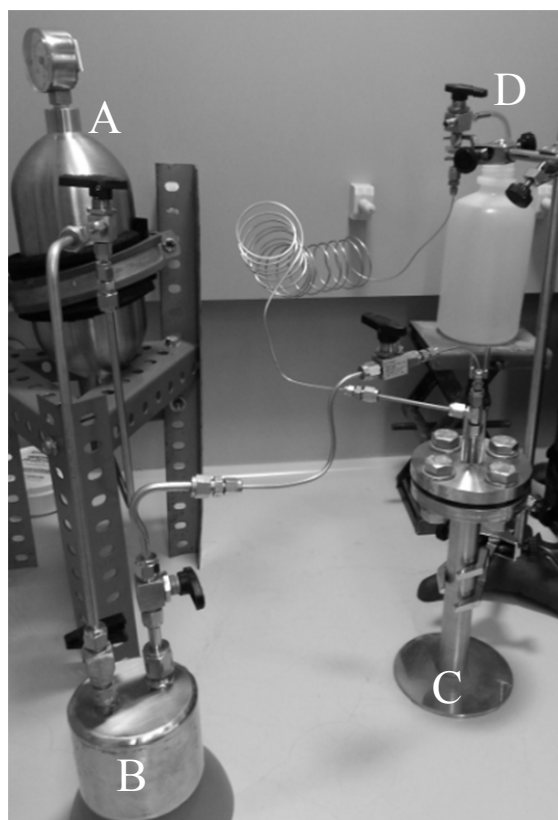


Figure 3.12: Sample transport setup. A) high pressure nitrogen cylinder B) solution C) measuring cell D) collector vessel.

To conclude, Table 3.1 shows the source and purity of the materials used in the measurements.

Table 3.1: Source and purity of materials

Material	Supplier	Purity
Ammonia	Carbueros Metálicos	99.98 %
Dimethyl phthalate	Sigma-Aldrich	99.0 %
Ethylene glycol	Sigma-Aldrich	99.5 %
Lithium bromide	Morton Thiokol Inc	99.0 %
Lithium nitrate	Sigma-Aldrich	98.0 %
Mercury	Sigma-Aldrich	99.9995 %
Multiwalled CNTs	Bayer MaterialScience	95.0 %
Platinum Wire + Teflon	Panreac Quimica	99.999 %
Toluene	Sigma-Aldrich	99.5 %
Millipore water	Millipack 40	< 18.2 MΩ

3.4 Carbon Nanotubes (CNTs)

A quick review about different kinds of nanoparticles used in thermal conductivity enhancement was made in order to choose the best candidate for this application. It seems that metal nanoparticles are not suitable to the $\text{NH}_3 + \text{LiNO}_3$ absorption process due to the ease reaction with ammonia [87]. On the other hand, there is no chemical reaction taking place between CNTs and ammonia [76]. Therefore, CNTs seems to be suitable for being used in NH_3 working fluids. Other advantages are their extraordinary electrical and mechanical properties and high thermal conductivity [88]. Also, the acquisition prices reduction as a result of increasing demand and improvement of synthesis has made the use of CNTs a good candidate for this work.

This section presents a more detailed description about preparation of the binary nanofluid (CNTs + $\text{NH}_3 + \text{LiNO}_3$), including chemical treatment for stable and homogeneous suspension.

Chapter 3: Experimental Setup

Also, some important parameters related to effective thermal conductivity of carbon nanotubes are introduced since their effects will be considered.

All the binary nanofluids samples were prepared by a two-step method, in which the commercially multi-walled carbon nanotubes are first treated by oxidation and then the dry powder is dispersed into the base fluids in a second processing step. In this case, the desired quantity of CNTs is weighed directly in the mixing cell before the ammonia has been introduced (See section 3.3).

In the present contribution, we choose commercially multi-walled carbon nanotubes (MWNTs). Some of the important parameters given by the supplier are presented in Table 3.2 and Figure 3.13 shows a TEM image of MWNTs.

Table 3.2: Specifications of commercial multi wall carbon nanotubes

Property	Value	Unit	Method
Purity	>95	%	Elementary analysis
Number of walls	3 - 15	-	TEM
Outer diameter	20 - 30	nm	TEM
Inner diameter	5 - 10	nm	TEM
Length	10 - 30	μm	SEM
Bulk density	0.28	$\text{g} \cdot \text{cm}^{-3}$	EN ISO 60

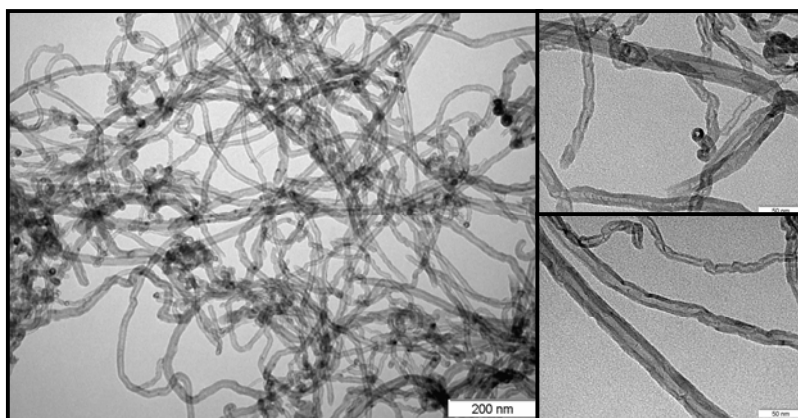


Figure 3.13: TEM image of multi-walled carbon nanotubes.

3.4.1 Chemical Treatment of Carbon Nanotubes and Stability Study

The most desired features in the binary nanofluids are stability, negligible agglomeration and high thermal conductivity. This means nanofluids are not merely liquid-solid mixtures and some special preparation is needed. Before the CNTs were introduced into the base fluid, they were subjected to a chemical treatment to achieve a better dispersion and suspension. We have been able to prepare an uniform dispersion solution and prevented agglomeration modifying the surface properties of CNTs by oxidation on the structural integrity through nitric acid (70 %) and hydrogen peroxide (35 %) and then washed with deionized water until a neutral pH of 7 [89].

Treatment: MWCNTs were dispersed in nitric acid (70 %) in a glass beaker under constant magnetic stirring for 48 h at 343 K. Also, the hydrogen peroxide (35 %) was added dropwise (10 % of the amount of nitric acid) into the glass beaker. After that, the resulting dispersion was diluted in deionized water and filtered. The resulting solid was washed up to neutral pH of 7, and the sample was dried in a furnace at 393 K during 12 hours.

Despite the oxidation treatment, after sample preparation with the binary nanofluid it was observed how CNTs in the base fluid tend to agglomerate to form clusters, which will eventually become unstable and settle out of the solutions. Several special requirements are necessary to carry on experimental measurements in the binary nanofluid, such as homogeneous and uniform suspension, stability and low agglomeration of particles. Thus, some energy is required to break clusters into smaller constituents. In this study, an ultrasonic bath was employed to break nanotubes clusters in the binary nanofluid separating aggregates. This technique involve immersing the binary nanofluid sample in a ultrasonic bath capable of generating ultrasonic pulses of 110 W at 40 kHz (See Figure 3.14). Then, before conducting thermal conductivity measurements, binary nanofluid sample was sonicated in the ultrasonic bath for 1 h. preventing agglomeration and ensuring uniform dispersion of nanotubes.

Chapter 3: Experimental Setup



Figure 3.14: Ultrasonic water bath

Finally, a stable binary nanofluid during approximately 8 h is achieved without the addition of any dispersants. Figure 3.15 shows on the left the binary nanofluid with 0.01 wt.% untreated CNTs in 40 wt.% $\text{NH}_3 + \text{LiNO}_3$ after 1 day at rest, almost all CNTs quickly agglomerate leaving fluid transparent. On the other hand, in the same conditions, treated CNTs on right are well dispersed and suspended in the working fluid.

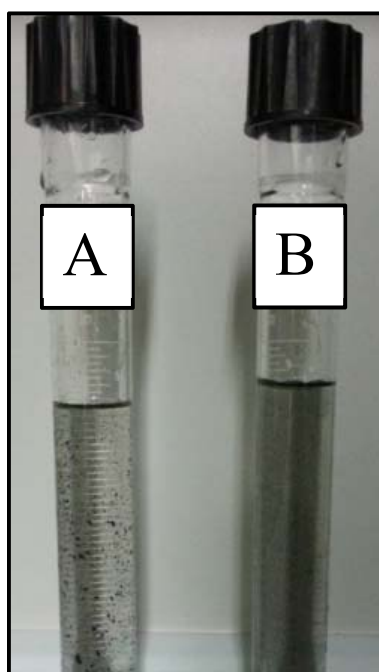


Figure 3.15: Comparison of the visualization of CNTs 0.01 wt.% binary nanofluid without (A) and with (B) oxidation treatment after 1 day.

One of the key parameters to prepare a stable binary nanofluid is the CNTs concentration. In this study, the distribution stability is verified visually from the agglomeration and sedimentation by comparing suspensions with 0.005 wt.%, 0.01 wt.%, 0.02 wt.% and 0.2 wt.% of CNTs in 40 wt.% $\text{NH}_3 + \text{LiNO}_3$, which are typical concentrations used in other studies [90], [91], [92].

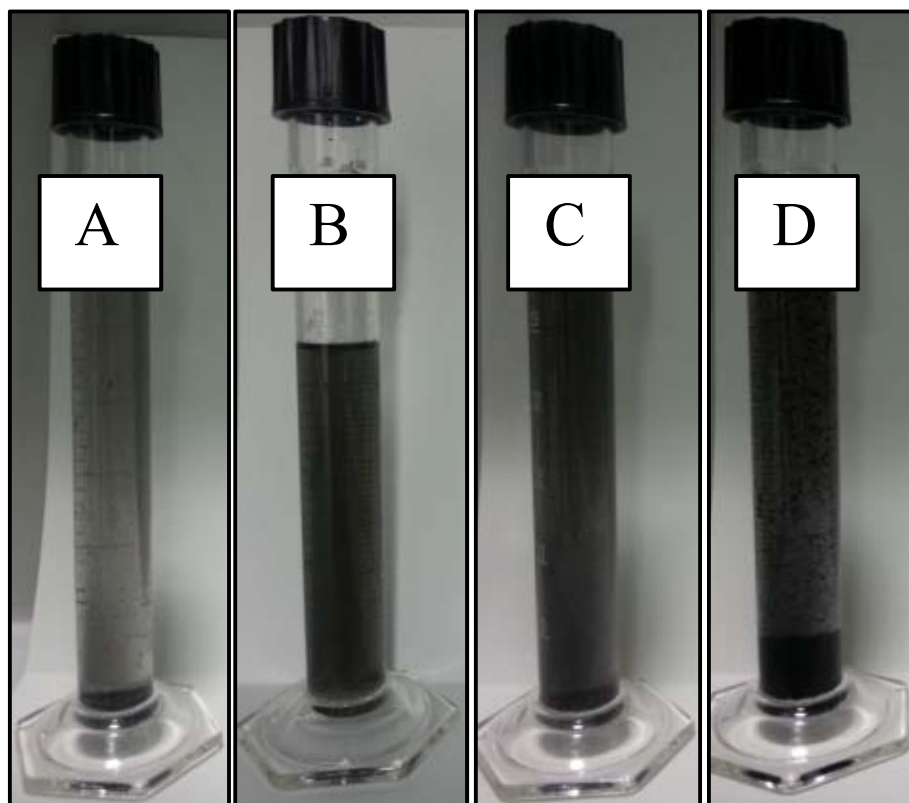


Figure 3.16: Visualization of distribution stability of CNTs suspension in $\text{NH}_3 + \text{LiNO}_3$ mixture (A) 0.005 wt.% (B) 0.01 wt.% (C) 0.02 wt.% and (D) 0.2 wt.%.

The prepared solutions were left to stand for a few hours before visual inspection (See Figure 3.16). Stable and homogeneous dispersions could be seen in Figure 3.16 up to the 0.02 wt.% CNTs concentration, but distribution stability decrease in concentration of 0.2 wt.% showing agglomeration and considerable precipitation of particles at the bottom. Therefore it can be said, in terms of good distribution stability, that the concentrations of 0.005 wt.%, 0.01 wt.%, 0.02 wt.% of CNTs are equally good for our purpose.

3.5 Calibration Procedure

A series of calibrations were performed in this work. First, in order to check the assembly, the temperature coefficient of resistance (α) of each platinum wire and each glass capillary filled with mercury was determined from measurements of its resistance as a function of temperature by using the relation given in equation (3.1).

$$R = R_0(1 + \alpha \cdot T) \quad (3.1)$$

In this case the wire or capillary should not be heated, so the applied current was minimal (10 mA). An example of probe calibration, plotting electrical resistance (R) versus temperature (T) is shown in Figure 3.17.

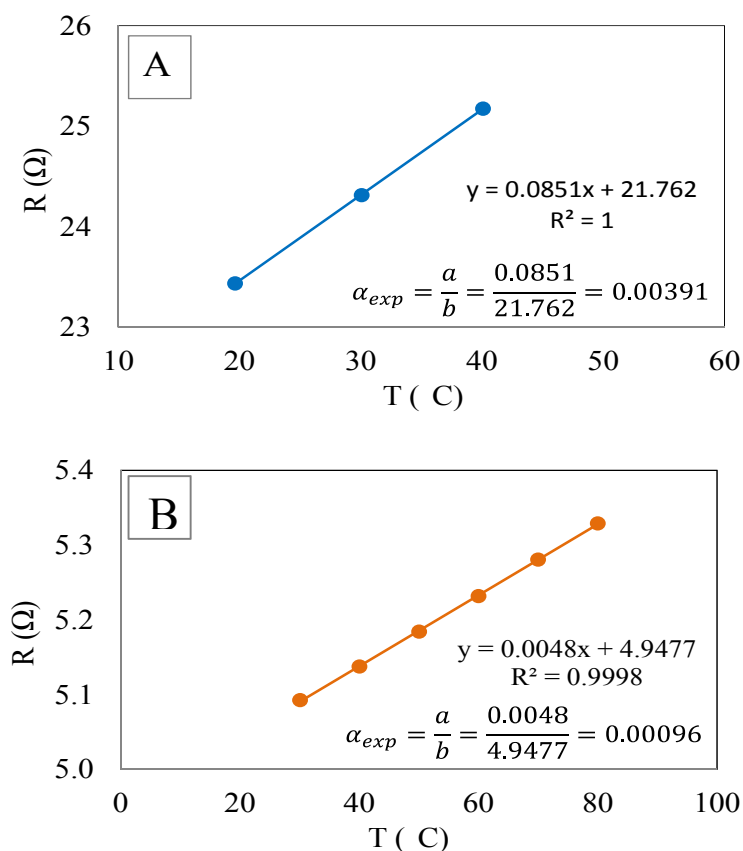


Figure 3.17: Resistance - Temperature relation for the A) Platinum B) Mercury

The average values obtained in the calibrations, from the slope of this linear relationship between resistance and temperature were $0.00390 \pm 0.00010 \text{ K}^{-1}$ for the platinum wire assembly and $0.00094 \pm 0.00003 \text{ K}^{-1}$ for the glass capillary assembly; These values were very close with the literature values of α for platinum 0.00392 K^{-1} and 0.00090 K^{-1} for mercury between $0 \text{ }^\circ\text{C}$ to $100 \text{ }^\circ\text{C}$ [78] and was considered to be an acceptable value.

Next, in the case of the platinum wire device, the calibration constant was determined (c in equation (2.3)) for each assembly with a new wire. For this, we make measurements of the thermal conductivity of pure water by using the standard reference data for the thermal conductivity of liquids [29]. The calibration constant is related to the finite length of the wire and the coating effect. The results from the calibration of each of the three assemblies used in this work are given in Table 3.3. The reported values of thermal conductivity were obtained by averaging the results of ten experiments at the three different temperatures.

Table 3.3: Calibration constants obtained from the thermal conductivity of water

Temperature (K)	k_{ref} ($\text{W}\cdot\text{m}^{-1}\cdot\text{K}^{-1}$)	k_{exp} ($\text{W}\cdot\text{m}^{-1}\cdot\text{K}^{-1}$)	c k_r/k_e
292.79	0.598	0.645	0.928
303.22	0.616	0.666	0.925
313.23	0.631	0.692	0.911
292.71	0.598	0.649	0.921
303.19	0.616	0.673	0.917
313.23	0.631	0.689	0.915
293.37	0.598	0.641	0.934
303.16	0.616	0.658	0.936
313.16	0.631	0.684	0.922

By taking the ratios of the reference value of thermal conductivity, the obtained values for c were between 0.911 and 0.936. In these measurements three different assemblies were used due to the fragility of the device.

Chapter 3: Experimental Setup

Finally, the apparatus and method were validated by measuring an electrically conductive fluid in order to corroborate that the coated wire and the coated brass rods work properly. No electrically conductive fluid could be found to use as a reference fluid and it was decided to use $\text{H}_2\text{O} + \text{LiNO}_3$ since this electrically conductive solution has similar compounds to the working mixtures measured in this study. Results were compare with the values given by Aseyev (1999) [93] and the average and maximum relative difference obtained was 1.7 % and 2.9 %, respectively (See Table 3.4).

Table 3.4: Deviations of the ammonia/lithium nitrate measured thermal conductivities from their literature values [93]

$\text{H}_2\text{O} + \text{LiNO}_3$ (30 wt.%)			
k ($\text{W}\cdot\text{m}^{-1}\cdot\text{K}^{-1}$)			
T (K)	k_{exp}	K_{ref}	*dev. (%)
312.95	0.560	0.577	-2.9
312.95	0.571	0.577	-1.0
312.95	0.570	0.577	-1.2
312.95	0.567	0.577	-1.8
312.95	0.594	0.577	2.9
312.95	0.580	0.577	0.52

$$*dev = \frac{k_{exp} - k_{ref}}{k_{ref}} \cdot 100$$

On the other hand, for the glass capillary system a calibration constant (c) is not used. In this case, in order to account the end effect and the nonuniform cross sectional area of the single capillary, the effective length (L_{eff}) for each assembly with a new glass capillary was determined (3.2) from measurements of the thermal conductivity of pure water [29].

$$L_{eff} = \frac{I^2 \cdot R}{4 \cdot \pi \cdot \frac{d\Delta T}{d \ln t} \cdot k_{ref}} \quad (3.2)$$

The reported value of effective length was obtained by averaging the results of ten experiments at three different temperatures to analyse any change with respect to temperature. By taking the average of the effective lengths presented in Table 3.5 the obtained value is 9.61 ± 0.54 cm and temperature dependence was not observed. For these measurements only one assembly was used due to the robustness of the device.

Table 3.5: Effective length of ten experiments at three temperatures

$L_{eff}(m)$ at 305.26 K									
0.1033	0.0988	0.0958	0.1084	0.0964	0.0946	0.0977	0.0959	0.0956	0.1064
$L_{eff}(m)$ at 313.22 K									
0.0983	0.0954	0.0924	0.0983	0.1023	0.0967	0.0953	0.1028	0.0922	0.0976
$L_{eff}(m)$ at 323.20 K									
0.0979	0.0856	0.0889	0.0916	0.0905	0.0927	0.0980	0.0900	0.0978	0.0855

With this effective length, the assembly was validated by comparing measurements with the values of reference fluids such as toluene, dimethyl phthalate and ethylene glycol suggested by IUPAC [94]. Other fluid with similar characteristics than the target mixture such as water + lithium nitrate (30 wt.%) has been measured and the data was compared with the values given by Aseyev, 1999 [93].

Table 3.6: Thermal conductivity of reference fluids measured with the mercury filled glass capillary

T (K)	Toluene ($W \cdot m^{-1} \cdot K^{-1}$)			Dimethyl phthalate ($W \cdot m^{-1} \cdot K^{-1}$)		
	k_{exp}	K_{ref}	dev(%)	k_{exp}	K_{ref}	dev(%)
303.15	-----	-----	-----	0.152	0.147	3.4
313.15	0.131	0.127	3.1	0.147	0.146	0.7
323.15	0.127	0.124	2.4	0.147	0.144	2.1
333.15	0.122	0.121	0.8	0.142	0.143	-0.7
343.15	0.119	0.118	0.8	0.141	0.142	-0.7
353.15	0.114	0.115	-0.9	0.136	0.140	-2.9

Chapter 3: Experimental Setup

T (K)	Ethylene glycol ($\text{W}\cdot\text{m}^{-1}\cdot\text{K}^{-1}$)			$\text{H}_2\text{O} + \text{LiNO}_3$ ($\text{W}\cdot\text{m}^{-1}\cdot\text{K}^{-1}$)		
	k_{exp}	K_{ref}	dev(%)	k_{exp}	K_{ref}	dev(%)
303.15	-----	-----	-----	0.582	0.580	0.3
313.15	0.257	0.255	0.8	0.596	0.595	0.2
323.15	0.257	0.256	0.4	0.606	0.608	-0.3
333.15	0.255	0.257	-0.8	0.616	0.619	-0.5
343.15	0.258	0.257	0.4	-----	-----	-----
353.15	0.250	0.257	-2.7	-----	-----	-----

Table 3.6 contains these experimental measurements and the comparison between the reference fluids. The average and maximum relative difference obtained was 1.2 % and 3.4 %, respectively.

To conclude, the two assemblies used in this work (platinum wire and glass capillary) were calibrated. First, verifying the linear dependence of the resistance with temperature, through the temperature coefficient of resistance (α). Second, determining the calibration constant (c) related to the finite length of the wire and the coating effect for the platinum wire, and the effective length (L_{eff}) of the glass capillary in order to account the end effect and the nonuniform cross sectional area. And finally, verifying the apparatus and method by measuring reference fluids and comparing the results with published values (See Table 3.7).

Table 3.7: Calibration parameters for platinum wire and glass capillary devices

Device	α (K^{-1})	c	L_{eff} (cm)	avg. dev(%)	max. dev(%)
Platinum wire	0.00390 ± 0.00010	0.911 - 0.936	----	1.7	2.9
Glass capillary	0.00094 ± 0.00003	----	9.61 ± 0.54	1.2	3.4

3.6 Experimental Procedure

The experimental procedure for each assembly used in this work (platinum wire and glass capillary) was the same, being the only difference the intensity applied. The procedure for each measurement was as follows.

Once the measurement cell was filled with the mixture, it was immersed in a water bath to adjust and control the temperature. After temperature equilibrium had been achieved (45 min.), the bath was stopped to prevent any vibration of the cell during measurement. The system was powered by the current source, and the nanovoltmeter was used to measure the voltage rise due to heating as a function of time. The Agilent VEE program used to control both instruments is given in Appendix A: Computer Programs. The applied constant intensity in the platinum wire was 0.1 A with an offset voltage of about 2 V. This resulted in temperature rise of approximately 3 °C. For the glass capillary, the applied constant intensity was between 0.2 to 0.3 A with an offset voltage of around 1.5 V and temperature rise approximately 3 - 6 °C. Each experimental run consist of around 370 points measured during the experimental time lasted about 6 seconds. Ten runs were carried out at each temperature and the average thermal conductivity obtained was noted. Five minutes between readings were allowed for temperatures to re-equilibrium.

The resistance of the wire/capillary (R) was then calculated from the Ohm's Law (3.3):

$$R = \frac{V}{I} \quad (3.3)$$

This resistance was converted to the temperature rise using equation (3.6):

$$\Delta T = T_{wire} - T_{bath} \quad (3.4)$$

$$T_{wire} = a \cdot R + b \quad (3.5)$$

Chapter 3: Experimental Setup

$$\Delta T = a \cdot R + b - T_{bath} \quad (3.6)$$

Coefficients a and b from equation (3.5) were found from a previous calibration of the temperature versus resistance (See section 3.5).

The heat dissipated per unit length (q) was determined from:

$$q = \frac{I^2 \cdot \bar{R}}{L} \quad (3.7)$$

Where \bar{R} is the average resistance during the chosen time interval.

A plot of ΔT versus $\ln t$ was made and the slope in the time interval from 0.3 to 2.7 seconds was calculated using a least squares fit. Finally, with all these parameters the thermal conductivity of the mixture can be calculated by equation (3.8).

$$k = \frac{q}{4 \cdot \pi \cdot \left(\frac{d\Delta T}{d \ln t} \right)} \quad (3.8)$$

3.7 Uncertainty estimation

The purpose of this section is the evaluation of measurement uncertainty in accordance with the EA- 4/02 of the European Cooperation for Accreditation [95]. There are two major methods in the literature in evaluation of uncertainty:

- Type A evaluation of measurement uncertainty; from the statistical distribution of the quantity values from series of measurements, and can be characterized by standard deviations (Normal distribution).

- Type B evaluation of measurement uncertainty; can also be characterized by standard deviations, evaluated from probability density functions based on experience or other information (Rectangular distribution).

In most experiments the direct measurement of a quantity rarely occurs. Then, the measurement model is based in a mathematical relation among all quantities known to be involved in a measurement, called Propagation of Uncertainty. Formally, the output quantity about which information is required (Y), is often related to input quantities about which information is available (X_1, X_2, \dots, X_n), by a measurement model in the form of:

$$Y = f(X_1, X_2, \dots, X_n) \quad (3.9)$$

When the uncertainties of thermal conductivity was evaluated, the following input quantities were taken into account: pressure, temperature, sample preparation, heat generation and the slope between ΔT vs $\ln(t)$. In order to identify all the input sources of uncertainty contributions in the thermal conductivity measurements a “fish-bone” diagram was made (See Figure 3.18).

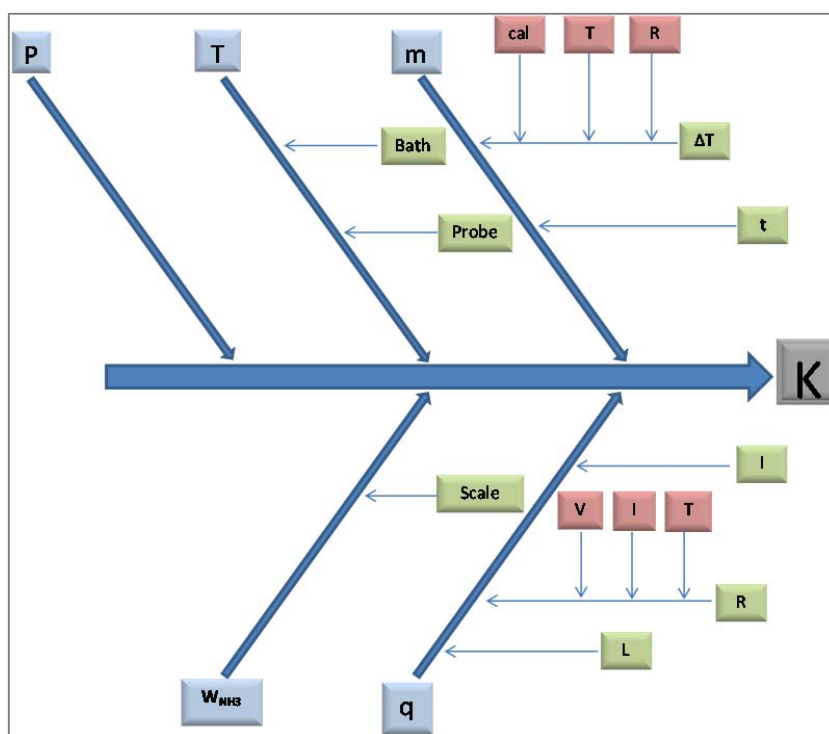


Figure 3.18: Fish-bone diagram of the uncertainty contributors

Chapter 3: Experimental Setup

When all the uncertainty sources for each input quantity were determined, they were multiplied by their sensitivity coefficient (c_i) and summed to calculate the combined standard uncertainty (u_c) given by equation (3.10), which is known as the law of propagation of uncertainty.

$$u_c^2(Y) = c_1^2 \cdot u^2(X_1) + c_2^2 \cdot u^2(X_2) + \dots + c_n^2 \cdot u^2(X_n) \quad (3.10)$$

The sensitivity coefficient (c_i) was calculated as the partial derivative of the function with respect to input quantity and describes how the estimate output quantity (Y) would be influenced by small changes in the estimates input quantities (X).

$$c_i = \frac{\partial f}{\partial X_i} \quad (3.11)$$

Input sources of uncertainties are the relation of estimate standard deviation and the probability distribution. If it is a normal distribution then the divisor value is equal 1. On the other hand if the distribution is rectangular then the divisor value is $\sqrt{3}$.

$$u(X_i) = \frac{\text{Estimate}}{\text{Divisor}} \quad (3.12)$$

The combined standard uncertainty (u_c) has a level of confidence of 68.27 %. If the purpose of the uncertainty statement is to provide coverage with a high level of confidence, then an expanded uncertainty (U) is obtained by equation (3.13), where k is the coverage factor.

$$U(Y) = k \cdot u(Y) \quad (3.13)$$

In this study, the value of the coverage factor is equal 2 and the expanded uncertainty is assumed to provide a level of confidence of 95.45 %.

Next, details are given on how to determine each of the uncertainty contributions for the input quantities, related to thermal conductivity measurements. More information can be found in Appendix B: Uncertainty.

PRESSURE (P)

The equipment used for measuring the pressure in the system was a manometer WIKA Model 232.35.

The uncertainty source associated with the pressure measurement was the resolution, adopted from the equipment catalogue.

The expanded uncertainty value was calculated as 0.6 bar.

TEMPERATURE (T)

Temperature was controlled by a thermostat (Selecta Digiterm 100) and measured with a precision thermometer (Automatic System Laboratories F205 MKII using a PT100 probe).

The uncertainty sources associated with the thermostat bath are stability and homogeneity and for the thermometer are calibration, drift, resolution and repeatability evaluated by experiments and adopted from the equipment catalogue.

The expanded uncertainty value was calculated as 0.04 K.

SAMPLE PREPARATION (S)

The precision balance METTLER Toledo PR2003 was used to weight all the compounds involved in the sample preparation.

The uncertainty sources associated with the sample preparation are resolution, calibration, linearity and repeatability, given by the equipment catalogue.

The expanded uncertainty value was calculated as 0.02 wt.%

Chapter 3: Experimental Setup

HEAT GENERATION (q)

In this case several uncertainty sources are involved. One of these contributors is the length of the wire or capillary. A vernier caliper was used to measure the length of the platinum wire and ten different measurements were made. Then, the uncertainty sources associated with this are resolution and standard deviation. For the capillary, the length was determined by calibration with a reference fluid (water). Then, the uncertainty sources associated with this are intensity, resistance, slope, thermal conductivity and standard deviation. The uncertainty associated with the intensity and the resistance is given by the acquisition system and are resolution, repeatability and drift.

Finally, the combined expanded uncertainty for the heat generation were $0.021 \text{ W}\cdot\text{m}^{-1}$ and $0.015 \text{ W}\cdot\text{m}^{-1}$ for the platinum wire and for the glass capillary, respectively.

SLOPE (m)

The slope is related by the temperature rise of the wire or capillary and the logarithm of time. The temperature rise is given by the calibration equation (3.6) and the uncertainty sources associated with this are the calibration parameters calculated by a least squares fit, temperature and resistance determined previously. For time, the resolution was involved.

Then, the expanded uncertainty for the slope were $0.91 \text{ K}\cdot\text{s}^{-1}$ and $13.63 \text{ K}\cdot\text{s}^{-1}$ for the platinum wire and for the glass capillary, respectively.

THERMAL CONDUCTIVITY (k)

Finally, with all the uncertainty contributors calculated, the uncertainty of the thermal conductivity is determined by the law of propagation with those variables that directly affect such as heat generation and slope.

Then, the expanded uncertainty for the thermal conductivity were $0.017 \text{ W}\cdot\text{m}^{-1}\cdot\text{K}^{-1}$ and $0.025 \text{ W}\cdot\text{m}^{-1}\cdot\text{K}^{-1}$ for the platinum wire and for the glass capillary, respectively.

In conclusion, all the uncertainty contributions to the thermal conductivity were calculated for each assembly used in this work. In both, the most critical cases were used for the uncertainty calculations. Table 3.8 resumes the most important uncertainties parameters used in this work for both devices.

Table 3.8: Expanded uncertainty values (K=2)

Device	P (bar)	T (K)	NH_3 (wt.%)	k ($\text{W}\cdot\text{m}^{-1}\cdot\text{K}^{-1}$)
Platinum wire	0.6	0.04	0.02	0.017
Glass capillary	0.6	0.04	0.02	0.025

Although which other insulated hot wire apparatus are capable of higher accuracy, the glass capillary filled with mercury has confirmed to be convenient for our purpose and can be used over a broader range of conditions, especially in regard to the nature of the fluids studied. During the experimental time it was observed how the glass capillary is much handier than the platinum wire. Although this construction has high-accuracy, the fragility of the wire assembly limits its use. A more rugged construction is the glass capillary technique, which is especially suited for these kinds of fluids, as it can withstand high temperatures without current leaks while maintaining enough stability for our purpose. When the platinum wire was used to measure $\text{NH}_3 + \text{H}_2\text{O}$ three different assemblies were needed because the wire breaks ease. On the other hand, with only one capillary assembly all the rest of fluids ($\text{NH}_3 + \text{LiNO}_3$, $\text{NH}_3 + \text{LiNO}_3 + \text{H}_2\text{O}$ and $\text{NH}_3 + \text{LiNO}_3 + \text{CNTs}$) were measured including the respective calibration fluids.

Chapter 4

4. Results and Discussion

Thermal conductivity data, obtained experimentally, for different working fluids such as $\text{NH}_3 + \text{H}_2\text{O}$, $\text{H}_2\text{O} + \text{LiBr}$ and $\text{NH}_3 + \text{LiNO}_3$ are presented first in this chapter, followed by the measurements on the ternary mixtures $\text{NH}_3 + \text{LiNO}_3 + \text{H}_2\text{O}$ and $\text{NH}_3 + \text{LiNO}_3 + \text{CNTs}$.

This section, also discusses the thermal conductivity enhancement of carbon nanotubes or water over those of the base fluid ($\text{NH}_3 + \text{LiNO}_3$) alone. Finally, the effect of using a different concentration of carbon nanotubes or water on the thermal conductivity enhancement is debated.

4.1 Thermal Conductivity of $\text{NH}_3 + \text{H}_2\text{O}$

Due to the scanty experimental data available in the literature, the measurement on thermal conductivity of $\text{NH}_3 + \text{H}_2\text{O}$ working fluid has been considered at different compositions and temperatures. The motivation behind is the disagreements found among literature data (See section 2.2.2 and Figure 2.8). In order to clarify these discrepancies between the reported experimental data and to extend the range of available data on high ammonia concentrations, the thermal conductivity of $\text{NH}_3 + \text{H}_2\text{O}$ mixtures containing 0.1 to 0.5 ammonia mass fraction has been measured at temperatures between 293.15 and 313.15 K and a constant pressure of 1.5 MPa.

Results were obtained using the coated platinum wire device showed in Figure 3.1 section 3.1.1. The maximum deviation from the average value never exceed 2.9 %, and the uncertainty in the measurements is $0.017 \text{ W}\cdot\text{m}^{-1}\cdot\text{K}^{-1}$ (More detail in section 3.5 and 3.7).

Chapter 4: Results and Discussion

The measurements were repeated ten times for each temperature and composition. The resulting average values are presented in Table 4.1. Also, the average values are plotted versus its composition in Figure 4.1.

Table 4.1: Thermal conductivity for NH₃+H₂O at several temperatures and compositions

T (K)	K_{exp} (W·m ⁻¹ ·K ⁻¹)				
	$w_I=0.1026$	$w_I=0.2007$	$w_I=0.3079$	$w_I=0.4012$	$w_I=0.5040$
293.15	0.512	0.478	0.448	0.423	0.406
303.15	0.527	0.491	0.457	0.429	0.412
313.15	0.550	0.499	0.472	0.444	0.410

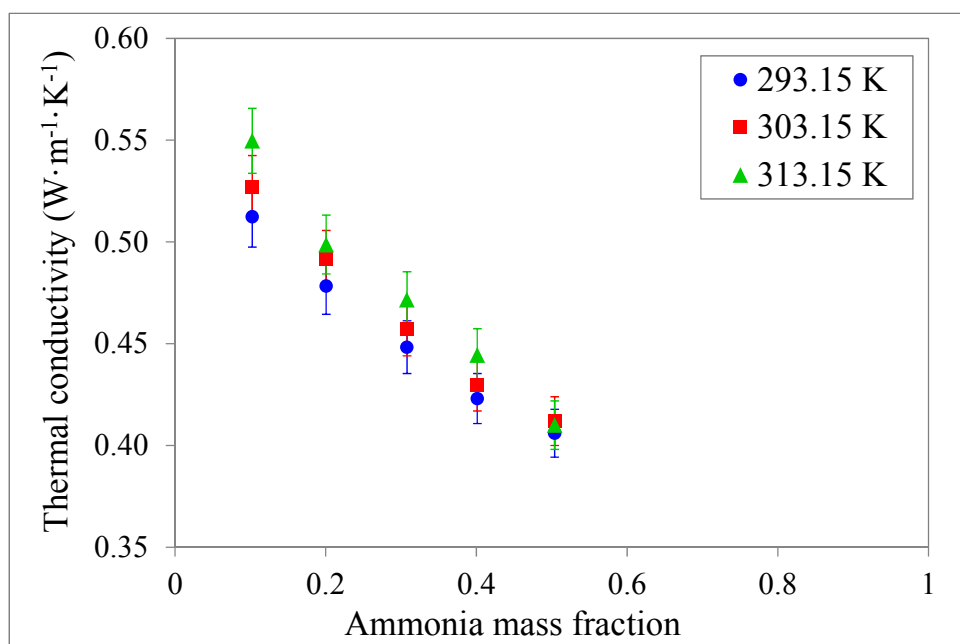


Figure 4.1: Thermal conductivity for NH₃+H₂O at several temperatures and compositions

Results show that the thermal conductivity of NH₃+H₂O mixtures increases with temperature and decreases with ammonia mass fraction for mass fractions below 0.5.

The values measured at 293.15 K and 303.15 K are plotted together with the literature values at similar temperatures in Figure 4.2. Our data agreed with the data published by Braune (1937) [54] and Lees (1898) [53], but were significantly different from the data reported by Baranov (1997) [56] and Chernen'kaya *et al.* (1972) [55]. It is difficult to provide reasons for these discrepancies since the authors did not give enough information about their techniques, methodologies, purity of the mixtures, etc. But, it is known that Baranov and Chernen'kaya used different techniques than the hot wire method, which could be a possible reason.

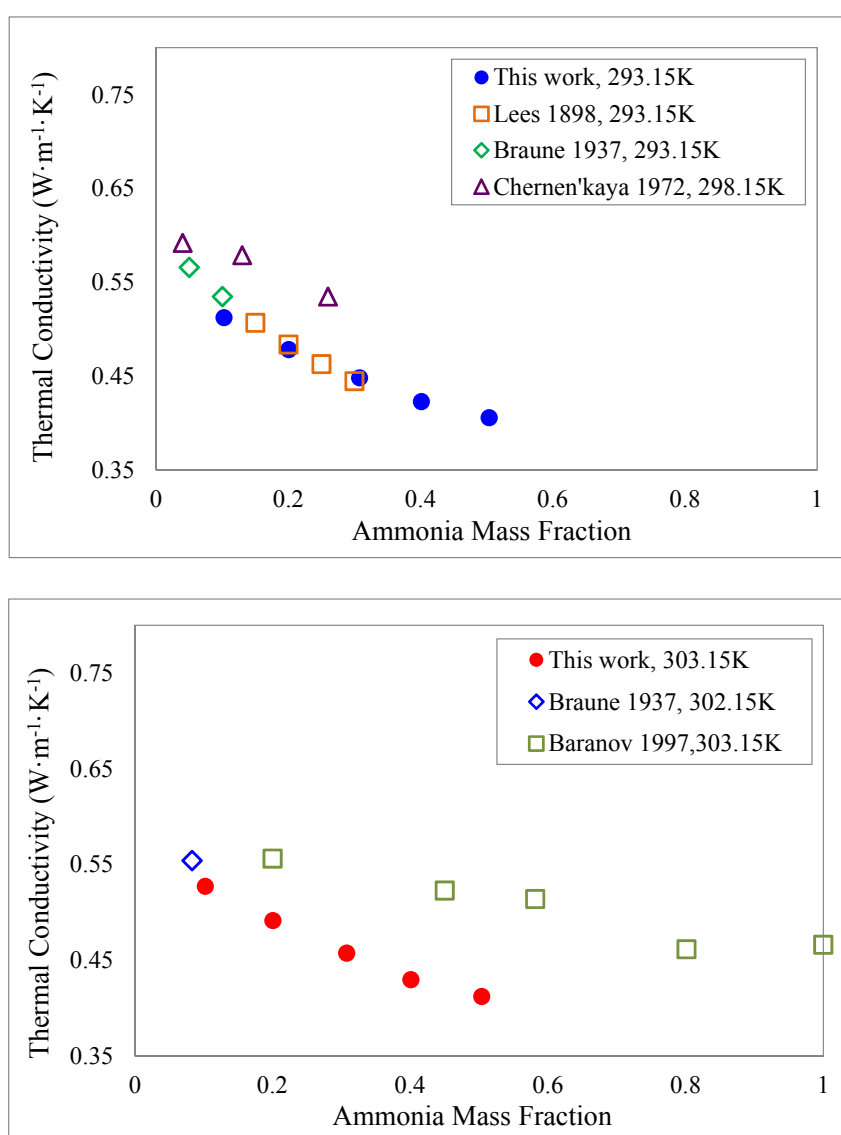


Figure 4.2: Thermal conductivity comparison between our experimental values and the literature data for NH₃ + H₂O mixtures

Chapter 4: Results and Discussion

4.2 Thermal Conductivity of H₂O + LiBr

Thermal conductivity values for H₂O + LiBr mixtures are well known, and several experimental data can be found in the literature [17], [18], [19], [20], [21] (See section 2.2.1). Moreover there is a correlation in function of temperature and weight percent of lithium bromide [21]. Therefore, one composition of H₂O + LiBr solution was measured at 40 wt. % LiBr in the temperature range from 298.15 to 428.15 K and a constant pressure of 1.5 MPa in order to confirm these available data with our system. The equipment used in these measurements was a glass capillary filled with mercury provided by Teja Thermodynamic Research Group in Georgia Institute of Technology. The characteristics of the device are 9.76 cm of length and 50 μm of inner diameter. The maximum deviation from the average value never exceeded 2.0 %.

Each data point presented in Table 4.2 represents the average of five experimental runs. Also, the experimental data were compared with the correlation proposed by DiGuilio *et al.*, [21] with a maximum deviation of 1.2 %.

Table 4.2: Thermal conductivity of H₂O + LiBr and comparison with literature data

T (K)	k_{exp} (W·m ⁻¹ ·K ⁻¹)	K_{ref} (W·m ⁻¹ ·K ⁻¹)	dev(%)
297.40	0.477	0.473	0.9
323.59	0.507	0.511	-0.8
352.14	0.537	0.534	0.6
374.80	0.554	0.547	1.2
399.32	0.564	0.558	1.0
427.67	0.567	0.563	0.8

Results are plotted in Figure 4.3 together with the correlation proposed by DiGuilio *et al.*, in 1990 [21]. Our data agreed with the literature data following the same trend where thermal conductivity increases significantly with temperature up to 400 K where this increase is more slightly.

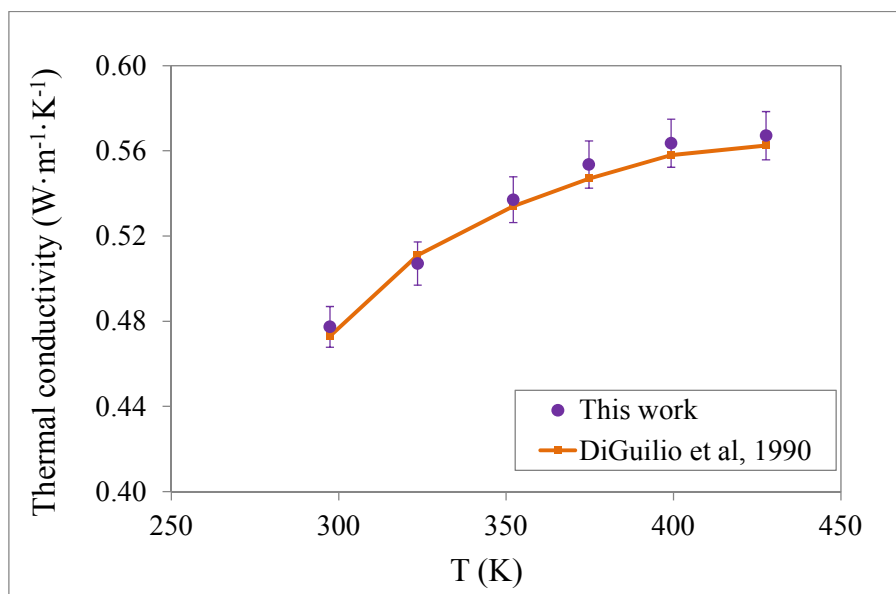


Figure 4.3: Thermal conductivity comparison between our experimental values and the literature data for $\text{H}_2\text{O} + \text{LiBr}$ mixtures

4.3 Thermal Conductivity of $\text{NH}_3 + \text{LiNO}_3$

$\text{NH}_3 + \text{LiNO}_3$ is a new mixture proposed as an alternative to the conventional working fluids for absorption cycles. No previous experimental studies have been found in the literature for this mixture. As was mentioned before in section 2.2.3 the only available data in the literature is the correlation proposed by Infante Ferreira in 1984 [8]. Other thermodynamics and transport properties of this mixture such as, vapor-liquid equilibrium, density, viscosity and heat capacity have been presented in previous works [11], [12] at temperatures between (293.15 and 353.15) K and a fixed pressure of 1.8 MPa. Then, in the absence of experimental data, and in order to complete the existing properties database for the mixture, the thermal conductivity from 0.3 to 0.6 in ammonia mass fraction, temperatures between 303.15 K and 353.15 K and a constant pressure of 1.5 MPa has been measured, and new data has been provided to the literature.

Chapter 4: Results and Discussion

Measurements were made using the glass capillary device filled with mercury showed in Figure 3.5 and section 3.1.2. Therefore, the maximum deviation from the average value never exceed 3.4 %, and the uncertainty in the measurements is $0.025 \text{ W}\cdot\text{m}^{-1}\cdot\text{K}^{-1}$ (For more detail see section 3.5 and 3.7).

The measurements were repeated ten times for each temperature and composition. The resulting average values are presented in Table 4.3. Also, the measured values are plotted versus its temperature in Figure 4.4.

Table 4.3: Thermal conductivity for NH_3 (1) + LiNO_3 (2) at several temperatures and ammonia mass fractions.

$k \text{ (W}\cdot\text{m}^{-1}\cdot\text{K}^{-1}\text{)}$					
$T \text{ (K)}$	$w_1=0.2966$	$w_1=0.3480$	$w_1=0.3988$	$w_1=0.5016$	$w_1=0.5960$
303.15	-----	0.356	0.350	0.360	0.385
313.15	0.350	0.348	0.331	0.342	0.371
323.15	0.344	0.342	0.323	0.331	0.362
333.15	0.333	0.337	-----	0.323	0.351
343.15	0.330	0.332	0.312	0.319	-----
353.15	0.331	0.323	0.305	-----	-----

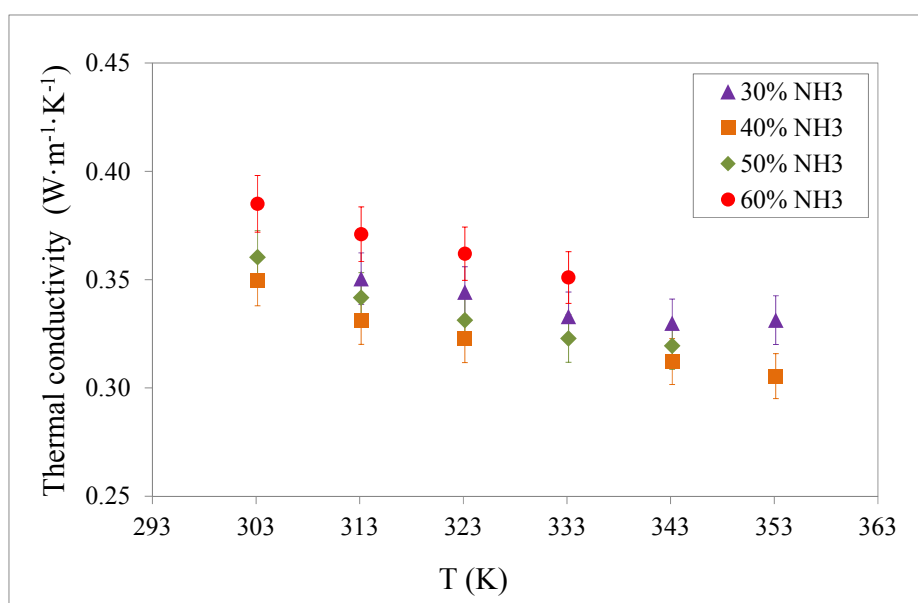


Figure 4.4: Thermal conductivity of NH_3 + LiNO_3 at several temperatures and compositions

Thermal conductivity values of the mixture were found to decrease when the temperature increases for all of the measured samples. Furthermore, for all of the studied temperatures, the minimum thermal conductivity was observed to be at 40 % of ammonia.

The experimental data of $\text{NH}_3 + \text{LiNO}_3$ mixture were compared with the calculated data obtained through the correlation proposed by Infante Ferreira (1984) [8] showing remarkable inconsistencies (See Figure 4.5). In terms of root mean square error the maximum deviation obtained was 132 %.

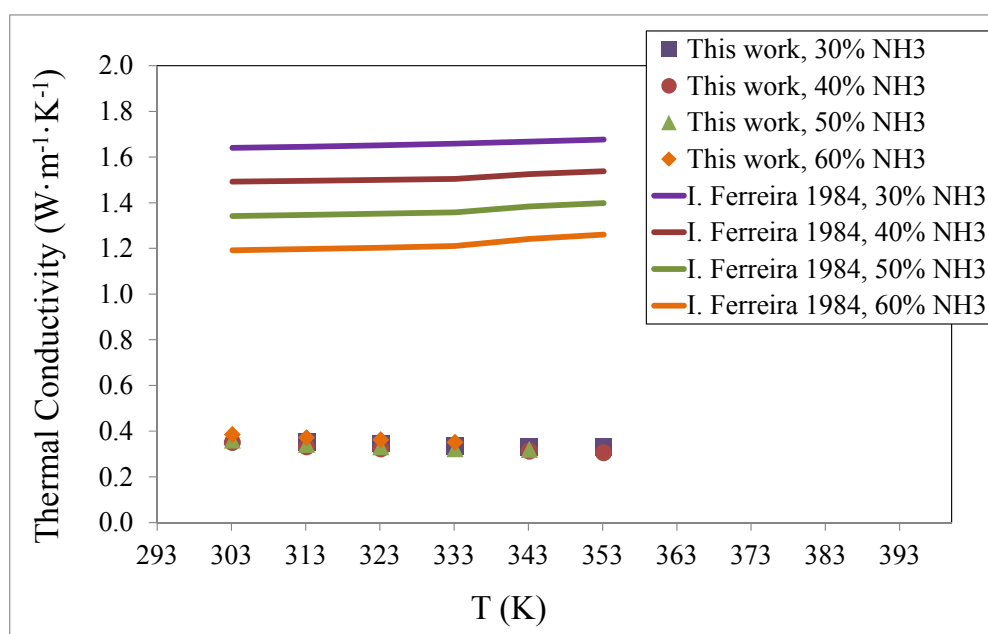


Figure 4.5: Thermal conductivity comparison between our experimental values and the calculated data proposed by Infante Ferreira (1984) for $\text{NH}_3 + \text{LiNO}_3$ mixtures

It can be seen how the obtained values by Ferreira are extremely higher than our experimental data. It is difficult to provide reasons for these discrepancies since the author did not measure the mixture; however, these results are much higher than thermal conductivity values expected for a liquid. For more detail about the procedure followed by Infante Ferreira see section 2.2.3.

4.4 Thermal Conductivity of $\text{NH}_3 + \text{LiNO}_3 + \text{H}_2\text{O}$

Comparing the thermal conductivity data of the three binary working fluids measured earlier, it can be observed that values for the new mixture $\text{NH}_3 + \text{LiNO}_3$ are in the order of $0.3 \text{ W}\cdot\text{m}^{-1}\cdot\text{K}^{-1}$ while $\text{NH}_3 + \text{H}_2\text{O}$ and $\text{H}_2\text{O} + \text{LiBr}$ are ranging around $0.4 \text{ W}\cdot\text{m}^{-1}\cdot\text{K}^{-1}$ and $0.5 \text{ W}\cdot\text{m}^{-1}\cdot\text{K}^{-1}$. Previous experimental studies of absorption cycles operating with this mixture have shown low rates of heat and mass transfer in the absorber [14], [15], [16] and finally experimental results obtained in this work have also lower thermal conductivity. Moreover, the high viscosity of the salt solution can limit the performance of the cycle. With the addition of water the viscosity could be reduced around 2-3 times [12], this reduction was also observed in the preparation of the sample.

Low thermal conductivity is a primary limitation in the development of energy-efficient heat transfer fluids that are required in absorption cycles. To overcome this limitation, the addition of water was proposed. Other authors used water as a method for augmenting heat and mass transfer processes but, thermal conductivity of the ternary mixture $\text{NH}_3 + \text{LiNO}_3 + \text{H}_2\text{O}$ never was measured. More information about earlier works with the ternary mixture is detailed in section 2.2.4.

In a previous works [64], [9], [63], [11], [12] thermodynamic and transport properties of this mixture such as, density, viscosity, heat capacity and vapor-liquid equilibrium have been measured. In this study thermal conductivity from 0.3 to 0.6 in ammonia mass fraction, temperatures between 303.15 K and 353.15 K and a constant pressure of 1.5 MPa is determined, with a water mass fractions in the absorbent solution ($\text{H}_2\text{O} + \text{LiNO}_3$) of 0.20 and 0.25.

The measurements were repeated ten times for each temperature and composition, giving an average value with a maximum deviation of 3.4 % and uncertainty in the measurements of $0.025 \text{ W}\cdot\text{m}^{-1}\cdot\text{K}^{-1}$ (See more detail in section 3.5 and 3.7). Glass capillary device filled with mercury showed in Figure 3.5 and section 3.1.2 was used for all the measurements.

Results for the two water mass fractions 0.20 and 0.25 are given in Table 4.4 and Table 4.5, respectively and also plotted together versus its temperature in Figure 4.6.

Table 4.4: Thermal conductivity for NH₃ (1) + LiNO₃ (2) + H₂O (3) at several temperatures and 0.2 in water mass fraction in the absorbent solution.

<i>T</i> (K)	<i>k</i> (W·m ⁻¹ ·K ⁻¹)			
	<i>w</i> _l =0.2985	<i>w</i> _l =0.3989	<i>w</i> _l =0.4984	<i>w</i> _l =0.5978
303.15	0.388	0.368	0.380	0.407
313.15	0.374	0.360	0.371	0.395
323.15	0.364	0.353	0.362	0.382
333.15	0.359	0.349	0.357	-----
343.15	0.352	0.347	-----	-----
353.15	0.350	0.342	-----	-----

Table 4.5: Thermal conductivity for NH₃ (1) + LiNO₃ (2) + H₂O (3) at several temperatures and 0.25 in water mass fraction in the absorbent solution.

<i>T</i> (K)	<i>k</i> (W m ⁻¹ K ⁻¹)			
	<i>w</i> _l =0.2986	<i>w</i> _l =0.3978	<i>w</i> _l =0.4992	<i>w</i> _l =0.5978
303.15	0.399	0.374	0.394	0.419
313.15	0.392	0.366	0.380	0.401
323.15	0.381	0.358	0.372	0.390
333.15	0.375	0.353	0.367	-----
343.15	0.368	0.349	-----	-----
353.15	0.370	0.348	-----	-----

Results for the ternary mixture follows the same trend than those for the binary (NH₃ + LiNO₃). The minimum values were observed to be at 40 % of ammonia for all of the studied temperatures, and thermal conductivity decreases slightly when the temperature increases for all of the measured samples.

Chapter 4: Results and Discussion

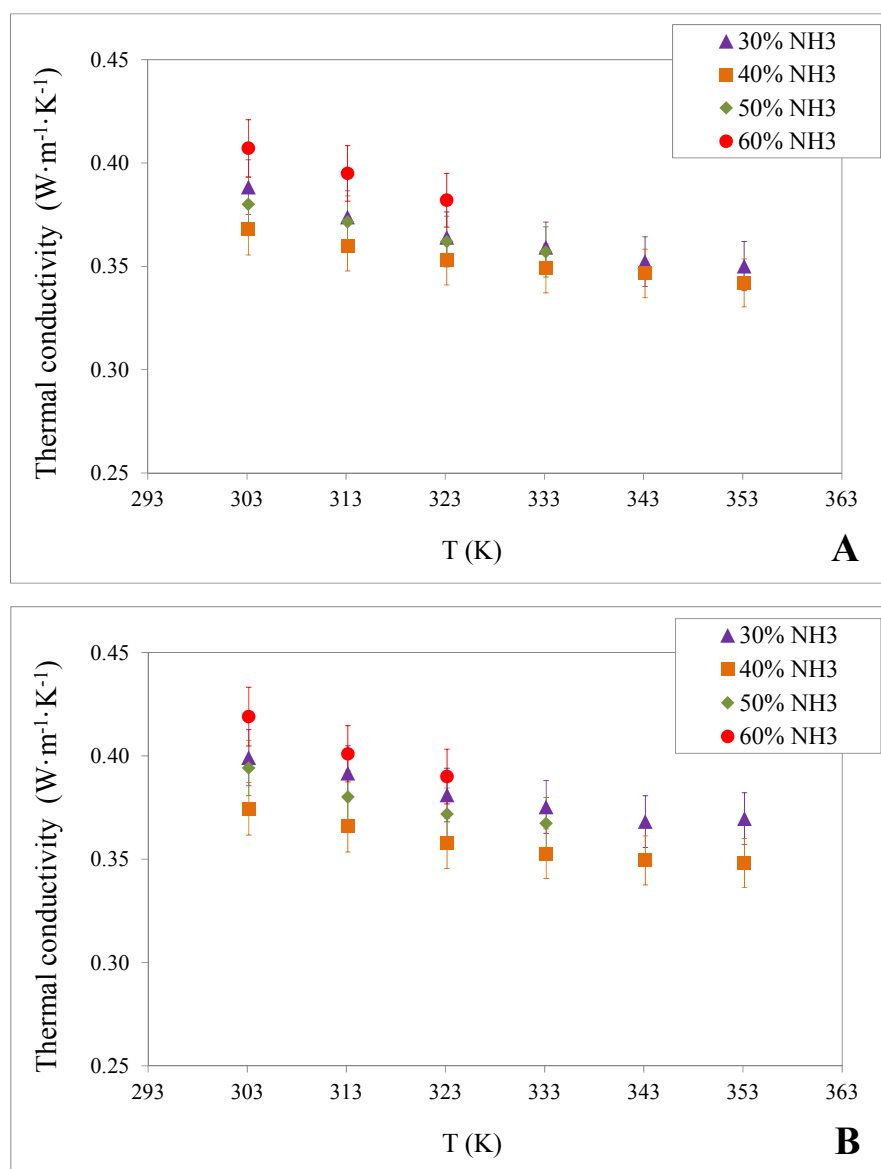


Figure 4.6: Thermal conductivity for $\text{NH}_3 + \text{LiNO}_3 + \text{H}_2\text{O}$ at several temperatures and compositions. A) 0.2 water mass fraction B) 0.25 water mass fraction

Finally, results obtained for the binary and the ternary mixture were plotted together (Figure 4.7) in order to analyse the effect of the water addition to the $\text{NH}_3 + \text{LiNO}_3$ mixture. Using a third component with high affinity for ammonia not only showed a decrease of the viscosity, it was also found that with the ternary mixture the average enhancement of thermal conductivity were up to 8 % and 11 % with 0.20 and 0.25 water mass fractions, respectively.

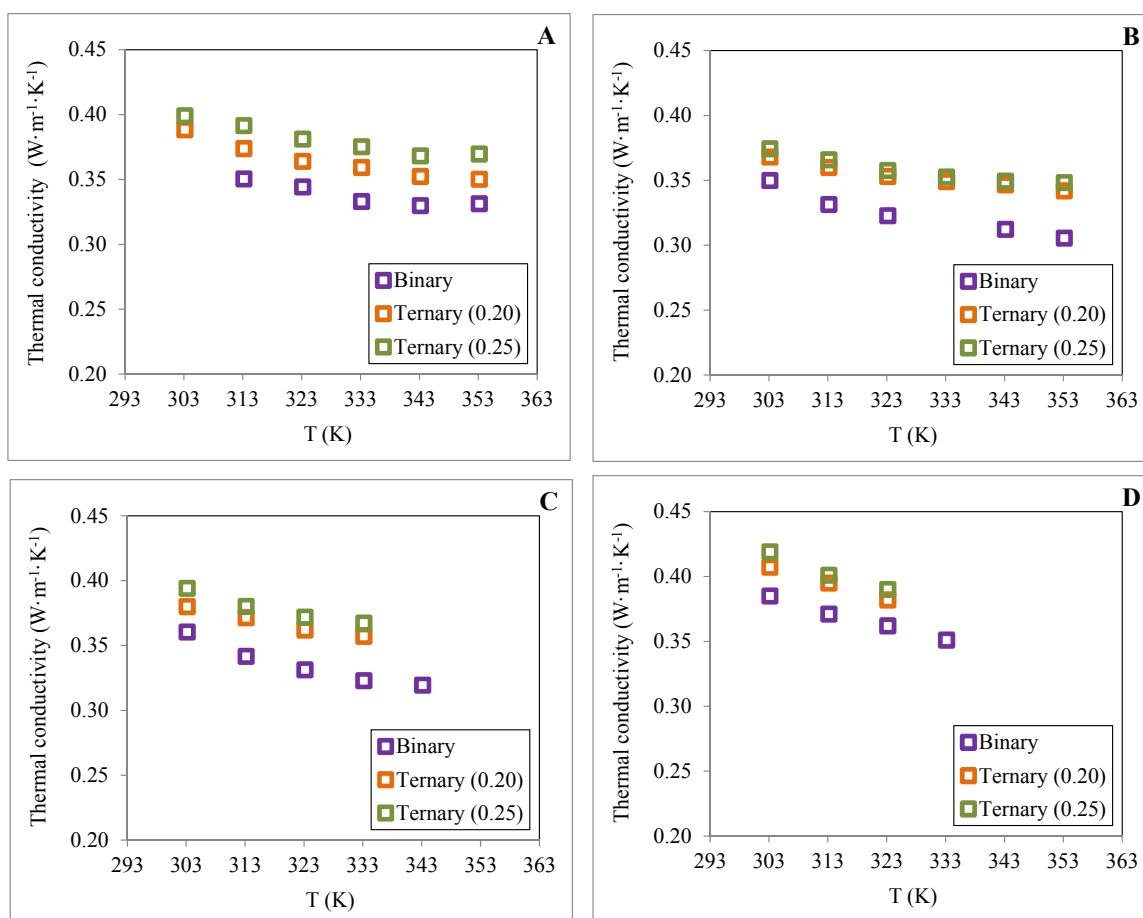


Figure 4.7: Effect of water addition to the binary mixture $\text{NH}_3 + \text{LiNO}_3$: (A) 0.3 mass fraction ammonia, (B) 0.4 mass fraction ammonia, (C) 0.5 mass fraction ammonia and (D) 0.6 mass fraction ammonia.

4.5 Thermal Conductivity of $\text{NH}_3 + \text{LiNO}_3 + \text{CNTs}$

Regarding to the low thermal conductivity for the binary mixture $\text{NH}_3 + \text{LiNO}_3$, other solution proposed for enhancing thermal properties of heat transfer fluids is the addition of carbon nanotubes (CNTs). In the last decade, a significant amount of experimental and theoretical research was made to investigate the thermophysical behaviour of nanofluids. In these studies, it was observed that a high thermal conductivity enhancement could be

Chapter 4: Results and Discussion

obtained with nanofluids, even in the case of very small particle volume fractions (See section 2.2.5 for more detail about previous works). This increase ratio (φ) is defined as the effective thermal conductivity of the nanofluid (k_{eff}) divided by the thermal conductivity of the base fluid (k_f).

$$\varphi = \frac{k_{eff} - k_f}{k_f} \cdot 100 \quad (4.1)$$

Thermal conductivity of $\text{NH}_3 + \text{LiNO}_3 + \text{CNTs}$ was measured using the glass capillary device filled with mercury designed and built in this study. Temperatures ranging from 303.15 K to 353.15 K, at 10 K intervals and a constant pressure of 1.5 MPa. Several samples were measured between 0.005 wt.% and 0.2 wt.% of CNTs at 40 wt.% of NH_3 in the binary mixtures. Latter at two different compositions of NH_3 (30 wt.% and 50wt.%) in the binary mixture and 0.01 wt.% of CNTs.

The measurements were repeated ten times for each temperature and composition to take into account the reproducibility. The average values are presented in Table 4.6, Table 4.7 and Table 4.8. The maximum deviation in the experimental data is 3.4 % and uncertainty in the measurements is $0.025 \text{ W}\cdot\text{m}^{-1}\cdot\text{K}^{-1}$ (See more detail in section 3.5 and 3.7).

Table 4.6: Effective thermal conductivity of CNTs nanofluids with $\text{NH}_3 + \text{LiNO}_3$ (40 wt.%) as the base fluid.

CNTs (wt.%)	T (K)	K_{eff} ($\text{W}\cdot\text{m}^{-1}\cdot\text{K}^{-1}$)	K_f ($\text{W}\cdot\text{m}^{-1}\cdot\text{K}^{-1}$)	φ (%)
0.005	303.27	0.360	0.350	2.9
0.005	313.23	0.347	0.331	4.8
0.005	323.21	0.338	0.323	4.6
0.005	333.20	0.334	-----	-----
0.005	343.19	0.331	0.312	6.1
0.005	353.11	0.325	0.305	6.6

Y. Cuenca, *Doctoral Thesis*, URV, Tarragona 2013

0.01	303.08	0.365	0.350	4.3
0.01	313.09	0.350	0.331	5.7
0.01	323.00	0.340	0.323	5.2
0.01	333.05	0.337	-----	-----
0.01	343.09	0.335	0.312	7.4
0.01	353.10	0.328	0.305	7.5
0.02	303.27	0.362	0.350	3.4
0.02	313.21	0.347	0.331	4.8
0.02	323.19	0.338	0.323	4.6
0.02	333.17	0.335	-----	-----
0.02	343.09	0.334	0.312	7.1
0.02	353.02	0.323	0.305	5.9
0.2	303.28	0.355	0.350	1.4
0.2	313.22	0.337	0.331	1.8
0.2	323.19	0.329	0.323	1.9
0.2	333.17	0.323	-----	-----
0.2	343.19	0.318	0.312	1.9
0.2	353.14	0.311	0.305	2.0

Table 4.7: Effective thermal conductivity of CNTs nanofluids with NH₃ + LiNO₃ (30 wt.%) as the base fluid.

CNTs (wt.%)	T (K)	K_{eff} (W·m ⁻¹ ·K ⁻¹)	K_f (W·m ⁻¹ ·K ⁻¹)	φ (%)
0.01	313.24	0.362	0.350	3.4
0.01	323.22	0.354	0.344	2.9
0.01	333.20	0.348	0.333	4.5
0.01	343.16	0.341	0.330	3.3
0.01	353.06	0.342	0.331	3.3

Chapter 4: Results and Discussion

Table 4.8: Effective thermal conductivity of CNTs nanofluids with NH₃ + LiNO₃ (50 wt.%) as the base fluid.

CNTs (wt.%)	<i>T</i> (K)	<i>K_{eff}</i> (W·m ⁻¹ ·K ⁻¹)	<i>K_f</i> (W·m ⁻¹ ·K ⁻¹)	<i>φ</i> (%)
0.01	303.26	0.377	0.360	4.7
0.01	313.22	0.362	0.342	5.8
0.01	323.16	0.351	0.331	6.0
0.01	333.13	0.342	0.323	5.9
0.01	343.10	0.338	0.319	6.0

Results presented in Table 4.6 show that the binary nanofluid, containing only a small amount of CNTs, has significantly higher effective thermal conductivity than the base fluid. For the NH₃ + LiNO₃ + CNTs binary nanofluid, the thermal conductivity can be enhanced up to 7.5 % at 0.01 wt.% of CNTs and 353.10 K. It was observed (See Figure 4.8) that the thermal conductivity ratios of the binary nanofluid not increase linearly with mass fraction of CNTs.

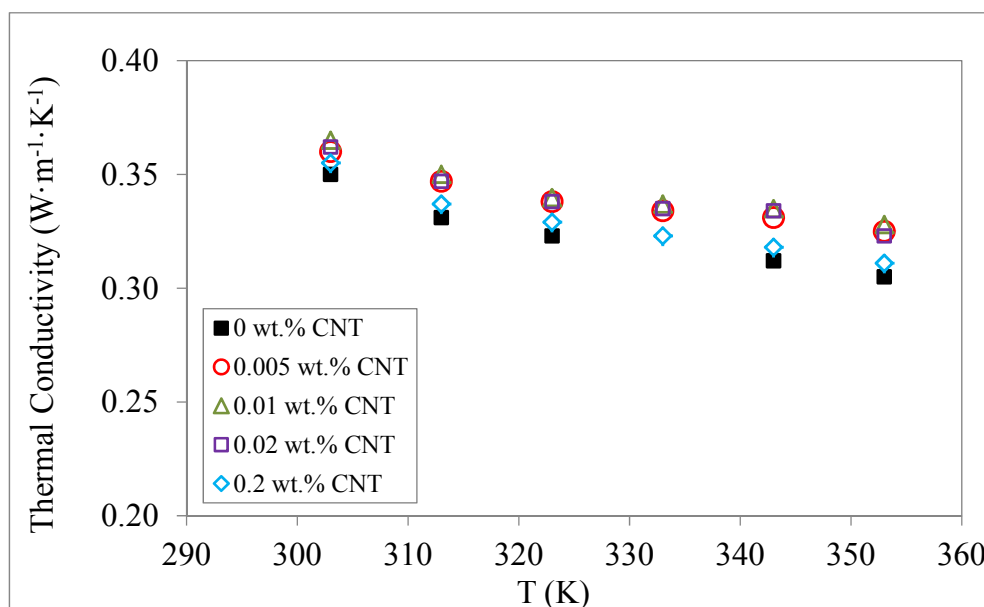


Figure 4.8: Thermal conductivity comparison of CNTs concentrations with NH₃ + LiNO₃ (40 wt.%) as the base fluid.

With small quantities of CNTs (0.005 wt.%, 0.01 wt.%, 0.02 wt.%), the thermal conductivity ratios are almost the same, but the binary nanofluid with 0.01 wt% of CNTs shows slightly higher results in all the cases. Nevertheless, with higher mass fraction of CNTs (0.2 wt.%), the thermal conductivity ratios are remarkably lower, probably due to the bad distribution stability showed in Figure 3.16.

Furthermore, the thermal conductivity ratios of the binary nanofluid were found to increase slightly with temperature for almost all of the measured samples. Then, it makes the binary nanofluid even more attractive for applications with high temperature.

Seeing that, 0.01 wt.% of CNTs was the optimum concentration, thermal conductivity measurements were made at different NH_3 mass fractions in the base fluid (See Table 4.7 and Table 4.8). In this case, the maximum enhancement of thermal conductivity for 0.01 wt.% of CNTs is 6.0 % at 50 wt.% of NH_3 and 343.10 K. Figure 4.9 shows that thermal conductivity ratios are similar for NH_3 mass fractions of 40 wt.% and 50 wt.% and, enhancement is significantly smaller for lower NH_3 mass fraction as 30 wt.%.

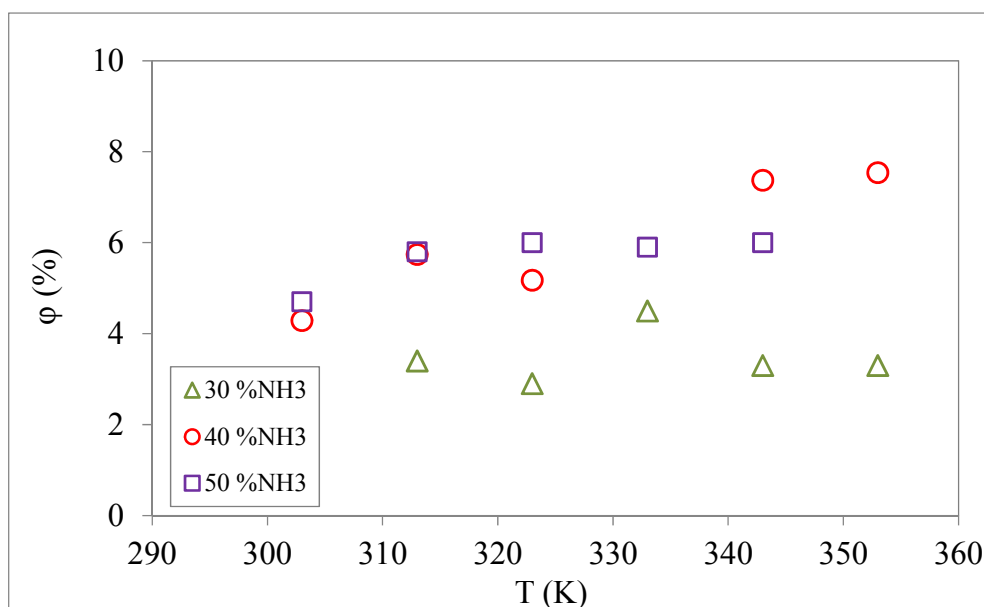


Figure 4.9: Thermal conductivity ratio comparison of NH_3 concentrations with 0.01 wt% of CNTs

Chapter 4: Results and Discussion

Some of the observed results are interesting but, the level of thermal conductivity enhancement with the addition of CNTs is significantly smaller than other experimental results for nanofluids reported in the literature. However, the conductivity enhancements found in this work are close of previously reported data by other authors [76], [77] who added nanoparticles into working pairs of absorption cycles.

Although it is beyond the scope of this work and the mechanisms leading to this enhancement are still under discussion, several researchers have discussed and proposed models that rely on the Brownian motion of the nanoparticles [97]. Brownian motion is the random movement of particles suspended in a fluid and possibly collide allowing transport heat between solid-solid, thereby increasing thermal conductivity [98]. Also, Brownian motion is found to dominate in small particles, low volume concentration, cylindrical shape and high temperatures [99], which could explain the causes of the increased thermal conductivity in our system.

On the other hand, this modest increase in conductivity has resulted in outstanding heat and mass transfer coefficients with these binary fluids [100], [87], [101], [102], [92], [103], and [104]. From studies, it is considered as possible reasons of the mass transfer enhancements mainly in bubble systems, induced micro disturbances and increase in the gas-liquid interfacial bubble area due to the motion and nanoparticles interaction. In addition, Krishnamurthy et al. 2006 [102] showed that an optimum volume fraction of nanoparticles could results in mass transfer enhancements higher than on the thermal conductivity.

4.6 Summary

Comparing the thermal conductivity data of the three binary working fluids measured in this work, it can be observed that values for the new mixture $\text{NH}_3 + \text{LiNO}_3$ are in the order of $0.3 \text{ W}\cdot\text{m}^{-1}\cdot\text{K}^{-1}$ while $\text{NH}_3 + \text{H}_2\text{O}$ and $\text{H}_2\text{O} + \text{LiBr}$ are ranging around $0.4 \text{ W}\cdot\text{m}^{-1}\cdot\text{K}^{-1}$ and $0.5 \text{ W}\cdot\text{m}^{-1}\cdot\text{K}^{-1}$. These lower thermal conductivity results confirm the low rates of heat and

mass transfer in the absorber, working with this mixture, as was predicted by other authors [14], [15], [16].

With the addition of water or carbon nanotubes in the binary mixture $\text{NH}_3 + \text{LiNO}_3$, results indicate an enhancement on the effective thermal conductivity in both cases. Using water as a third component with high affinity for ammonia not only decrease the viscosity of the mixture, it was also found an average enhancement of thermal conductivity up to 8 % and 11 % with 0.20 and 0.25 water mass fractions, respectively. On the other hand, results containing only a small amount of CNTs also suggest a thermal conductivity enhancement, but in this case this improvement is slightly lower than those for water. The maximum enhancement achieved was 7.5 % with 40 wt.% of NH_3 and 0.01 wt.% of CNTs.

Chapter 5

5. Modelling Thermal Conductivity

The difficulties in the thermal conductivity measurements of working fluids related to the high vapour pressure of the mixture have prompted the development of a predictive model which can be used to extend known information to other conditions of temperature and concentration, for which the thermal conductivity has not been measured.

Many correlations methods for thermal conductivity of general liquid mixtures available in the literature [96] were reviewed. The selected methods are described separately and evaluated later together with one of our target mixtures in this work ($\text{NH}_3 + \text{H}_2\text{O}$). After, these correlations were attempted to use with the other mixtures studied in this work such as $\text{NH}_3 + \text{LiNO}_3$ and $\text{NH}_3 + \text{LiNO}_3 + \text{H}_2\text{O}$. Neither of the mixtures was accurately fitted using these methods. Finally, a comprehensive model based in the local composition concept and taking account the electrolytes effect, has been used to correlate all the target mixtures.

Filippov Equation (1955) [58]

The equation (5.1) proposed by Filippov has been extensively tested for organic binary mixtures, although is not suitable for multicomponent mixtures.

$$k_m = w_1 k_1 + w_2 k_2 - 0.72 w_1 w_2 (k_2 - k_1) \quad (5.1)$$

The constant 0.72 may be replaced by an adjustable parameter when the binary mixture data are available. The choice of which component is number 1 or number 2 is made with criterion $k_2 \geq k_1$. The uncertainty found was less than 5 %.

Chapter 5: Modelling Thermal Conductivity

Jamieson, et al. Correlation (1975) [59]

Equation (5.2) was suggested for binary mixtures.

$$k_m = w_1 k_1 + w_2 k_2 - \alpha (k_2 - k_1) \left[1 - (w_2)^{1/2} \right] w_2 \quad (5.2)$$

As in the Filippov method the equation enables to estimate thermal conductivity for all types of binary mixtures with or without water. In this case the uncertainty was less than 3%. However, it cannot be extended to multicomponent mixtures. The adjustable parameter (α) is set equal to unity if mixture data are unavailable for regression purposes. The components are so selected that $k_2 \geq k_1$.

Baroncini, et al. Correlation (1984) [105]

Thermal conductivity can be estimated from equation (5.3) calculating the A parameter (5.4) from the reduced temperature of the mixture T_{rm} (5.5). Where, T_{c1} and T_{c2} are the pure component critical temperatures. The choice of which component is number 1 or number 2 is made with criterion $A_1 \leq A_2$.

$$k_m = \left[x_1^2 A_1 + x_2^2 A_2 + 2.2 \left(\frac{A_1^3}{A_2} \right)^{1/2} x_1 x_2 \right] \frac{(1 - T_{rm})^{0.38}}{T_{rm}^{1/6}} \quad (5.3)$$

$$A = \frac{k \cdot T_{rm}^{1/6}}{(1 - T_{rm})^{0.38}} \quad (5.4)$$

$$T_{rm} = \frac{T}{T_{cm}} \quad (5.5)$$

$$T_{cm} = x_1 T_{c1} + x_2 T_{c2} \quad (5.6)$$

The correlation was verified with 50 binary systems of organic liquids including those with highly polar components. Also, the method is not suitable for multicomponent mixtures. The average error found was about 3%.

Method of Rowley (1988) [106]

In this procedure, the liquid phase is modelled by using a two-liquid theory wherein the energetics of the mixture is assumed to favour local variations in composition. For a binary system of 1 and 2, thermal conductivity can be calculated by:

$$k_m = w_1 k_1 + w_2 k_2 + w_1 w_2 \left[\frac{G_{21} (k_{12} - k_1)}{w_1 + w_2 G_{21}} + \frac{G_{12} (k_{12} - k_2)}{w_2 + w_1 G_{12}} \right] \quad (5.7)$$

Where k_{12} is found from equation (5.8) and is a characteristic parameter for the thermal conductivity that expresses the interactions between 2 and 1 in $\text{W}\cdot\text{m}^{-1}\cdot\text{K}^{-1}$.

$$k_{12} = \frac{(w_1^*)^2 (w_2^* + w_1^* G_{12}) k_1 + (w_2^*)^2 (w_1^* + w_2^* G_{21}) k_2}{(w_1^*)^2 (w_2^* + w_1^* G_{12}) + (w_2^*)^2 (w_1^* + w_2^* G_{21})} \quad (5.8)$$

$$w_1^* = \frac{M_1 G_{21}^{1/2}}{M_1 G_{21}^{1/2} + M_2 G_{12}^{1/2}} \quad ; \quad w_2^* = 1 - w_1^* \quad (5.9)$$

To employ this technique, values for the liquid thermal conductivities of the pure components are required. In addition, the NRTL parameters G_{12} and G_{21} related with the activity coefficients and the polar solubility parameter must be found. Here the parameter values used were $G_{12}=2.0839$ and $G_{21}=0.3546$. The method was tested with data on 18 ternary mixtures founding an average absolute deviation of 1.86%.

Sun and Teja (2003) [107]

The equation (5.10) proposed initially by Bohne *et al*, 1984 [108] was used to correlate the thermal conductivity of ethylene glycol + water mixtures as a function of temperature and mass fraction. Coefficients A, B and C obtained by fitting the data of EG + Water are 0.14219, 0.38715 and -6.6551E-04, respectively. The maximum deviation found was 1.82%.

$$k_m = w_1 k_1 + w_2 k_2 + (k_1 - k_2) w_1 w_2 (A + B w_1 + C T) \quad (5.10)$$

Chapter 5: Modelling Thermal Conductivity

Then, the experimental data obtained in this work for $\text{NH}_3 + \text{H}_2\text{O}$ mixtures was attempted to correlate with the above equations proposed for general liquid mixtures, although in almost all cases these equations were used with organic systems.

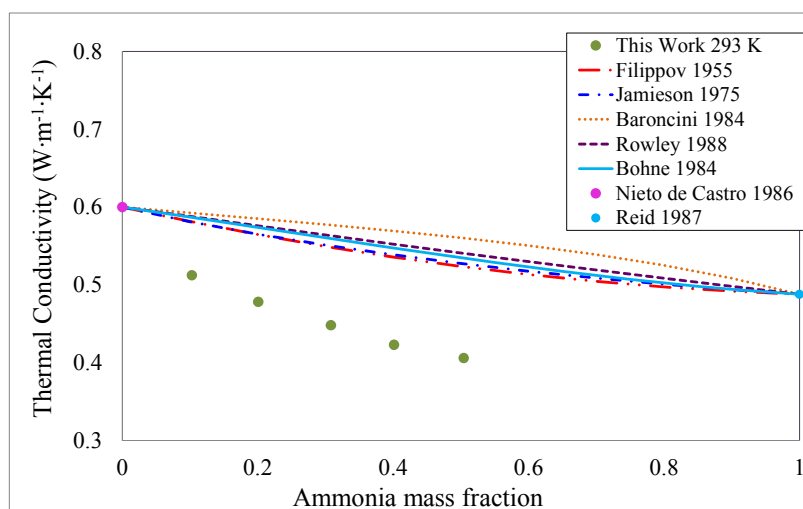


Figure 5.1: Comparison of some predictive methods with the experimental data of $\text{NH}_3 + \text{H}_2\text{O}$ at 293 K.

Figure 5.1 shows the comparison of those correlations, proposed for general liquid mixtures (most of them organic mixtures), with the experimental data of $\text{NH}_3 + \text{H}_2\text{O}$ at 293.15 K. Pure component thermal conductivities required in the calculations are also presented [29], [109]. It can be observed that using these methods with their original adjustable parameters would not yield coherent with those for $\text{NH}_3 + \text{H}_2\text{O}$ mixtures obtained experimentally, maybe because of the highly non-ideal nature of this fluid. These discrepancies have also been noted by Conde (2006) [57], who tried to correlate the experimental thermal conductivity of $\text{NH}_3 + \text{H}_2\text{O}$ mixtures available in the literature [53], [54], [55], [56] using the equations proposed by Filippov (1955) [58] and Jamieson et al. (1975) [59]. He found that neither of these equations was able to accurately fit all the published data.

Regarding to Figure 5.1, the equations proposed by Filippov, Jamieson and Bohne have reasonable agreement with experimental trends. The trend between Filippov and Jamieson equations is quite similar. Then, new fitting parameters have been found and replaced in the Filippov and Bohne equation. The question is whether the adjustable parameter should be independent of the temperature. In the Filippov equation, the adjustable parameter (X) was

related with temperature in the form of $[X = A + B \cdot T]$. The adjustable coefficients for both equations are presented in

Table 5.1, obtained by using the experimental data of $\text{NH}_3 + \text{H}_2\text{O}$ of this work.

Table 5.1: Adjustable parameters in the Filippov and Bohne equation with $\text{NH}_3 + \text{H}_2\text{O}$

(Filippov)		(Bohne)		
A	B	A	B	C
36.732	-0.108	8.119	-2.239	-0.108

The experimental values of $\text{NH}_3 + \text{H}_2\text{O}$ mixtures measured at 293.15 K, 303.15 K and 313.15 K are plotted in Figure 5.2, together with the calculated values by Filippov and Bohne equations using the new adjustable parameters shown in Table 5.1. Results show good agreement in both cases and the two equations are able to correlate the data equally well with a root mean square error of 1.1 % with Filippov and 0.8 % with Bohne.

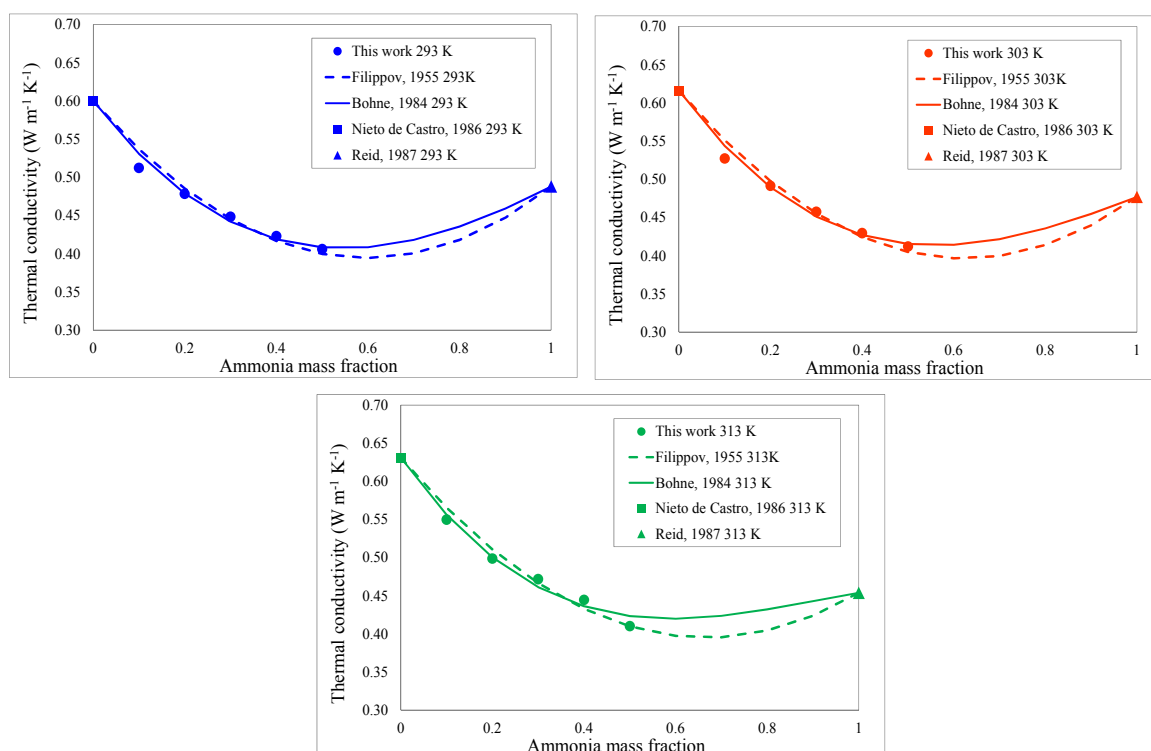


Figure 5.2: Comparison of Filippov and Bohne equation using the new fitting parameters with the experimental data of $\text{NH}_3 + \text{H}_2\text{O}$ at different temperatures.

Chapter 5: Modelling Thermal Conductivity

However, it was desired to find a method able to fit the experimental data of the three major mixtures studied in this work and used in absorption machines such as, $\text{NH}_3 + \text{H}_2\text{O}$, $\text{NH}_3 + \text{LiNO}_3$ and $\text{NH}_3 + \text{LiNO}_3 + \text{H}_2\text{O}$. Followed, the experimental data of $\text{NH}_3 + \text{LiNO}_3$ obtained in this work at the temperature range between 303.15 K to 353.15 K was attempted to correlate with the Filippov and Bohne equations. Now the adjustable parameter (X) in Filippov equation was related with the temperature and the mass fraction of ammonia in the form of $[X = A + B w_1 + CT]$ similar to Bohne equation. Coefficients for both equations are presented in Table 5.2, obtained by fitting the experimental data of $\text{NH}_3 + \text{LiNO}_3$.

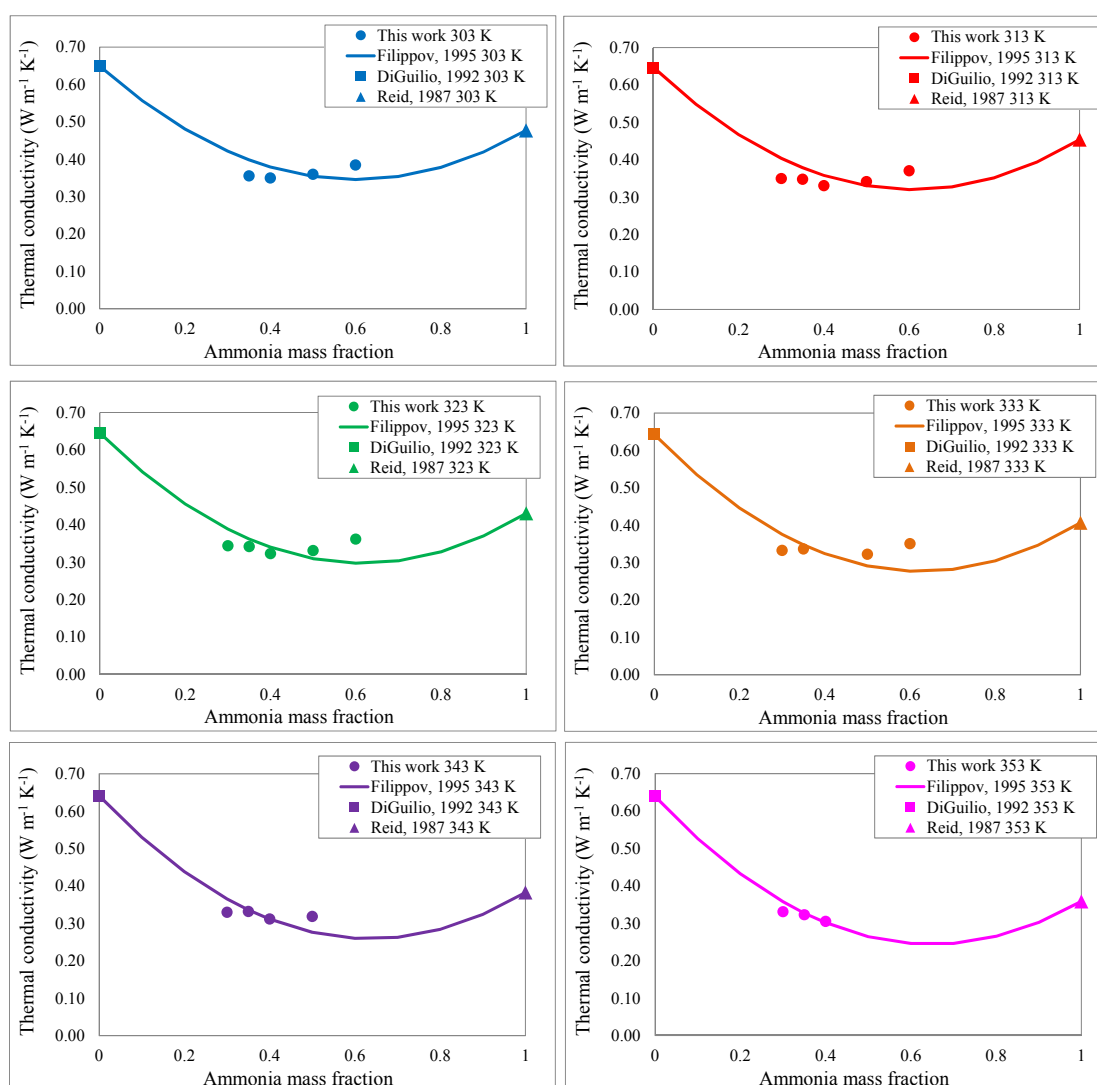


Figure 5.3: Comparison of Filippov equation with the experimental data of $\text{NH}_3 + \text{LiNO}_3$ at different temperatures

Table 5.2: Adjustable parameters in Filippov and Bohne equations with $\text{NH}_3 + \text{LiNO}_3$

(Filippov)			(Bohne)		
<i>A</i>	<i>B</i>	<i>C</i>	<i>A</i>	<i>B</i>	<i>C</i>
14.119	-0.032	-0.031	9.698	-7.080	-0.047

Neither of the temperatures was accurately fitted using the Filippov equation. Results in Figure 5.3 clearly show disagreement with the experimental trends.

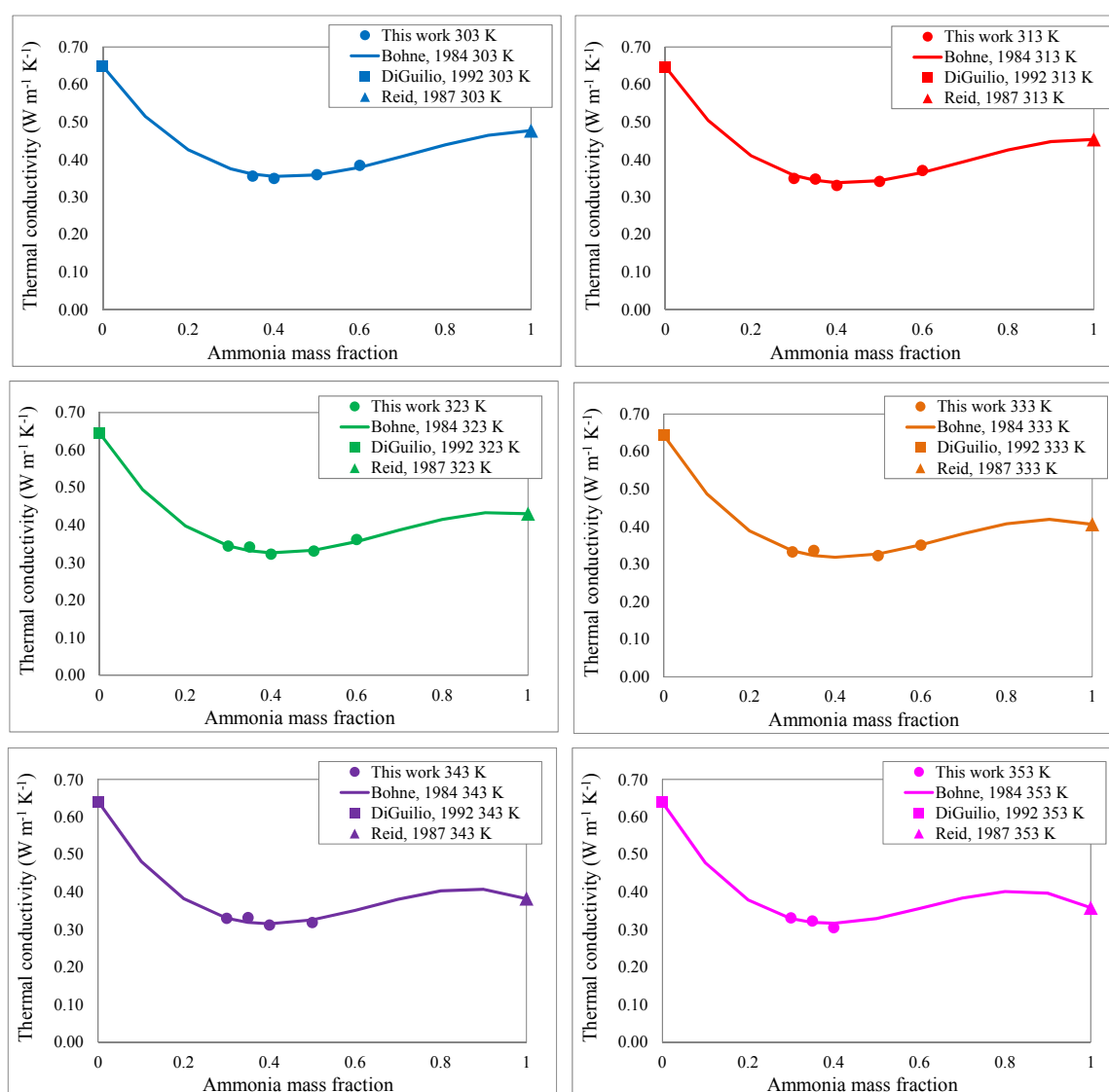


Figure 5.4: Comparison of Bohne equation with the experimental data of $\text{NH}_3 + \text{LiNO}_3$ at different temperatures

Chapter 5: Modelling Thermal Conductivity

Figure 5.4 shows experimental and calculated values for the $\text{NH}_3 + \text{LiNO}_3$ system using the correlation proposed by Bohne. This equation fit the data well over the temperature range but at high concentrations of ammonia the curve has a S-shape trend unusual in these systems. Therefore the equations proposed by Filippov and Bohne were able to accurately fit the experimental data of $\text{NH}_3 + \text{H}_2\text{O}$ mixtures but on the other hand, it was not able to correlate $\text{NH}_3 + \text{LiNO}_3$ mixtures over a wide range of temperatures.

After have tried different methods for general liquid mixtures it seems that the above equations can accurately fit $\text{NH}_3 + \text{H}_2\text{O}$ mixtures but on the other hand, the correlations disagree with the experimental data of $\text{NH}_3 + \text{LiNO}_3$. Probably the reason is the different behaviour of the mixture due to the electrolyte contribution. Hence, a new literature review involving electrolyte solutions was made. The published correlation methods have been reviewed [110] and the most widely used expression is that of Riedel, 1951 [17] (See equation (5.11)). It is a simple expression in terms of molar concentration (x_i) where the thermal conductivity of pure water and the ion contribution (α_i) are needed.

$$k = k_{\text{H}_2\text{O}} + \sum_i \alpha_i x_i \quad (5.11)$$

The equation is applicable to a multicomponent system, however is not recommended for high concentrations and strong acids and bases. Also, it is not accurate for systems that show complicated trends with maximum and minimums, such as our systems, where the thermal conductivity decreases first with the concentration of ammonia and then increase. Other correlations presented in the literature [110] for electrolyte solutions have similar restrictions of concentration and temperatures, or on the other hand the equations require much more information. Finally, a comprehensive model for calculating the thermal conductivity of aqueous, nonaqueous and mixed-solvent electrolyte systems has been chosen. Wang and Anderko (2008) [111] developed a model accounting the effect of electrolytes contribution by the Riedel coefficients (α_i), which quantified the contribution of individual ions, and a contribution of specific interactions between ions or neutral species (β_{ik}). Moreover, the model is based in the local composition concept embodied in the UNIQUAC and NRTL models and relies on the use of local area fractions for modelling

energy transport in liquid mixtures. It seems that these models are typically used for moderately and strongly non ideal binary mixtures. More in detail, the thermal conductivity of multicomponent solvent mixtures can be represented using surface area parameters and thermal conductivities of pure components in conjunction with a single binary parameter per solvent pair.

Then, the thermal conductivity of the binary solvent k_m in the Wang and Anderko (2008) model [111] is given by equation (5.12):

$$k_m = \sum_i^n w_i \sum_j^n \theta_{ji} k_{ji} \quad (5.12)$$

where w_i is the mass fraction of component i , θ_{ji} is the local area fraction which is the fraction of external sites around molecule j which are occupied by segments of molecule i determined from equation (5.13):

$$\theta_{ji} = \frac{\theta_j \tau_{ji}}{\sum_k^n \theta_k \tau_{ki}}, \quad \sum_j^n \theta_{ji} = 1 \quad (5.13)$$

where τ_{ji} and τ_{ki} are parameters related to the energetic interaction between the molecules. Such interactions play a minimal role in calculating thermal conductivity, and therefore these parameters may be set equal to 1. The average area fraction θ_j is defined by equation (5.14):

$$\theta_j = \frac{x_j Q_j}{\sum_k^n x_k Q_k} \quad (5.14)$$

where x_j is the mole fraction of component j , and Q_j is the surface area parameter for molecule j obtained by Bondi method (1960) [112] for NH_3 ($Q = 0.98$) and for H_2O ($Q=1.4$). Finally,

Chapter 5: Modelling Thermal Conductivity

$$k_{ij} = k_{ji} = (w_i^* k_i + w_j^* k_j) \cdot (1 - X_{ij}) \quad (5.15)$$

where k_i and k_j are the thermal conductivities of the pure components, w_i^* and w_j^* are determined from equation (5.16) and $X_{ij} = 0.5256$ is the adjustable binary parameter found by fitting the experimental data of $\text{NH}_3 + \text{H}_2\text{O}$.

$$w_i^* = \frac{Q_j M_i}{Q_j M_i + Q_i M_j}; \quad w_j^* = 1 - w_i^* \quad (5.16)$$

In this work the model based in the local composition concept was used to correlate the experimental data of $\text{NH}_3 + \text{H}_2\text{O}$ as a binary solvent. Results show that the model was able to correlate the data with good agreement in the experimental trend for all the studied temperatures (Figure 5.5).

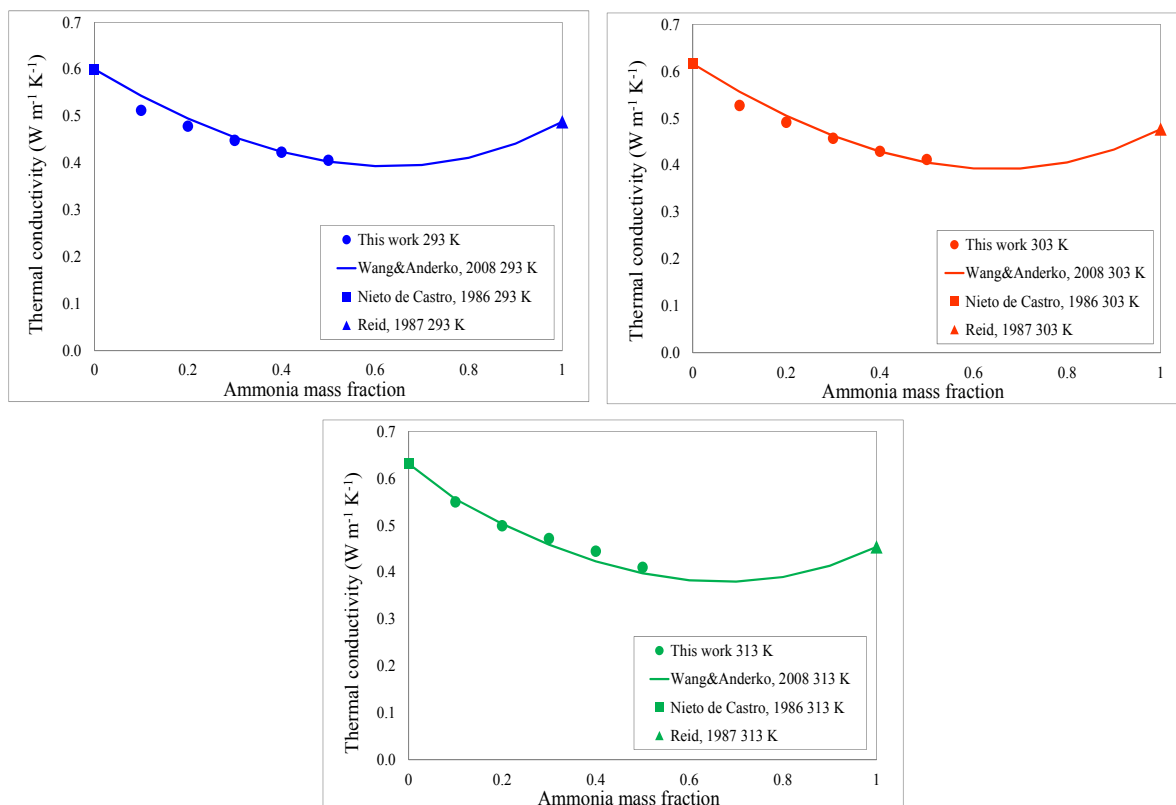


Figure 5.5: Comparison between calculated values by Wang and Anderko (2008) model and experimental data of $\text{NH}_3 + \text{H}_2\text{O}$ at different temperatures.

Once is confirmed that the model [111] correlate the binary mixed solvent studied in this work, now it is desired to correlate the values of thermal conductivity for the binary mixture $\text{NH}_3 + \text{LiNO}_3$, formed by a single solvent (NH_3) and an electrolyte solute (LiNO_3).

Thus, three contributions should be included for modelling thermal conductivity of electrolyte solutions: First, thermal conductivity of the solvent mixture (k_m); Second a contribution of individual ion-solvent interactions (Δk^s), quantified by Riedel's coefficients (α); Third, a contribution of interactions between pairs of species (Δk^{s-s}), quantified by a binary parameter (β) depending on the ionic strength between the solute and the solvent mixture.

Accordingly, the thermal conductivity of an electrolyte solution is expressed as a sum of the three contributions:

$$k = k_m + \Delta k^s + \Delta k^{s-s} \quad (5.17)$$

The contribution of individual ion in a mixed-solvent electrolyte solution can be expressed as:

$$\Delta k^s = \sum_j \sum_i x_j' x_i \alpha_{ij} \quad (5.18)$$

where x is the mole fraction, the subscripts j denotes the solvent components and i the solute ions. In this case the mole fraction of solvent is based in salt-free basis. For an electrolyte solution with a single solvent, equation (5.18) can be reduced to:

$$\Delta k^s = \sum_i x_i \alpha_i \quad (5.19)$$

A temperature dependence of the α_i coefficient is given by:

$$\alpha = \alpha_1 + \alpha_2 \exp[-0.023(T - 273.15)] \quad (5.20)$$

Coefficients α_1 and α_2 are determined on the basis of experimental data for binary electrolyte systems.

Chapter 5: Modelling Thermal Conductivity

The contributions of interactions between all species pairs are defined by:

$$\Delta k^{s-s} = \sum_j \sum_l \sum_i \sum_k x'_j x'_i f_i f_k \beta_{ijkl} \quad (5.21)$$

In cases when there is only one solvent, equation (5.21) reduces to:

$$\Delta k^{s-s} = \sum_i \sum_k f_i f_k \beta_{ik} \quad (5.22)$$

where the subscripts j and l are all solvent components and i and k are all solutes, f_i and f_k are the solute-only mole fraction of the species:

$$f_i = \frac{x_i}{\sum_m x_m} \quad (5.23)$$

The binary parameter β_{ijkl} between the species i and k in a solvent-mixture $j-l$ depends on the ionic strength in the form of:

$$\beta_{ijkl} = \beta_{ijkl}^{(1)} + \beta_{ijkl}^{(2)} I_x^2 + \beta_{ijkl}^{(3)} \exp\left(\beta_{ijkl}^{(0)} I_x\right) \quad (5.24)$$

This parameter is very important when thermal conductivity data extend to higher concentrations and when the system shows a complex behaviour. The parameter I_x is related with the mole fraction based ionic strength:

$$I_x = \frac{1}{2} \sum_{ions} z_i^2 x_i \quad (5.25)$$

A temperature dependence of each binary pair $\beta_{ijkl}^{(m)}$ ($m=1, 2, 3$) is given by:

$$\beta_{ijkl}^{(m)} = \beta_{ijkl}^{(m0)} \exp\left(\beta_{ijkl}^{(mT)} (T - 273.15)\right) \quad (5.26)$$

where $\beta_{ijkl}^{(m0)}$ and $\beta_{ijkl}^{(mT)}$ are adjustable parameters.

Thus, the model has been applied to the electrolyte mixture $\text{NH}_3 + \text{LiNO}_3$ with a single solvent (NH_3) and to the ternary mixture $\text{NH}_3 + \text{LiNO}_3 + \text{H}_2\text{O}$ with a mixed-solvent ($\text{NH}_3 + \text{H}_2\text{O}$).

In the first step of parameter regression, the coefficients α_1 and α_2 have been determined for individual ions based on experimental data for $\text{NH}_3 + \text{LiNO}_3$, and on literature data for aqueous solution ($\text{LiNO}_3 + \text{H}_2\text{O}$) [111]. For the ternary mixture, the adjustable coefficients α_1 and α_2 for each binary pair involved in the multicomponent solution were used. These parameters are collected in Table 5.3.

Table 5.3: Coefficients used in equation (5.20) for selected Ions.

Species	α_{1,NH_3}	α_{2,NH_3}	$\alpha_{1,\text{H}_2\text{O}}$	$\alpha_{2,\text{H}_2\text{O}}$
Li^+	-0.069565	-0.165749	-0.207041	0.057691
NO_3^-	-0.663428	-0.321705	-0.422374	0.033717

The parameters $\beta_{ijkl}^{(m0)}$ and $\beta_{ijkl}^{(mT)}$ have been determined by regressing the experimental data of this work for $\text{NH}_3 + \text{LiNO}_3$ and $\text{NH}_3 + \text{LiNO}_3 + \text{H}_2\text{O}$. These parameters are summarized in Table 5.4.

Table 5.4: Interaction parameters used in equation (5.26) for each studied mixture.

System	$\beta_{ijkl}^{(10)}$	$\beta_{ijkl}^{(11)}$	$\beta_{ijkl}^{(20)}$	$\beta_{ijkl}^{(21)}$
$\text{NH}_3 + \text{LiNO}_3$	-0.2724402	-0.4180173	5.6252506	0.0080053
$\text{NH}_3 + \text{LiNO}_3 + \text{H}_2\text{O}$	2.7176499	-0.0292327	3.1001896	-0.0292332

The parameters $\beta_{ijkl}^{(30)}$, $\beta_{ijkl}^{(31)}$ and $\beta_{ijkl}^{(0)}$ were set equal to 0 for the indicated pairs [111].

Figure 5.6 and Figure 5.7 compare the predictions with the experimental data of this work for $\text{NH}_3 + \text{LiNO}_3$ and $\text{NH}_3 + \text{LiNO}_3 + \text{H}_2\text{O}$ systems. The results that have been obtained indicate that there are a high degree of consistency between experimental al calculated trends over wide range of temperature and composition. Therefore, the experimental data

Chapter 5: Modelling Thermal Conductivity

obtained in this work made it possible to evaluate the model parameters with a high level of confidence.

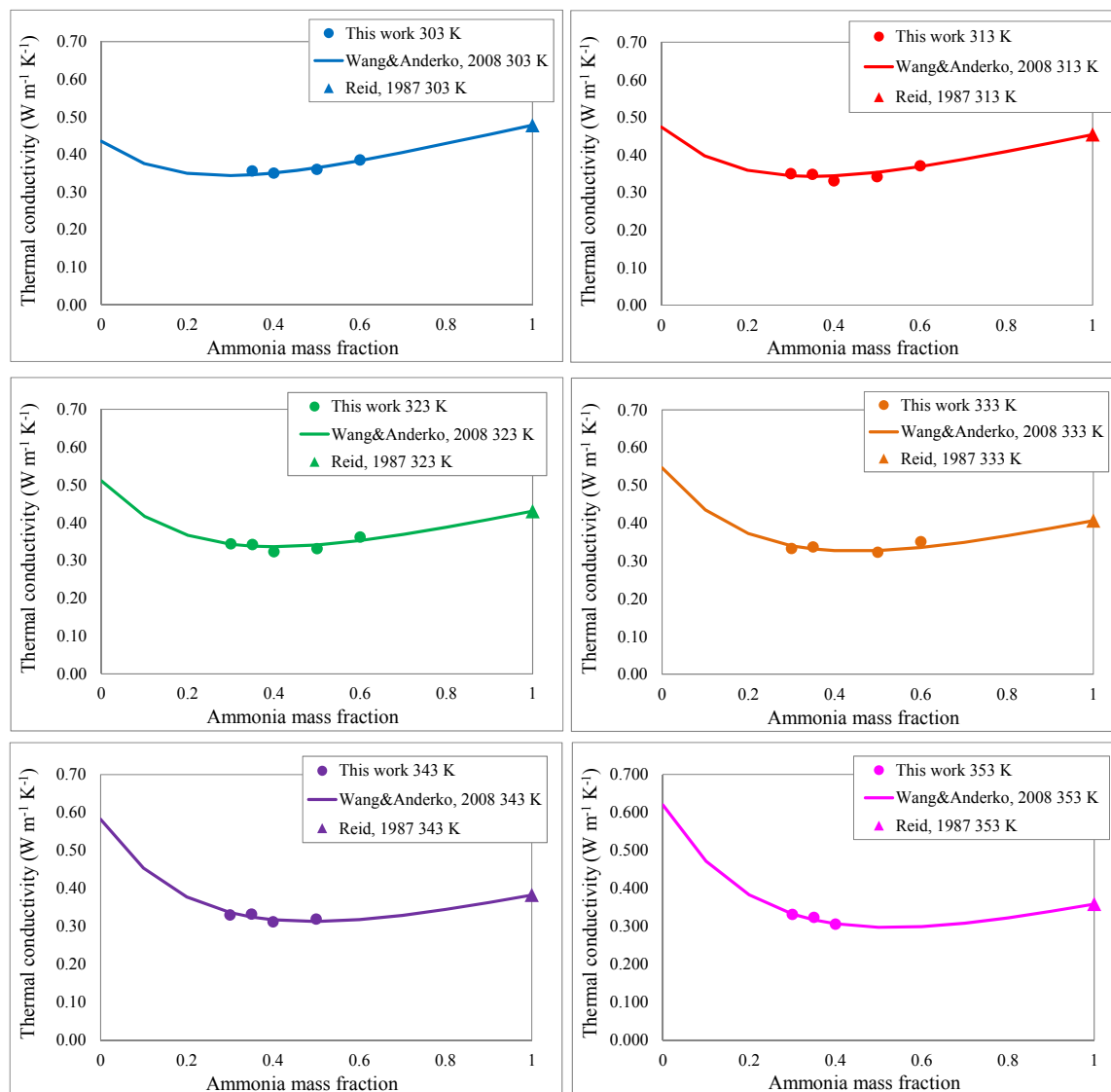


Figure 5.6: Comparison between calculated values by Wang and Anderko (2008) model and experimental data of $\text{NH}_3 + \text{LiNO}_3$ at different temperatures.

Finally, by using the adjustable parameters given in Table 5.3 and Table 5.4 the binary and ternary mixture $\text{NH}_3 + \text{LiNO}_3$ and $\text{NH}_3 + \text{LiNO}_3 + \text{H}_2\text{O}$ were correlated with a root mean square error of 0.8 % and 1.5 %, respectively.

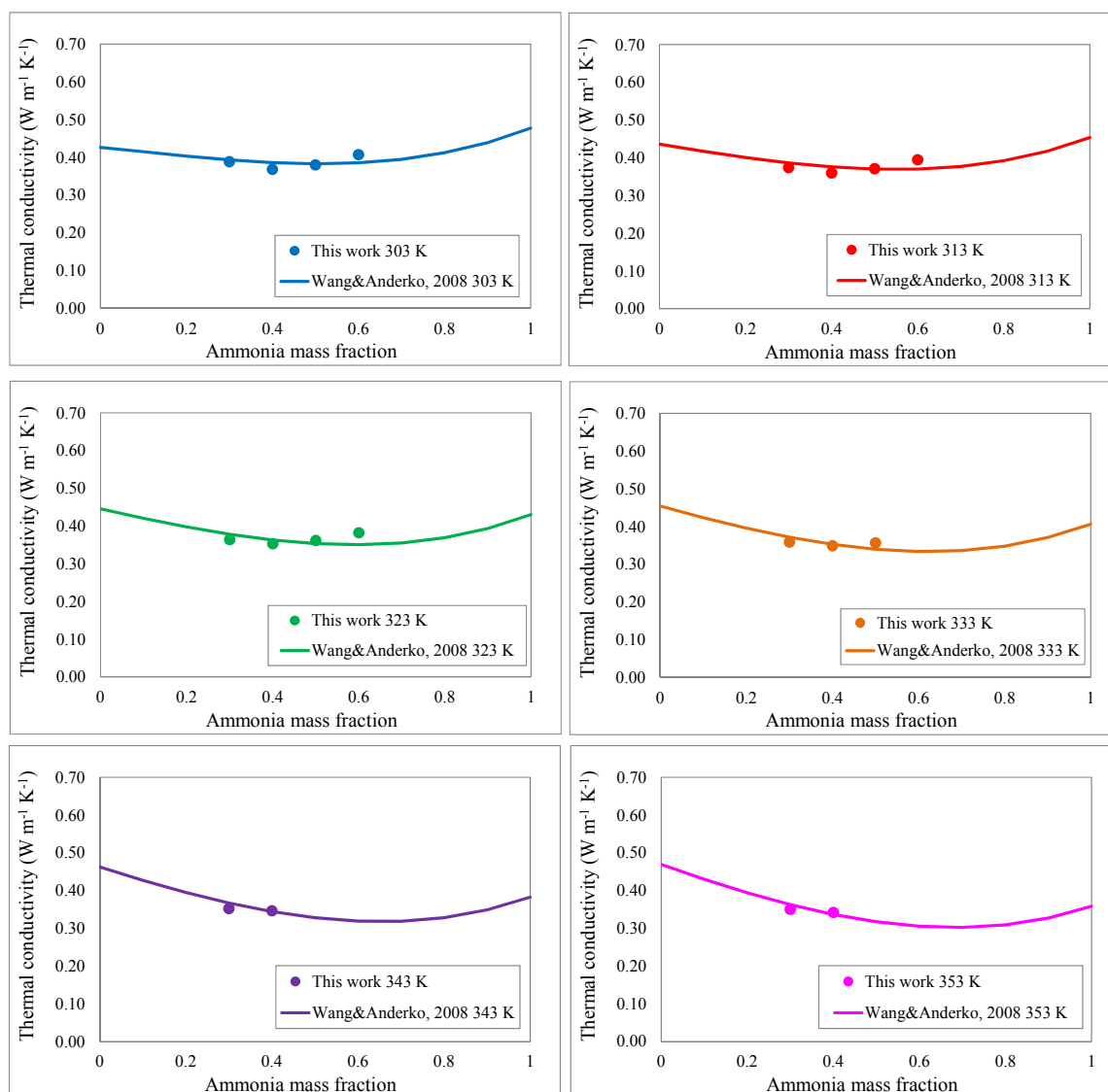


Figure 5.7: Comparison between predicted values by Wang and Anderko (2008) model and experimental data of $\text{NH}_3 + \text{LiNO}_3 + \text{H}_2\text{O}$ (20%) at different temperatures.

SUMMARY

Table 5.5 shows the correlations and models used in this work for each mixture. As was presented earlier not all the correlations were suitable for the different mixtures measured in this work. In order to use a single model suitable to correlate all the systems involved in this study, finally Wang and Anderko model [111] based in the local composition concept

Chapter 5: Modelling Thermal Conductivity

and ion contribution was appropriate for calculating the thermal conductivity of aqueous, nonaqueous and electrolyte systems.

Table 5.5: Correlations and models used in this work for each mixture

Working Fluid	Filippov [58]	Bohne [108]	Wang&Anderko [111]
NH ₃ + H ₂ O	YES	YES	YES
NH ₃ + LiNO ₃	NO	NO	YES
NH ₃ + LiNO ₃ + H ₂ O	-	-	YES

Therefore, all the mixtures were correlated by this model and the obtained deviation in terms of root mean square error for each system are presented in Table 5.6.

Table 5.6: Root Mean Square Error for all the measured systems with Wang&Anderko model

Working Fluid	RMSE
NH ₃ + H ₂ O	1.4 %
NH ₃ + LiNO ₃	0.8 %
NH ₃ + LiNO ₃ + H ₂ O (20 %)	1.5 %
NH ₃ + LiNO ₃ + H ₂ O (25 %)	1.7 %

Chapter 6

6. Hot Wire Numerical Studies

Numerical simulations have been performed for the THW method in order to exactly represent the geometry of the measurement sensor (glass capillary) and to analyse the coating effect of the wire (glass thickness).

It seems that finite element method (FEM) is a powerful computational technique for approximate solutions to a variety of engineering problems having complex domains subjected to general boundary conditions. Hence, in this study FEM is implemented to validate the simplifications in the mathematical model. A commercially available finite element package ANSYS is used for this numerical analysis.

Using the finite element program ANSYS, the analysis system is carried out by transient thermal in a 2D behaviour axisymmetric geometry. The main tasks of mesh generation, processing (calculations) and graphical representation of results are embedded under a common interface to enable the interaction with all the parts in a single environment.

First it is necessary to determine the geometry of the system. Figure 6.1 shows the computational domain used in the numerical simulations formed by three regions: the mercury part, the insulation layer, which would be the thickness of the glass capillary, and the fluid to be measured.

Thermophysical properties (density, specific heat and thermal conductivity) are assigned to the domain according to each one of these regions. Table 6.1 shows the values used in this work for each material at 343 K with their corresponding literature reference.

Chapter 6: Hot Wire Numerical Studies

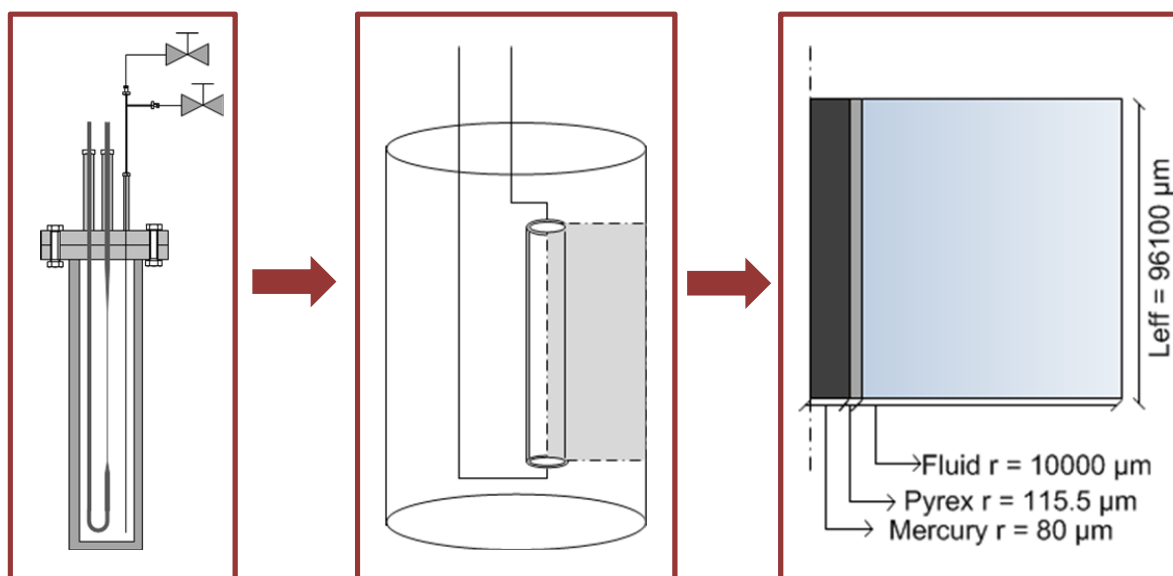


Figure 6.1: 2D-Axisymmetric geometry used in the numerical simulations

Table 6.1: Thermophysical properties for ANSYS

Fluids	Density ($\text{kg}\cdot\text{m}^{-3}$)	Specific Heat ($\text{J}\cdot\text{kg}^{-1}\cdot\text{K}^{-1}$)	Thermal Conductivity ($\text{W}\cdot\text{m}^{-1}\cdot\text{K}^{-1}$)
Mercury [114] ^a [115] ^b	13424 ^a	138 ^a	9.04 ^b
Pyrex 7740 [116] ^c [117] ^d	2230 ^c	810 ^d	1.18 ^c
Toluene [94]	822	1854	0.118
Dimethyl phthalate [94]	1145	346	0.142
Ethylene glycol [94]	1078	2447	0.257
$\text{NH}_3 + \text{LiNO}_3$ (40%) [12] ^e [This work] ^f	1096.9 ^e	2818 ^e	0.312 ^f
$\text{NH}_3 + \text{LiNO}_3 + 20\% \text{H}_2\text{O}$	1032.2 ^e	3103 ^e	0.347 ^f

Discretization of the solution domain into an appropriate computational mesh is the next important step in the finite element simulation. Main factors in the selection of a particular mesh design are the domain geometry, the required accuracy and the cost of computations. A self-adapting mesh of structured quadratic elements with 71027 nodes was used taking in account factors such as; consistency of the adopted mesh with the domain geometry, increase the accuracy of the solution by bonded refinement in the heat transfer region and optimize the computational time by mesh independence test. The mesh independence test

was carried out for 3 different types of mesh regarding their density. First, run an initial simulation with an initial mesh and ensure convergence. Second, refine the mesh globally, for around 2 times the initial mesh size. Run the simulation and compare the temperature increase (ΔT) value from mesh 2 against the value from mesh 1. Since they are not within an acceptable value this means that the solution is changing because of the mesh resolution, and hence the solution is not yet independent of the mesh. Then, mesh 2 is refined again globally two times. In this case when results from mesh 2 are compared with results from mesh 3 they are the same within our allowable tolerance. Now, the solution of mesh 2 is independent of the mesh. The best way to check for a mesh independent solution is to plot the results for each mesh. This is illustrated below in Figure 6.2 where there are three results. Between mesh 1 and mesh 2 there has been a jump in the value of interest (ΔT), but increasing the mesh refinement results are very similar. Consequently, for further analysis we can use mesh 2 as it will give us a result within tolerance and will reduce the simulation run time. This process should be carried out once, and next time for a similar problem the same mesh sizing can be applied.

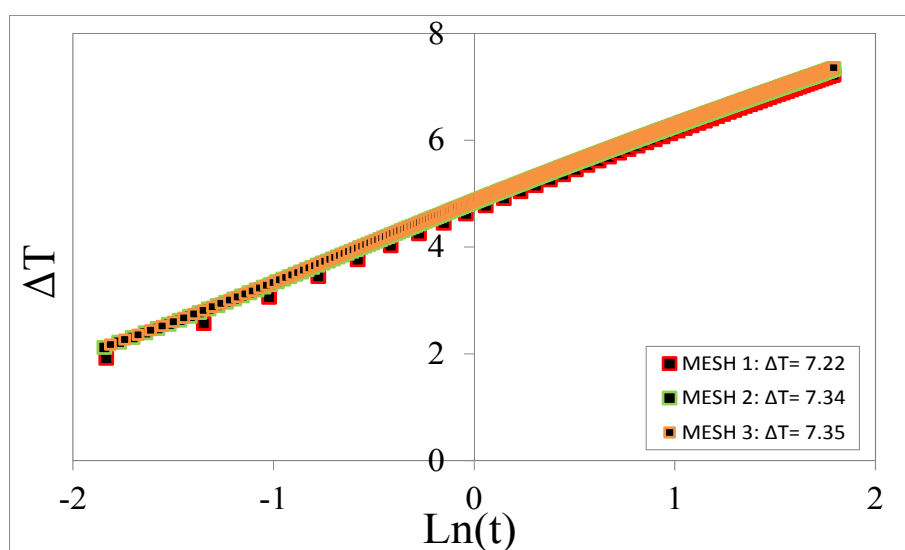


Figure 6.2: Example of mesh independence study for dimethyl phthalate

Once the mesh has been designed, appropriate initial and boundary conditions need to be defined. All the simulations were made with an initial temperature of 343 K and the internal heat generation applied to the mercury was in the order of $1E+8 \text{ W}\cdot\text{m}^{-3}$ with an intensity

Chapter 6: Hot Wire Numerical Studies

value around 0.2 A. This value was determined by using the experimental data of this work. Analysis settings were established as the experimental data used in this work, where the internal heat was applied in 1 step with a maximum time period of 6 seconds.

Figure 6.3 shows an example of one simulation (with Toluene) in order to display the mesh with the refinement in the wall boundary layer where heat gradients are larger, and the temperature profile after 6 seconds.

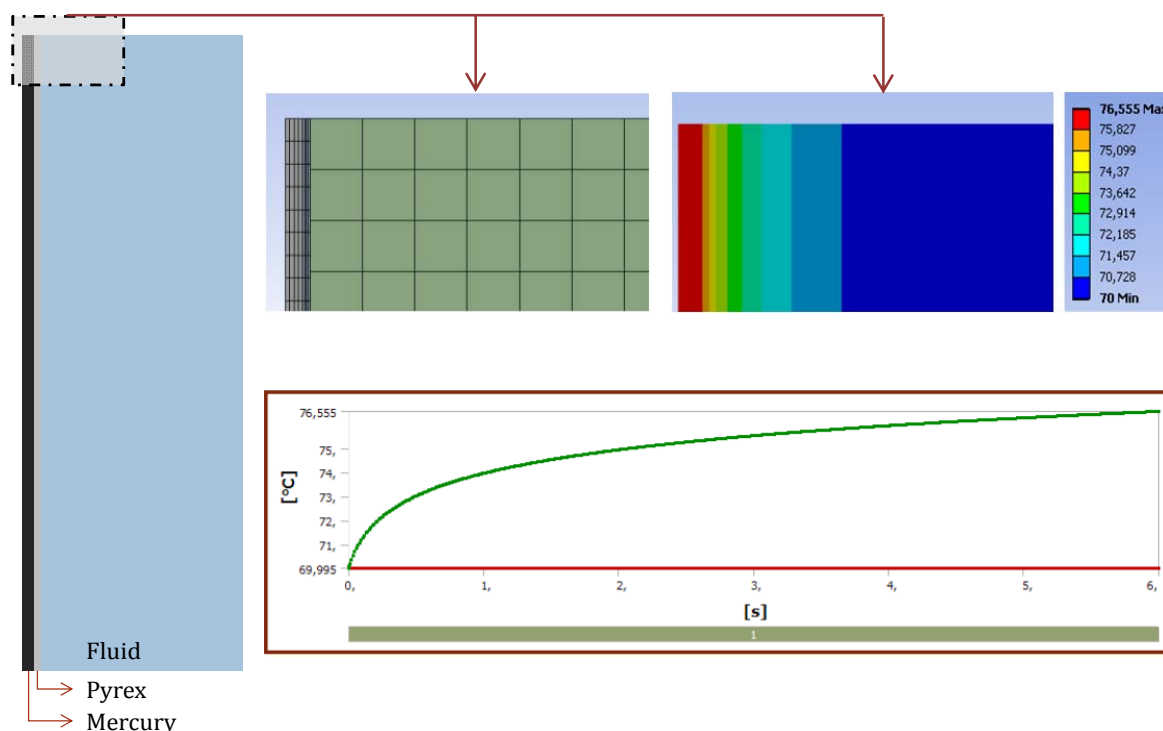


Figure 6.3: 2D-Axisymmetric geometry meshed and the temperature profile for Toluene at 343 K.

It can be verified that temperature profile is only in the x axis which means there are not bi-dimensional effects. Then, from the 2D model it was observed that the sensor is thinner and longer enough, which satisfying the assumption made in the mathematical model of hot wire infinitely thin and long (See section 2.1.3). Also there is a big region without temperature change and this means an infinite medium which was other of the assumptions made in the mathematical model. Consequently, bi-dimensional effects can be neglected and a one dimensional model can be used in this study. However, the computational run

time for solving the 2D model is small in this problem, and finally it was decided to represent the length of the sensor in the numerical simulation in order to characterize the entire geometry.

Numerical analysis of the slope [ΔT vs $\ln(t)$]

After verifying that the model used in the simulations is consistent with the selected mesh and boundaries conditions, the results obtained by the numerical simulation for reference fluids (dimethyl phthalate, toluene and ethylene glycol) are compared with the experimental data in Figure 6.4 in order to analyse how the slope [ΔT vs $\ln(t)$] changes for both cases.

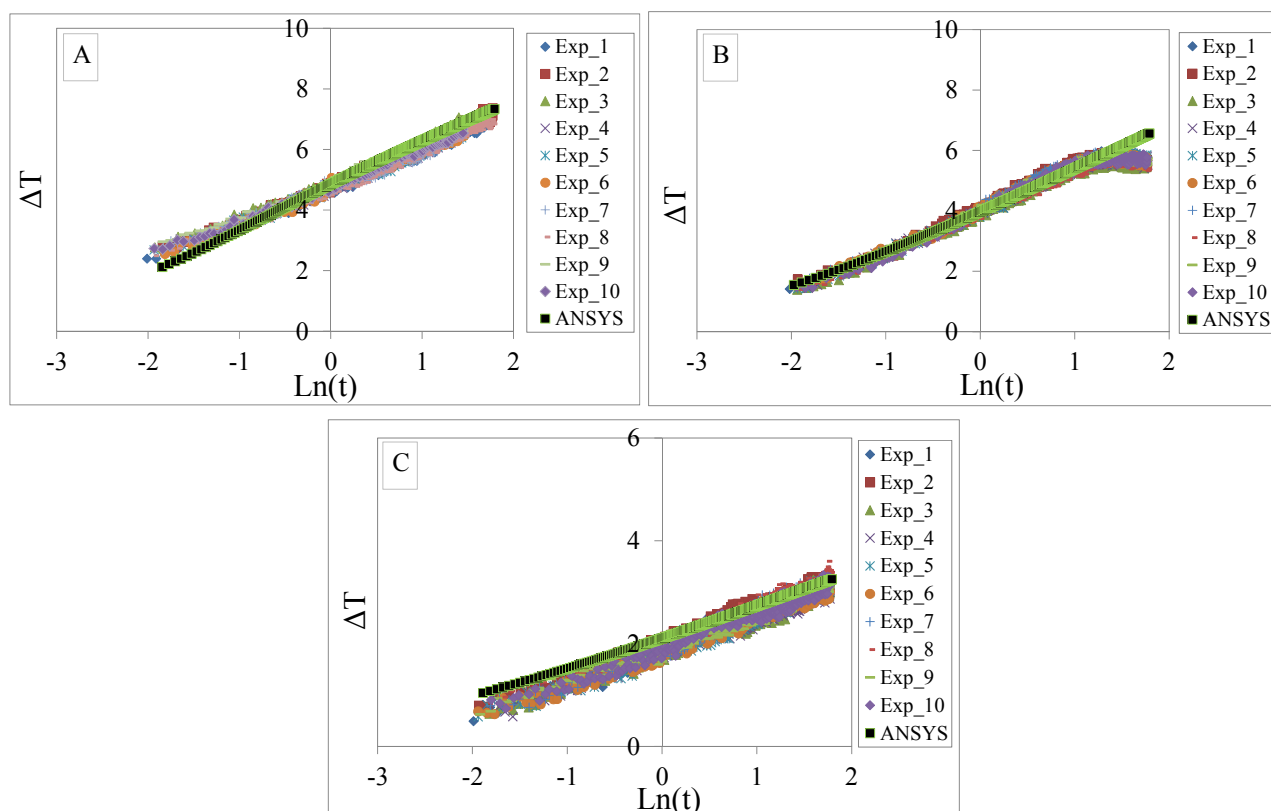


**Figure 6.4: Temperature rise comparison between numerical and experimental data for
A) Dimethyl phthalate B) Toluene and C) Ethylene glycol**

Good agreement between ANSYS calculated values and experimental temperature rise over their trend is observed in Figure 6.4. In order to compare the slope value obtained with the

Chapter 6: Hot Wire Numerical Studies

numerical calculations, and the experimental value used in the calculations of the thermal conductivity, the slope values obtained by ANSYS are plotted versus time. The slope value used for this comparison is the constant value with time in an intermediate interval. Figure 6.5 shows an example with Toluene.

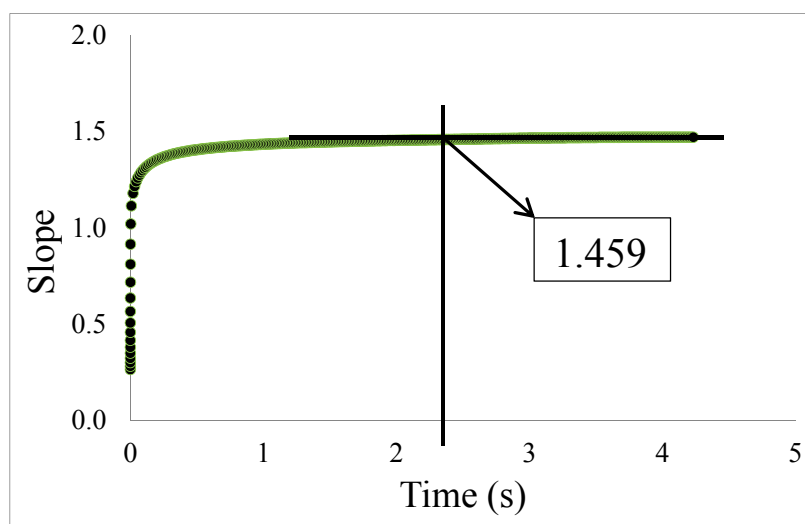


Figure 6.5: Slope selection for ANSYS data with Toluene

Then, using the thermal conductivity value from the literature for the three reference fluids, the slope for each system was calculated by ANSYS and was compared with the experimental measured value. The values obtained using finite element analysis is found to be in reasonable agreement with the experimental values (Table 6.2).

Table 6.2: Comparison between slope values for reference fluids.

Fluids	ANSYS	Experimental	dev (%)
Dimethyl phthalate	1.273	1.237	2.8
Toluene	1.459	1.476	1.2
Ethylene glycol	0.653	0.681	4.3

For the new working fluid proposed in this study ($\text{NH}_3 + \text{LiNO}_3$) and the ternary mixture ($\text{NH}_3 + \text{LiNO}_3 + \text{H}_2\text{O}$) the slope was also calculated numerically and compared with the experimental trend. Figure 6.6 shows good agreements for both cases.

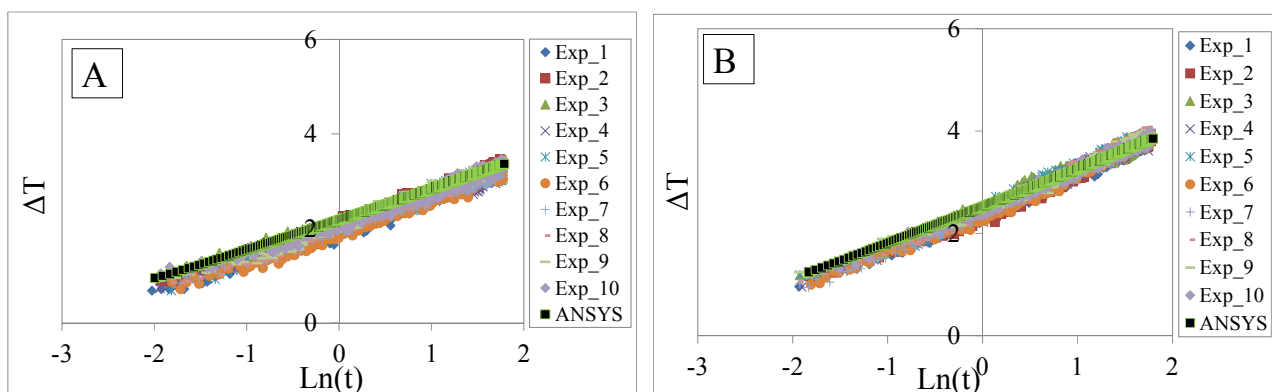


Figure 6.6: Temperature increase comparison between numerical and experimental data for A) $\text{NH}_3 + \text{LiNO}_3$ (40%) and B) $\text{NH}_3 + \text{LiNO}_3 + \text{H}_2\text{O}$ (20%)

Thermal conductivity estimation by ANSYS

In this case, the experimental values of slope were used to calculate the thermal conductivity values for each system by ANSYS. Table 6.3 shows the comparison between experimental and calculated values of thermal conductivity with literature values. Results using finite elements analysis have slightly better agreement than those with the measured values. Nevertheless, both results were in a reasonable agreement with literature data.

Table 6.3: Comparison between thermal conductivity values ($\text{W}\cdot\text{m}^{-1}\cdot\text{K}^{-1}$)

Fluids	Reference	Calculated	Experimental	dev _{CALC}	dev _{EXP}
Dimethyl phthalate	0.142	0.142	0.141	0.0 %	0.7 %
Toluene	0.118	0.118	0.119	0.0 %	0.8 %
Ethylene glycol	0.257	0.256	0.258	0.3 %	0.4 %

Numerical analysis of the coating effects

The objective of this analysis is to understand better the coating effect in the experimental technique. The mathematical model used in this work [28] takes into account the effect on temperature distribution due to thin insulation coating of the wire. The purpose here is to determine how the glass capillary thickness affects the outcome of the transient hot wire

Chapter 6: Hot Wire Numerical Studies

system, by solving numerically the problem with and without this thickness over the source.

The computational domain used in the numerical simulations was the same as the geometry shown in Figure 6.1. First, simulations were made taking in account the three regions: Region 1, the mercury domain, Region 2, the coating domain and Region 3, the fluid domain. On the other hand, with same conditions the simulation was run without Region 2.

The main interest of this analysis is to investigate how the slope [ΔT vs $\ln(t)$] changes due to the presence of the coating. Figure 6.7 shows the temperature rise with coating and without coating for Toluene at 343 K with the time axis in logarithmic scale. Also it can be seen that the presence of the coating changes slightly the temperature profile giving lower values of ΔT . However, the presence of the coating does not change the slope. Moreover, Figure 6.7 shows the lineal relationship between temperature and time presented before for the analytical and for the experimental results.

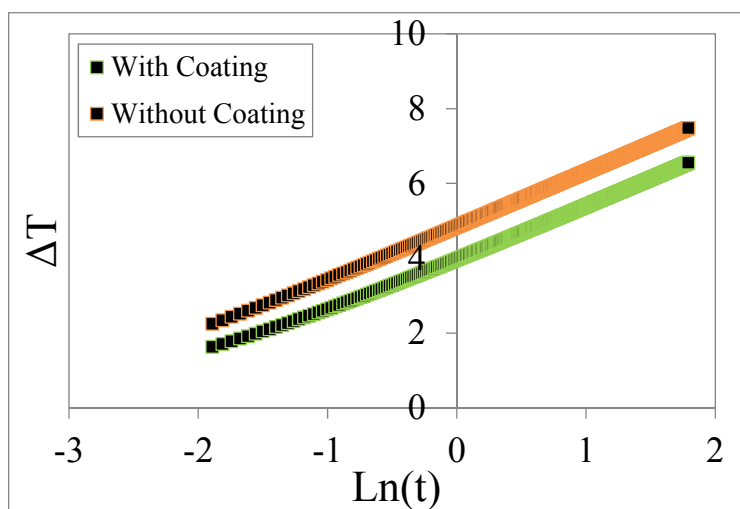


Figure 6.7: Temperature profiles for Toluene at 343 K with coating and without coating

Calculated values of the slope with and without the coating are presented in Table 6.4. The maximum deviation obtained was 0.68 %. Since the slope is an important parameter to determine final values of thermal conductivity, from the simulation can be confirmed than

the effect of the glass capillary thickness does not affect the final result of thermal conductivity.

Table 6.4: Simulation analysis for the coating effect

Fluid	Slope without coating	Slope with coating	Deviation
Toluene	1.47	1.46	0.68 %

In the experiments, the effect of the glass capillary thickness is taking account by determining the effective length experimentally with a reference fluid (See section 3.5). Since the thickness of the glass will change in each new glass capillary, the effective length has to be determined before each set of measurements in each new assembly.

Chapter 7

7. Conclusions

The originally proposed objectives in this study have been carried out, which were the experimental measurement of thermal conductivity of working fluids for absorption cycles. The commercial working fluids $\text{NH}_3 + \text{H}_2\text{O}$ and $\text{H}_2\text{O} + \text{LiBr}$ have been first measured. Available data in the literature for this property is scanty, especially for $\text{NH}_3 + \text{H}_2\text{O}$ at high temperatures and concentrations, and the data shows remarkable inconsistencies. Then, the experimental database available in the literature has been extended with this study. On the other hand, for $\text{H}_2\text{O} + \text{LiBr}$ mixture the available experimental data in the literature shows good agreement and was measured in a wide range of temperature and concentrations. Then, in this study $\text{H}_2\text{O} + \text{LiBr}$ mixture was measured in order to validate the data with our system. Later, the thermal conductivity for the new mixture $\text{NH}_3 + \text{LiNO}_3$ has been also measured. It is a promising mixture for solar activated refrigeration systems; however results show lower thermal conductivity values than those for the commercial working fluids. To overcome this limitation, the addition of water or carbon nanotubes to the new mixture was proposed. Finally, the thermal conductivity enhancement of the ternary mixtures $\text{NH}_3 + \text{LiNO}_3 + \text{H}_2\text{O}$ and $\text{NH}_3 + \text{LiNO}_3 + \text{CNTs}$ was studied in accordance with the main aim of this thesis, and in order to find the optimal conditions to design a highly effective absorption machine.

A transient hot wire system capable to measure the thermal conductivity of electrically conducting fluids and high vapour pressure mixtures was designed and used in this work. At the end, two different approaches were used for thermal conductivity measurements: The first one was based in the common method, using a platinum wire coated by Teflon, with 25 μm of diameter and 10-12 cm of length. The second device was a variant of the

Chapter 7: Conclusions

classical method based in the liquid metal probe concept, using a single glass capillary filled with mercury with 160 μm of inner diameter and 9.6 cm of length.

The apparatus and method were validated by comparing measurements with the values of reference fluids such as toluene, dimethyl phthalate and ethylene glycol. Also, water lithium nitrate as an electrically conductive fluid with similar characteristics than the target mixtures was measured. The maximum relative difference obtained was 2.9 % for the platinum wire device and 3.4 % for the glass capillary device.

Thermal conductivity of $\text{NH}_3 + \text{H}_2\text{O}$ mixtures containing 0.1 to 0.5 ammonia mass fraction has been measured at temperatures between 293.15 and 313.15 K and a constant pressure of 1.5 MPa using the coated platinum wire device. Uncertainties in the data were estimated to be less than $0.017 \text{ W}\cdot\text{m}^{-1}\cdot\text{K}^{-1}$. The obtained thermal conductivity values are in the order of $0.50 \text{ W}\cdot\text{m}^{-1}\cdot\text{K}^{-1}$.

Thermal conductivity of $\text{H}_2\text{O} + \text{LiBr}$ mixtures containing 0.4 LiBr mass fraction has been measured in the temperature range from 298.15 to 428.15 K and a constant pressure of 1.5 MPa using a glass capillary device. In this case the maximum deviation was 2.0 % and the obtained values of thermal conductivity are ranging around $0.55 \text{ W}\cdot\text{m}^{-1}\cdot\text{K}^{-1}$.

Thermal conductivity of $\text{NH}_3 + \text{LiNO}_3$ and $\text{NH}_3 + \text{LiNO}_3 + \text{H}_2\text{O}$ have been measured between 303.15 and 353.15 K and a constant pressure of 1.5 MPa containing 0.3 to 0.6 in ammonia mass fraction, for the ternary mixture the water mass fraction considered in the absorbent was 0.20 and 0.25. Using the glass capillary device, the uncertainties in the data were estimated to be less than $0.025 \text{ W}\cdot\text{m}^{-1}\cdot\text{K}^{-1}$. For the binary mixture, thermal conductivity values are around $0.30 \text{ W}\cdot\text{m}^{-1}\cdot\text{K}^{-1}$. On the other hand, for the ternary mixture values are ranging around $0.40 \text{ W}\cdot\text{m}^{-1}\cdot\text{K}^{-1}$.

Lastly, thermal conductivity of $\text{NH}_3 + \text{LiNO}_3 + \text{CNTs}$ was measured using the glass capillary device between 303.15 and 353.15 K and a constant pressure of 1.5 MPa. Several samples were measured between 0.005 and 0.2 wt.% of CNTs at 0.4 in ammonia mass fraction. Latter at two different compositions of ammonia (0.3 and 0.5) and 0.01 wt.% of CNTs. Uncertainties in the data were estimated to be less than $0.025 \text{ W}\cdot\text{m}^{-1}\cdot\text{K}^{-1}$ and thermal conductivity values are around $0.35 \text{ W}\cdot\text{m}^{-1}\cdot\text{K}^{-1}$.

Uniform dispersion in the binary nanofluid was achieved by oxidation on the structural integrity through nitric acid. Also, the influence of some important parameters on stability was studied and the concentration of nanoparticles was found to be a key parameter.

It is interesting to spot that thermal conductivity enhancement of the ternary mixture has been confirmed in this work. The ternary mixture with 0.25 of water in the absorbent solution shows the higher thermal conductivity enhancement up to 11 % in this study.

With the addition of carbon nanotubes, results also indicate an enhancement of the effective thermal conductivity. All the concentrations of CNTs analysed here have shown an improvement in the thermal conductivity. However, small quantities of CNTs showed greater potential and the optimal CNT content in the absorbent was 0.01 wt.% presenting an increase on its thermal conductivity up to 7.5 %.

Concluding, both cases indicate an enhancement in thermal conductivity but, this improvement is less with CNTs addition than with water addition.

In order to extend the experimental data obtained in this work to other conditions of temperature and concentration, many correlation methods for thermal conductivity in general liquid mixtures have been evaluated. Neither of these correlations was suitable to fit all the mixtures measured in this work. It was necessary to include the contributions due to the electrolyte behaviour involved in the measured mixtures. Finally, the experimental data collected in this study were correlated with temperature and composition by using a model based in the local composition concept and Riedel coefficients for electrolyte effect [111]. New interaction parameters were fitted using the experimental data of this study and the model was able to correlate the two systems: $\text{NH}_3 + \text{H}_2\text{O}$ and $\text{NH}_3 + \text{LiNO}_3$ equally well, with a root mean square error of 1.4 % and 0.8 %, respectively. In addition, the model was also used to predict the thermal conductivity of the ternary mixture $\text{NH}_3 + \text{LiNO}_3 + \text{H}_2\text{O}$; in this case the obtained root mean square error was 1.5 % and 1.7 %, for 0.20 and 0.25 in water mass fraction, respectively.

Numerical simulations using a finite element method have been performed in order to exactly represent the geometry of the measurement sensor and validate the adopted

Chapter 7: Conclusions

assumptions in the mathematical model. Commercially available software, ANSYS, was used for this numerical analysis. The experimental values of the slope (ΔT vs $\ln t$) obtained by the numerical solution were compared with the values obtained by the analytical solution and good agreements were observed, with an average deviation of 2.7 %. Later, the experimental values of slope were used to calculate the thermal conductivity for each reference fluid by ANSYS. Thermal conductivity values obtained by numerical and analytical solution were compared with literature data and both results were in a reasonable agreement. The maximum relative difference was 0.3 % and 0.8 % for analytical and numerical data respectively.

The glass capillary thickness was analysed in the outcome of the transient hot wire system, by solving numerically the heat equation for the line source case, in order to analyse the coating effect in the measurement of the thermal conductivity. It has been shown that the coating does not affect too much the results of the measurements with a maximum slope deviation of 0.68 %. However, this deviation was corrected by determining the effective length of the capillary experimentally, in order to diminish the error in the measurement of the thermal conductivity.

References

- [1] AFEC, “Directiva 2010/31/UE del Parlamento Europeo y del Consejo de 19 de mayo de 2010, relativa a la eficiencia energética de los edificios,” 2010.
- [2] L. Pérez-Lombard, J. Ortiz, and C. Pout, “A review on buildings energy consumption information,” *Energy and Buildings*, vol. 40, no. 3, pp. 394–398, Jan. 2008.
- [3] IDAE, “Análisis del consumo energético del sector residencial en España,” 2011.
- [4] U. SBCI, “Buildings & Climate Change—A Summary for Decision-Makers,” 2009.
- [5] P. Ananthanarayanan, *Basic Refrigeration and Air Conditioning*, McGraw-Hill Publishing Company Limited, 2005.
- [6] P. Srihirin, S. Aphornratana, and S. Chungpaibulpatana, “A review of absorption refrigeration technologies,” *Renewable and Sustainable Energy Reviews*, vol. 5, no. 4, pp. 343–372, Dec. 2001.
- [7] Z. T. Marcriss RA, Gutraj JM, “Absorption fluid data survey: final report on worldwide data,” 1988.
- [8] C. I. Ferreira, “Thermodynamic and physical property data equations for ammonia-lithium nitrate and ammonia-sodium thiocyanate solutions,” *Solar Energy*, vol. 32, pp. 231–236, 1984.
- [9] M. K. Aggarwal and R. S. Agarwal, “Thermodynamic properties of lithium nitrate-ammonia mixtures,” *International Journal of Energy Research*, vol. 10, no. 1, pp. 59–68, Jan. 1986.

References

- [10] M. Venegas, M. Izquierdo, M. de Vega, and a. Lecuona, "Thermodynamic study of multistage absorption cycles using low-temperature heat," *International Journal of Energy Research*, vol. 26, no. 8, pp. 775–791, Jun. 2002.
- [11] S. Libotean, D. Salavera, M. Valles, X. Esteve, and A. Coronas, "Vapor–Liquid Equilibrium of Ammonia + Lithium Nitrate + Water and Ammonia + Lithium Nitrate Solutions from (293.15 to 353.15) K," *Journal of Chemical & Engineering Data*, vol. 52, no. 3, pp. 1050–1055, May 2007.
- [12] S. Libotean, A. Martín, D. Salavera, M. Valles, X. Esteve, and A. Coronas, "Densities, Viscosities, and Heat Capacities of Ammonia + Lithium Nitrate and Ammonia + Lithium Nitrate + Water Solutions between (293.15 and 353.15) K," *Journal of Chemical & Engineering Data*, vol. 53, no. 10, pp. 2383–2388, Oct. 2008.
- [13] K. Antonopoulos and E. Rogdakis, "Performance of solar-driven ammonia-lithium nitrate and ammonia—sodium thiocyanate absorption systems operating as coolers or heat pumps in Athens," *Applied Thermal Engineering*, vol. 16, no. 2, pp. 127–147, 1996.
- [14] Infante Ferreira C.A., "Operating characteristics of NH₃-LiNO₃ and NH₃-NaSCN absorption refrigeration machines," in *Proceedings of 19th International Congress of Refrigeration*, 1995, pp. 321–328.
- [15] Heard, C.L., Ayala, R., Best, R., "An experimental comparison of an absorption refrigerator using ammonia/water and ammonia/lithium nitrate," in *Proceedings of the International Sorption Heat Pump Conference, Montreal, Canada*, 1996, pp. 245–252.
- [16] M. . Abdulateef, J.M., Sopian, K., Alghoul, "Solar absorption refrigeration systems and comparison of the performances using ammonia-water, ammonia-lithium nitrate and ammonia-sodium thiocyanate," *International Journal of Mechanical and Materials Engineering (IJMME)*, vol. 3, no. 1, pp. 17–24, 2008.

- [17] L. Riedel, “Die Wärmeleitfähigkeit von wässrigen Lösungen starker Elektrolyte,” *Chemie Ingenieur Technik - CIT*, vol. 23, no. 3, pp. 59–64, Feb. 1951.
- [18] T. Uemura & S. Hasaba, “Studies on Methanol-Lithium Bromide-Zinc Bromide Absorption Refrigerating Machine,” *Refrig Japan*, vol. 38, p. 19, 1963.
- [19] Alloush. Gosney. Wakeham., “A transient hot-wire instrument for thermal conductivity measurements in electrically conducting liquids at elevated temperatures,” *Int J Thermophysics*, vol. 3, pp. 225–235, 1982.
- [20] K. Kawamata, Y. Nagasaka, and A. Nagashima, “Measurements of the thermal conductivity of aqueous LiBr solutions at pressures up to 40 MPa,” *International Journal of Thermophysics*, vol. 9, no. 3, pp. 317–329, May 1988.
- [21] A. . DiGuilio, R.M., Lee, R.J., Jeter, S.M, Teja, “Properties of Lithium Bromide-Water solutions at high temperatures and concentrations-I Thermal Conductivity,” *ASHRAE Trans*, vol. 96, pp. 702–708, 1990.
- [22] J. Castro, C. Oliet, I. Rodríguez, and a. Oliva, “Comparison of the performance of falling film and bubble absorbers for air-cooled absorption systems,” *International Journal of Thermal Sciences*, vol. 48, no. 7, pp. 1355–1366, Jul. 2009.
- [23] Y. T. Kang and J.-K. Kim, “Comparisons of Mechanical and Chemical Treatments and Nano Technologies for Absorption Applications,” *HVAC&R Research*, vol. 12, pp. 807–819, Aug. 2006.
- [24] S. U. . Choi, “Enhancing thermal conductivity of fluids with nanoparticles, developments and Applications of Non-Newtonian Flow,” in *ASME International Mechanical Engineering Congress & Exposition*, 1995, pp. 99–105.
- [25] S. K. Das, S. U. S. Choi, W. Yu, and T. Pradeep, *Nanofluids : Science and Technology*. Hoboken, NJ, USA: John Wiley & Sons, Inc., 2007.

References

- [26] M. Ehmke, H.J., Renz, “Ternary working fluids for absorption systems with salt-liquid mixtures as absorber,” in *IIF, IIR Congress Commission B1*, 1983.
- [27] H. Bokelmann, “Presentation of new working fluids for absorption heat pumps,” in *International Sorption Heat Pump Conference*, 1985.
- [28] Y. Nagasaka and A. Nagashima, “Absolute measurement of the thermal conductivity of electrically conducting liquids by the transient hot-wire method,” *Journal of Physics E: Scientific ...*, vol. 14, pp. 1435–1440, 1981.
- [29] C. . Nieto de Castro, “Standard reference data for the thermal conductivity of liquids,” *Journal of Physical and Chemical Reference Data*, vol. 15, pp. 1073–1086., 1986.
- [30] T. M. Tritt, *Thermal Conductivity: Theory, Properties, and Applications (Physics of Solids and Liquids)*. Klower Academic/Plenum Publishers, New York, 2004.
- [31] M. J. Assael, K. D. Antoniadis, and W. a. Wakeham, “Historical Evolution of the Transient Hot-Wire Technique,” *International Journal of Thermophysics*, vol. 31, no. 6, pp. 1051–1072, Sep. 2010.
- [32] J. Priestley, *Experiments and Observations Relating to Various Branches of Natural Philosophy; with a Continuation of the Observations on Air, vol. II*. London: Pearson and Rollason, 1781.
- [33] “W.R. Grove, J. Franklin Inst. 46, 358 (1848).”
- [34] “G. Magnus, J. Franklin Inst. 72, 130 (1861).”
- [35] “G. Magnus, Philos. Mag. IV 22, 85 (1861).”
- [36] J. Tyndall, “Heat Considered as a Mode of Motion,” *Being a Course of Twelve Lectures Delivered at the Royal Institution of Great Britain in the Season in 1862 (Longman, Green, Longman, Roberts, & Green, London, 1863), p. 239.*

- [37] “J.C. Maxwell, *Philos. Mag.* IV 19, 19 (1860).”
- [38] “J.C. Maxwell, *Philos. Mag.* IV 20, 21 (1860).”
- [39] “R.J.E. Clausius, *Philos. Mag.* IV 23, 417 (1862).”
- [40] “R.J.E. Clausius, *Philos. Mag.* IV 23, 512 (1862).”
- [41] “A. Schleiermacher, *Ann. Phys. Chem.* 270, 623 (1888).”
- [42] Sophus Weber, “Untersuchungen über die Wärmeleitfähigkeit der Gase. II,” *Annals of Physics*, vol. 359, no. 22, pp. 437–462, 1917.
- [43] S. Stålhane, B., Pyk, “Ny Metod for Bestamning Av Varmelednings-Koefficienter,” *Teknisk Tidskrift*, vol. 61, p. 389, 1931.
- [44] J.W. Haarman, “*Physica*,” vol. 52, pp. 605–619, 1971.
- [45] J. Healy, “The Theory of the Transient Hot-Wire Method for Measuring Thermal Conductivity,” *Physica C*, vol. 82, pp. 392–408, 1976.
- [46] A. DiGuilio, R.M., Teja, “Thermal conductivity of aqueous salt solutions at high temperatures and concentrations,” *Industrial & Engineering Chemistry Research*, vol. 31, pp. 1081–1085, 1992.
- [47] J. G. Bleazard and A. S. Teja, “Thermal Conductivity of Electrically Conducting Liquids by the Transient Hot-Wire Method,” *Journal of Chemical & Engineering Data*, vol. 40, no. 4, pp. 732–737, Jul. 1995.
- [48] T. Fujii, M., Zhang, X., Imaishi, N., Fujiwara, S., Sakamoto, “Simultaneous measurements of thermal conductivity and thermal diffusivity of liquids under microgravity conditions,” *International Journal of Thermophysics*, vol. 18, pp. 327–339, 1997.

References

- [49] Carslaw H S. Jaeger J C., *Conduction of heat in solids*. USA: Oxford University Press, 1959.
- [50] I. . Hensel, W.E. Harlowe, “Compositions for absorption refrigeration system,” *US Pat*, vol. 3, pp. 643–455, 1972.
- [51] T. Iyoki, S. Iwasaki, S. Kuriyama, Y. Uemura, “Solubilities for the Two Ternary Systems Water + Lithium Bromide + Lithium Iodide and Water + Lithium Chloride + Lithium Nitrate at Various Temperatures,” *Journal of Chemical & Engineering Data*, vol. 38, pp. 396–398, 1993.
- [52] Iyoki, S. Yamanaka, R. Uemura, “Physical and thermal properties of the water-lithium bromide-lithium nitrate system,” *International Journal of Refrigeration*, vol. 16, pp. 191–200, 1993.
- [53] C. E. Lees, “On the thermal conductivities of single and mixed solids and liquids and their variation with temperature,” *Philosophical Transactions of the Royal Society of London*, vol. 191, pp. 399–440, 1898.
- [54] B. Braune, “Disseration Universitat Leipzig,” 1937.
- [55] G. . Chernen’kaya, E.I., Vernigora, “. Experimental determination of the thermal conductivity of aqueous salt and ammonia solutions at 25 and 50°C,” *Zh. Prikl. Khim*, vol. 8, pp. 1704–1707, 1972.
- [56] A. B. Baranov, A.N., Churagulov, B.R., Kalina, A.I., Sharikov, F.Yu., Zharov, A.A., Yoroslavtsev, “The investigation of ammonia water gas and liquid mixtures properties.” Report on the Workshop on Thermophysical Properties of Ammonia/Water mixtures. NISTIR, Boulder, Colorado, pp. 59–67, 1997.
- [57] M. Conde, *Thermophysical properties of NH₃ + H₂O mixtures for the industrial design of absorption refrigeration equipment*. Zurich: M.Conde Engineering, 2006, pp. 12–15.

- [58] L. . Filippov, "Thermal Conductivity of Organic Liquids," *Vestnik Mosk. gos. Univ. Ser. 3 Fiz., Astron.*, vol. 15, p. 61, 1955.
- [59] J. . Jamieson, D.T., Irving, J.B., Tudhope, "Liquid thermal conductivity," Edinburg, 1975.
- [60] D.-W. Sun, "Comparison of the performances of NH₃-H₂O, NH₃-LiNO₃ and NH₃-NaSCN absorption refrigeration systems," *Energy Conversion and Management*, vol. 39, pp. 357–368, 1998.
- [61] G. C. B. and F. Daniels, "Concentrated solutions of NaSCN in liquid ammonia: solubility, density, vapor pressure, viscosity, thermal conductance, heat of solution, and heat capacity," *Journal of the American Chemical Society*, vol. 84, p. 1075, 1962.
- [62] H. E. Kok, "De vertikale film absorber in de NH₃-absorptie koelinstallatie," Laboratory for refrigeration and indoor climate technology, Delft University of Technology, 1973.
- [63] A. Reiner, R.H. Zaltash, "Evaluation of ternary ammonia/water fluids for GAX and regenerative absorption cycles," Report ORNL/CF-91/263, 1991.
- [64] H. . Ehmke, "Doctoral Thesis," Universität Essen, Germany, 1984.
- [65] A. Manago, "Research and Development on working fluids and transport phenomena in advanced absorption heat pumps," ANNEX 14 2, Final report, 4-1, 1995.
- [66] A. Bothe, "Das Stoffsystem NH₃-LiNO₃/H₂O für den Einsatz in Absorptionskreisläufen," Universität Duisburg-Essen, Germany, 1989.
- [67] R. Moreno-Quintanar, G., Rivera, W., Best, "Comparison of the experimental evaluation of a solar intermittent refrigeration system for ice production operating with the mixtures NH₃/LiNO₃ and NH₃/LiNO₃/H₂O," *Renewable Energy*, vol. 38, pp. 62–68, 2012.

References

- [68] C. Oronel, C. Amaris, M. Bourouis, and M. Vallès, “Heat and mass transfer in a bubble plate absorber with $\text{NH}_3/\text{LiNO}_3$ and $\text{NH}_3/(\text{LiNO}_3 + \text{H}_2\text{O})$ mixtures,” *International Journal of Thermal Sciences*, vol. 63, pp. 105–114, 2013.
- [69] L. . Eastman, J.A., Choi, S., Li, S., Yu, W., Thompson, “Anomalously increased effective thermal conductivities of ethylene glycol-based nanofluids containing copper nanoparticles,” *Applied Physics Letters*, vol. 78, pp. 718–720, 2001.
- [70] M. Xie, H.Q., Lee, H., Youn, W., Choi, “Nanofluids containing multiwalled carbon nanotubes and their enhanced thermal conductivities,” *Applied Physics Letters*, vol. 94, pp. 4967–4971, 2003.
- [71] P. Keblinski, J. Eastman, and D. Cahill, “Nanofluids for thermal transport,” *Materials Today*, vol. 8, pp. 36–44, 2005.
- [72] J. . Hwang, Y.J., Ahn, Y.C., Shin, H.S., Lee, C.G., Kim, G.T., Park, H.S., Lee, “Investigation on characteristics of thermal conductivity enhancement of nanofluids,” *Applied Physics*, vol. 6, pp. 1068–1071, 2006.
- [73] C. H. Li and G. P. Peterson, “Experimental investigation of temperature and volume fraction variations on the effective thermal conductivity of nanoparticle suspensions (nanofluids),” *Journal of Applied Physics*, vol. 99, no. 8, p. 084314, 2006.
- [74] C. Pang, J.-Y. Jung, and Y. T. Kang, “Thermal conductivity enhancement of Al_2O_3 nanofluids based on the mixtures of aqueous NaCl solution and CH_3OH ,” *International Journal of Heat and Mass Transfer*, vol. 56, no. 1–2, pp. 94–100, Jan. 2013.
- [75] and K. Y. . Kim, J.K., Jung J.Y., Kim, J.H., Kim, M.G., Kashiwagi, T., “The effect of chemical surfactants on the absorption performance during $\text{NH}_3/\text{H}_2\text{O}$ bubble absorption process,” *International Journal of Refrigeration*, vol. 29, pp. 170–177, 2006.

- [76] Y. Ma, X., Su, F., Chen, J., Zhang, “Heat and mass transfer enhancement of the bubble absorption for a binary nanofluid,” *Journal of Mechanical Science and Technology*, vol. 21, pp. 1813–1818, 2007.
- [77] Y. . Jung, J.Y., Cho, C., Lee, W.H., Kang, “Thermal conductivity measurement and characterization of binary nanofluids. Int. J. Heat Mass Tran,” *International Journal of Heat and Mass Transfer H*, vol. 54, pp. 1728–1733, 2011.
- [78] D. . Giancoli, *Physics: Principles with Applications*. Prentice Hall, 1995.
- [79] M. . Lazarus, G.A, Nandigana, V., Senthil, K.G., Dhasan, “Experimental study on forced convective heat transfer with low volume fraction of CuO/Water Nanofluid,” *Energies*, vol. 2, pp. 97–119, 2009.
- [80] “E. McLaughlin, J.F.T. Pittman, Philos. Trans. R. Soc. London, Ser. A 270, 557 (1971).”
- [81] H. M. Roder, “A Transient Hot Wire Thermal Conductivity Apparatus for Fluids,” *JOURNAL OF RESEARCH of the National Bureau of Standards*, vol. 86, pp. 457–493, 1981.
- [82] S. G. S. Beirão, M. L. V. Ramires, M. Dix, and C. a. N. Castro, “A New Instrument for the Measurement of the Thermal Conductivity of Fluids,” *International Journal of Thermophysics*, vol. 27, no. 4, pp. 1018–1041, Aug. 2006.
- [83] N. Hoshi, Omotani, “Transient method to measure the thermal conductivity of high-temperature melts using a liquid-metal probe,” *Rev. Sci. Instrum*, vol. 52, pp. 755–758, 1981.
- [84] DiGuilio. Lee. Jeter. Teja, “Properties of Lithium Bromide - Water Solutions at High Temperatures and Concentrations I. Thermal Conductivity,” *ASHRAE Transactions*, vol. 96, 1990.

References

- [85] S. Garnier, J.P., Maye, J.P., Saillard, J., Thévenot, G., Kadjo, A., Martemianov, “A new transient hot-wire instrument for measuring the thermal conductivity of electrically conducting and highly corrosive liquids using small samples,” *International Journal of ...*, vol. 29, pp. 468–482, 2008.
- [86] W. C. Williams, “Experimental and Theoretical Investigation of Transport Phenomena in Nanoparticle Colloids (Nanofluids) by,” 2006.
- [87] J.-K. Kim, J. Y. Jung, and Y. T. Kang, “Absorption performance enhancement by nano-particles and chemical surfactants in binary nanofluids,” *International Journal of Refrigeration*, vol. 30, no. 1, pp. 50–57, Jan. 2007.
- [88] E. Dresselhaus, M.S., Dresselhaus, G., Charlier, J.C., Hernandez, “Electronic, thermal and mechanical properties of carbon nanotubes,” *Philosophical Transactions of the Royal Society of London*, vol. 362, pp. 2065–2098, 2004.
- [89] V. Datsyuk, M. Kalyva, K. Papagelis, J. Parthenios, D. Tasis, a. Siokou, I. Kallitsis, and C. Galiotis, “Chemical oxidation of multiwalled carbon nanotubes,” *Carbon*, vol. 46, no. 6, pp. 833–840, May 2008.
- [90] K. I. Kang, Y.T., Kim, H.J., Lee, “Heat and mass transfer enhancement of binary nanofluids for H₂O/LiBr falling film absorption process,” *International Journal of Refrigeration*, vol. 31, no. 5, pp. 850–856, Aug. 2008.
- [91] S. Neetu, J., Ramaprabhu, “Synthesis and thermal conductivity of copper nanoparticle decorated multiwalled carbon nanotubes based nanofluids,” *The Journal of Physical Chemistry*, vol. 112, pp. 9315–9319, 2208.
- [92] J. K. Lee, J. Koo, H. Hong, and Y. T. Kang, “The effects of nanoparticles on absorption heat and mass transfer performance in NH₃/H₂O binary nanofluids,” *International Journal of Refrigeration*, vol. 33, no. 2, pp. 269–275, Mar. 2010.

- [93] G. G. Aseyev, *Electrolytes Properties of Solutions: Methods for calculation of multicomponent systems and experimental data on thermal conductivity and surface tension*. Begell House, Inc. Publishers, New York, Wallingford, U.K, 1999, p. 607.
- [94] K. N. Marsh, *Recommended Reference Materials for the Realization of Physicochemical Properties*. Blackwell Scientific Publications. Boston., 1987.
- [95] EA-4/02., “Expression of the Uncertainty of Measurement in Calibration, European Cooperation for Accreditation.,” 1999.
- [96] J. M. P. & B. E. P. R. C. Reid, “The Properties of Gases & Liquids, 4th Edition.” McGraw-Hill, Inc., p. 557, 1987.
- [97] S. Krishnamurthy, P. Bhattacharya, P. E. Phelan, and R. S. Prasher, “Enhanced mass transport in nanofluids.,” *Nano letters*, vol. 6, no. 3, pp. 419–23, Mar. 2006.
- [98] J. A. Keblinski, P., Phillpot, S.R., Choi, S.U.S., Eastman, “Mechanisms of heat flow in suspensions of nano-sized particles (nanofluids),” *International Journal of Heat and Mass Transfer*, vol. 45, pp. 855–863., 2002.
- [99] S. Savithiri, A. Pattamatta, and S. K. Das, “Scaling analysis for the investigation of slip mechanisms in nanofluids.,” *Nanoscale research letters*, vol. 6, no. 1, p. 471, Jan. 2011.
- [100] J.-K. Kim, J. Y. Jung, and Y. T. Kang, “The effect of nano-particles on the bubble absorption performance in a binary nanofluid,” *International Journal of Refrigeration*, vol. 29, no. 1, pp. 22–29, Jan. 2006.
- [101] Y. Ma, X., Su, F., Chen, J., Zhang, “Heat and mass transfer enhancement of the bubble absorption for a binary nanofluids,” *Journal of Mechanical Science and Technology*, vol. 21, pp. 1813–1818, 2007.

References

- [102] X. Ma, F. Su, J. Chen, T. Bai, and Z. Han, "Enhancement of bubble absorption process using a CNTs-ammonia binary nanofluid," *International Communications in Heat and Mass Transfer*, vol. 36, no. 7, pp. 657–660, Aug. 2009.
- [103] Y. T. Pang, C., Wu, W., Sheng, W., Zhang, H., Kang, "Mass transfer enhancement by binary nanofluids (NH₃/H₂O + Ag nanoparticles) for bubble absorption process," *International Journal of Refrigeration*, vol. 35, pp. 2240–2247, 2012.
- [104] Y. T. Kim, J.K., Jung, J.Y., Kang, "Heat and mass transfer enhancement for falling film absorption process by SiO₂ binary nanofluids," *International Journal of Refrigeration*, vol. 35, pp. 645–651, 2012.
- [105] L. G. P. P. Baroncini C, "No Thermal Conductivity of Organic Liquid and Binary Mixtures: Measurements and Prediction Method.," *International Journal of Thermophysics.*, vol. 5, pp. 387–401, 1984.
- [106] M. Rowley, R. L. White, G. L.; Chiu, "Ternary Liquid Mixture Thermal Conductivities.," *Chemical Engineering Science.*, vol. 43, pp. 361–371, 1988.
- [107] T. Sun and A. Teja, "Density, viscosity, and thermal conductivity of aqueous ethylene, diethylene, and triethylene glycol mixtures between 290 K and 450 K," *Journal of Chemical & Engineering Data*, vol. 48, pp. 198–202, 2003.
- [108] E. Bohne, D., Fischer, S., Obermeier, "Thermal conductivity, density, viscosity, and prandtl numbers of ethylene glycol+water mixtures.," *Physical Chemistry*, vol. 88, pp. 739–742, 1984.
- [109] B. E. P. Robert C. Reid, John M. Prausnitz, *The properties of gases and liquids, Second Edition, Robert C. Reid and Thomas K. Sherwood, McGraw-Hill, New York(1966). 646 pages*, vol. 15, no. 6. 1969, pp. 802–802.
- [110] A. . Horvath, *Handbook of aqueous electrolyte solutions. Physical properties estimation and correlation methods*. John Wiley and Sons Inc, New York., 1985.

- [111] P. Wang and A. Anderko, "Modeling thermal conductivity of concentrated and mixed-solvent electrolyte systems," *Industrial & Engineering Chemistry Research*, vol. 47, pp. 5698–5709, 2008.
- [112] A. Bondi, *Physical properties of molecular crystals, liquids and gases*. John Wiley and Sons Inc, New York.
- [113] A. Wang, P., Anderko, "A specification-based model for mixed-solvent electrolyte systems," *Fluid Phase Equilibria*, vol. 203, pp. 141–176, 2002.
- [114] D. R. Lide, *Handbook of Chemistry and Physics*. 71st ed. CRC Press Inc., Boca Raton, FL., 1991.
- [115] Ho, C.Y., Powell, R.W., "Thermal conductivity of the elements," *Journal of Physical and Chemical Reference Data*, vol. 1, pp. 279–421, 1972.
- [116] "Corning Incorporated website." .
- [117] Y. S. Touloukian E. H. Buyco, *Thermophysical Properties of Matter: Specific heat: metallic elements and alloys*. IFI/Plenum, New York, 1970.

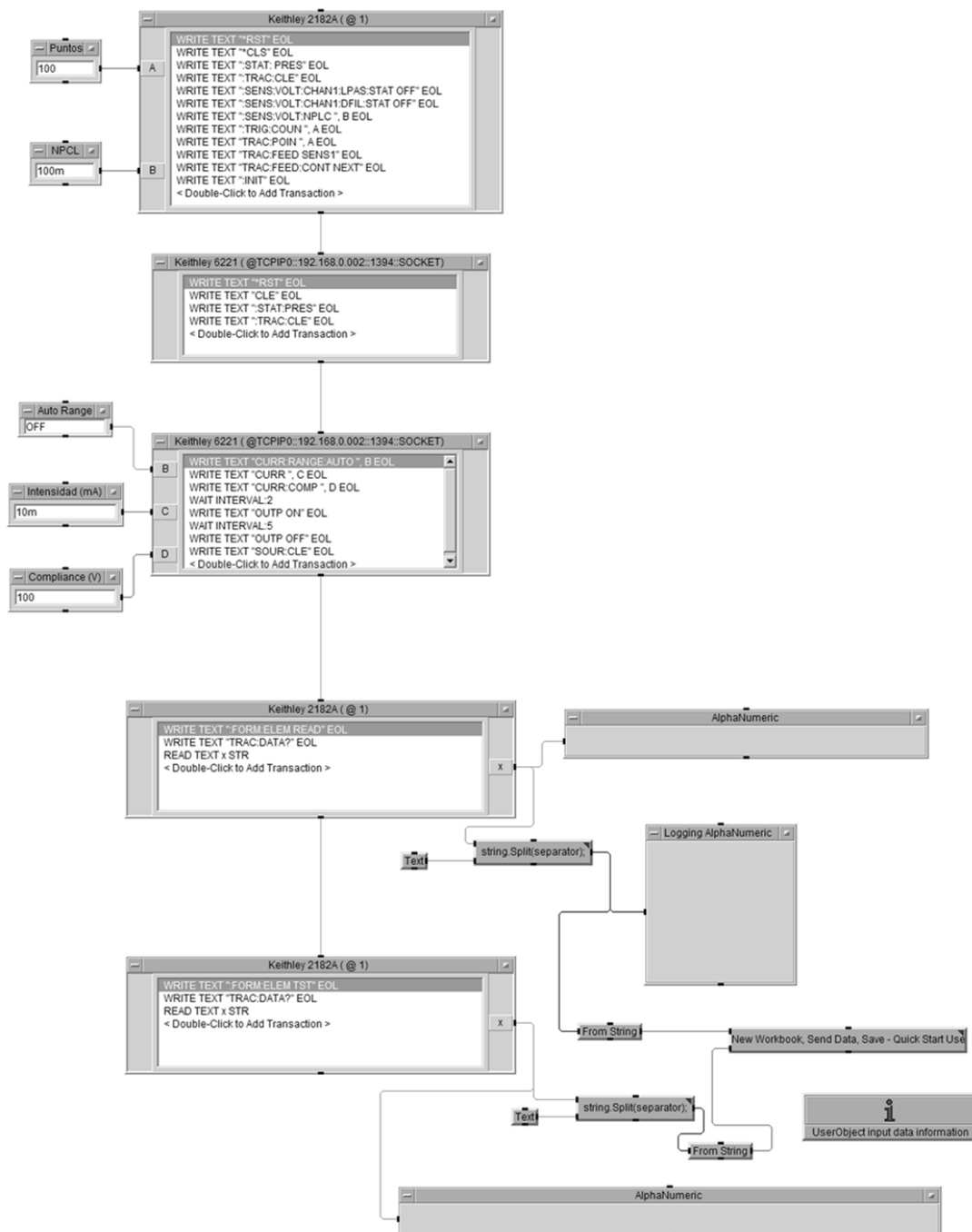
UNIVERSITAT ROVIRA I VIRGILI
EXPERIMENTAL STUDY OF THERMAL CONDUCTIVITY OF NEW MIXTURES FOR ABSORPTION CYCLES AND THE EFFECT OF
THE NANOPARTICLES ADDITION
Yolanda Cuenca Martínez
Dipòsit Legal: T.1561-2013

APPENDIX

UNIVERSITAT ROVIRA I VIRGILI
EXPERIMENTAL STUDY OF THERMAL CONDUCTIVITY OF NEW MIXTURES FOR ABSORPTION CYCLES AND THE EFFECT OF
THE NANOPARTICLES ADDITION
Yolanda Cuenca Martínez
Dipòsit Legal: T.1561-2013

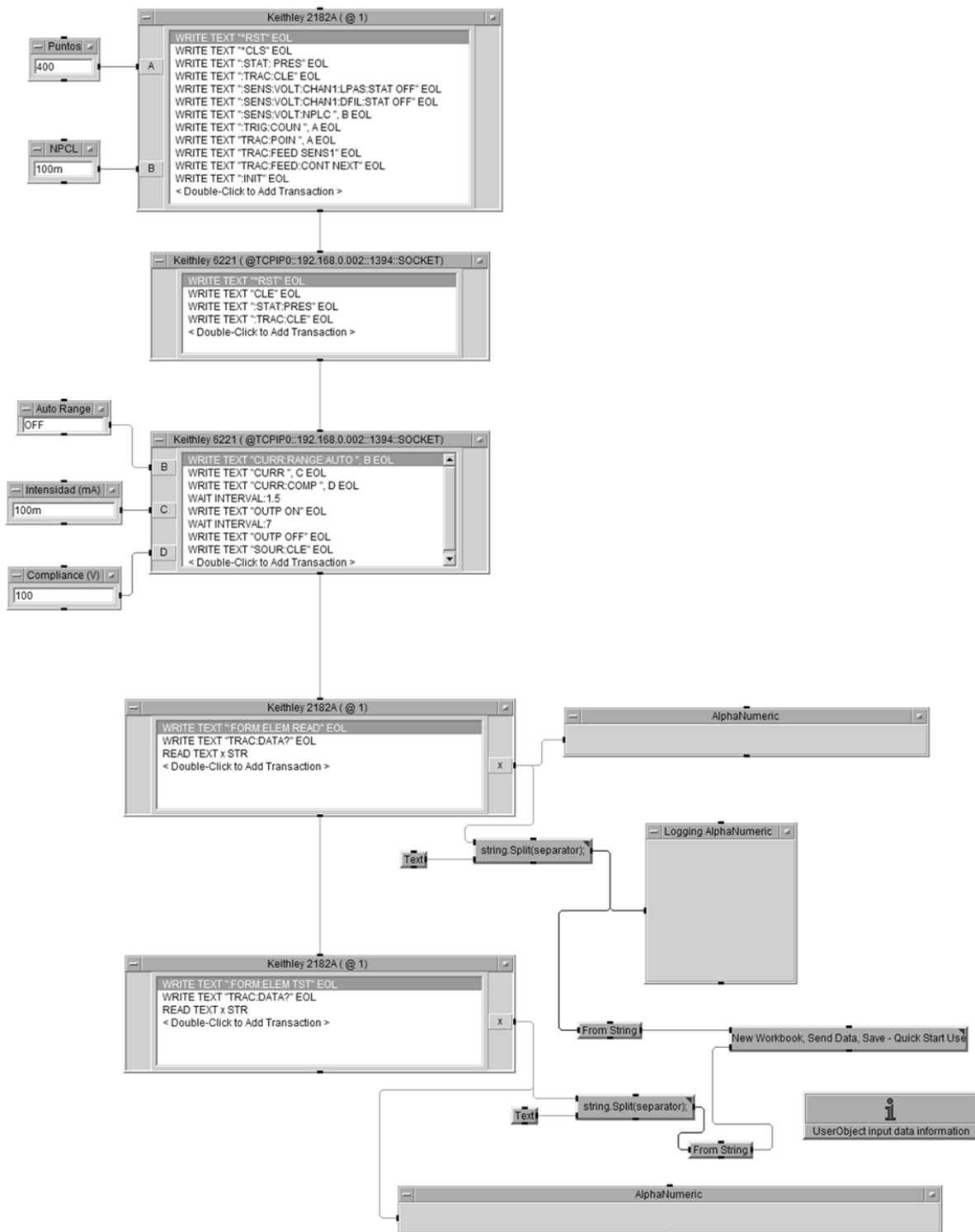
Appendix A: Computer Programs

Data acquisition program with Agilent VEE for Platinum Hot Wire Cell
(CALIBRATION)

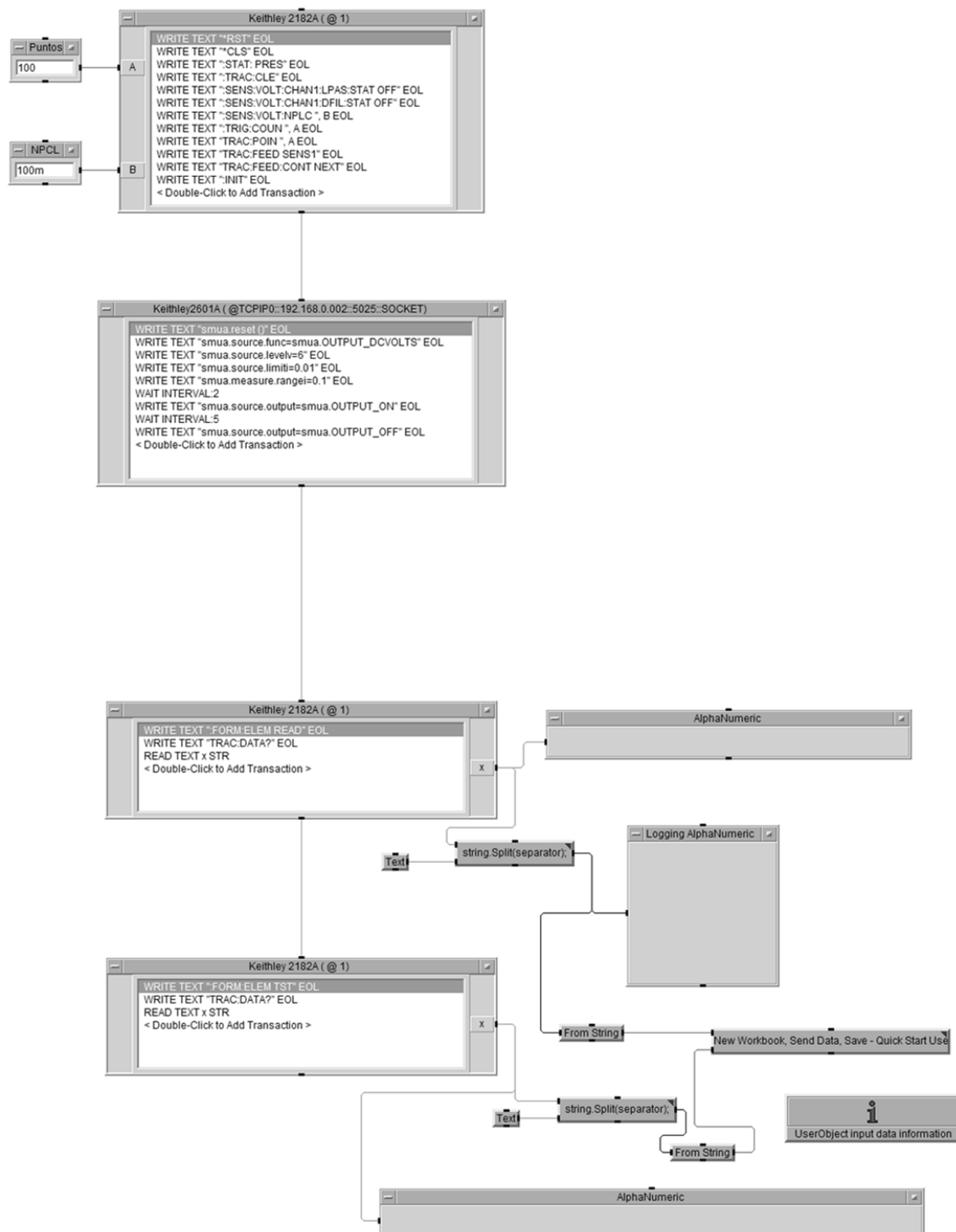


Appendix A

Data acquisition program with Agilent VEE for Platinum Hot Wire Cell (EXPERIMENTAL)

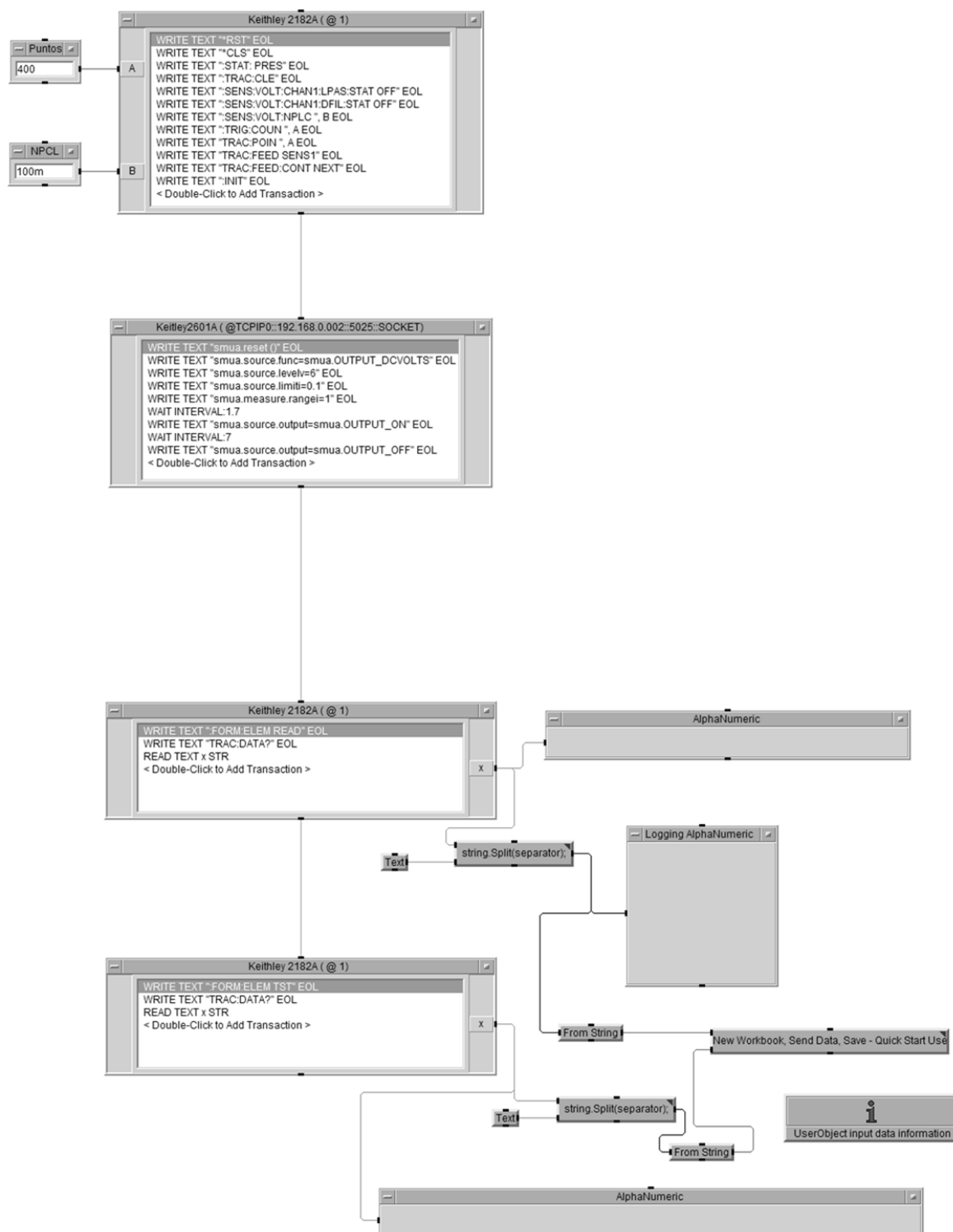


Data acquisition program with Agilent VEE for Single Capillary Cell (CALIBRATION)



Appendix A

Data acquisition program with Agilent VEE for Single Capillary Cell (EXPERIMENTAL)



Appendix B: Uncertainty

Pressure Uncertainty for both devices

Manometer WIKA model 232.35					
Source	Units	Estimate	Divisor	Sensitivity Coefficient	$u^2(t)$
Resolution	bar	1	3.464	1	0.0833
$u(P)$					0.2887
$U(P)$				K=2	0.6

U(P)	0.6
-------------	------------

Temperature Uncertainty for both devices

Thermostat P-Selecta digiterm 100					
Source	Units	Estimate	Divisor	Sensitivity Coefficient	$u^2(t)$
Stability	K	0.020	1.732	1	1.33E-04
Homogeneity	K	0.0100	1.732	1	3.33E-05
$u(T)$					0.0129
$U(T)$				K=2	0.0258
Probe PT100 + Precision Thermometer F250 MK II					
Source	Units	Estimate	Divisor	Sensitivity Coefficient	$u^2(t)$
Calibration	K	0.015	2	1	5.63E-05
Drift	K	0.015	1.732	1	7.50E-05
Resolution	K	0.01	3.464	1	8.33E-06
Repeatability	K	0.0067	1	1	4.44E-05
$u(T)$					0.0136
$U(T)$				K=2	0.0271

U(T)	0.04
-------------	-------------

Appendix B

Sample Preparation Uncertainty for ammonia + water

balance METTLER Toledo PR2003					
Source	Units	Estimate	Divisor	Sensitivity Coefficient	$u^2(t)$
Resolution	g	0.01	3.464	1	8.33E-06
Calibration	g	0.01	1	1	1.00E-04
Linearity	g	0.005	1	1	2.50E-05
Repeatability	g	0.003	1	1	9.00E-06
u(s)					0.0119
U(s)				K=2	0.0239
Mass Water					
Source	Units	Estimate	Divisor	Sensitivity Coefficient	$u^2(t)$
Empty cell	g	0.0119	1	1	1.42E-04
Water cell	g	0.0119	1	1	1.42E-04
u(s)					0.0169
U(s)				K=2	0.0337
Mass Ammonia					
Source	Units	Estimate	Divisor	Sensitivity Coefficient	$u^2(t)$
Empty cell	g	0.0119	1	1	1.42E-04
Ammonia cell	g	0.0119	1	1	1.42E-04
u(s)					0.0169
U(s)				K=2	0.0337
Mass fraction of Ammonia (%)					
Source	Units	Estimate	Divisor	Sensitivity Coefficient	$u^2(t)$
Ammonia mass	g	0.0169	1	0.00532	8.05E-09
Water mass	g	0.0169	1	-0.00134	5.08E-10
u(s)					9.25E-5
U(s)				K=2	0.00018

U(s)	0.0002
------	--------

In this case the sensitivity coefficient for the mass fraction of ammonia is:

$$w_{NH_3} = \frac{mass_{NH_3}}{mass_{NH_3} + mass_{H_2O}}$$

$$\frac{\partial w_{NH_3}}{\partial mass_{NH_3}} = \frac{(mass_{NH_3} + mass_{H_2O}) - mass_{NH_3}}{(mass_{NH_3} + mass_{H_2O})^2}$$

$$\frac{\partial w_{NH_3}}{\partial mass_{H_2O}} = \frac{-mass_{NH_3}}{(mass_{NH_3} + mass_{H_2O})^2}$$

Heat Generation Uncertainty for the platinum wire device

Length					
Source	Units	Estimate	Divisor	Sensitivity Coefficient	$u^2(t)$
Resolution	m	5.00E-05	3.464	1	2.08E-10
Std. Deviation	m	3.33E-04	1.000	1	1.11E-07
$u(l)$					0.00033
$U(l)$				K=2	0.0006673
Nanovoltmeter Keithley 2182A					
Source	Units	Estimate	Divisor	Sensitivity Coefficient	$u^2(t)$
Resolution	V	1.00E-06	3.464	1	8.33E-14
Repeatability	V	8.37E-05	1	1	7.00E-09
$u(V)$					0.00008370
$U(V)$				K=2	0.0001674
Current Source Keithley 6221					
Source	Units	Estimate	Divisor	Sensitivity Coefficient	$u^2(t)$
Resolution	A	1.00E-05	3.464	1	8.33E-12
Repeatability	A	1.50E-04	1	1	2.25E-08
Drift	A	1.00E-05	1	1	1.60E-09
$u(I)$					0.00015527
$U(I)$				K=2	0.0003105

Appendix B

Resistance					
Source	Units	Estimate	Divisor	Sensitivity Coefficient	$u^2(t)$
Voltage	V	8.37E-05	1	10	7.00E-07
Intensity	A	1.55E-04	1	-254.780	1.56E-03
Temperature	1/K	3.90E-03	1	0.08423	1.08E-07
u(R)					0.03956952
U(R)				K=2	0.0791390
Heat Generation (q)					
Source	Units	Estimate	Divisor	Sensitivity Coefficient	$u^2(t)$
Intensity	A	1.55E-04	1	46.32	5.17E-05
Resistance	Ohm	3.96E-02	1	0.09	1.29E-05
Length	m	3.34E-04	1	21.06	4.94E-05
u(q)					0.01067841
U(q)				K=2	0.0213568

U(q)	0.021
-------------	--------------

In this case the sensitivity coefficient for the resistance and the heat generation are:

$$R = \frac{V}{I}$$

$$\frac{\partial R}{\partial V} = \frac{1 \cdot I - 0 \cdot V}{I^2} = \frac{1}{I}$$

$$\frac{\partial R}{\partial I} = \frac{0 \cdot I - 1 \cdot V}{I^2} = \frac{-V}{I^2}$$

$$R = \frac{T}{a}$$

$$q = \frac{I^2 \cdot R}{L}$$

$$\frac{\partial q}{\partial I} = \frac{2 \cdot I \cdot R \cdot L - I^2 \cdot R \cdot 0}{L^2} = \frac{2 \cdot I \cdot R}{L}$$

$$\frac{\partial q}{\partial R} = \frac{I^2 \cdot 1 \cdot L - I^2 \cdot R \cdot 0}{L^2} = \frac{I^2}{L}$$

$$\frac{\partial q}{\partial L} = \frac{0 \cdot L - I^2 \cdot R \cdot 1}{L^2} = \frac{-I^2 \cdot R}{L^2}$$

Heat Generation Uncertainty for the glass capillary device

Length						
Source	Units	Estimate	Divisor	Sensitivity Coefficient	$u^2(t)$	
Intensity	A	1.95E-03	1	8.61E-02	2.82E-08	
Resistance	Ohm	3.25E-02	1	2.58E-03	7.05E-09	
Slope	K/s	6.81E+00	1	-2.88E-03	3.86E-04	
k water	W/m K	2.80E-04	1	-2.09E-02	3.41E-11	
k water	W/m K	6.10E-04	1	-2.09E-02	1.62E-10	
Std. Deviation	m	5.36E-03	1	1	2.87E-05	
u(I)					5.36E-03	
U(I)					K=2	0.011
Nanovoltmeter Keithley 2182A						
Source	Units	Estimate	Divisor	Sensitivity Coefficient	$u^2(t)$	
Resolution	V	0.000001000	3.464	1	8.33E-14	
Repeatability	V	0.0000575	1	1	3.31E-09	
u(V)					5.75E-05	
U(V)					K=2	0.0001150
Current Source Keithley 2601A						
Source	Units	Estimate	Divisor	Sensitivity Coefficient	$u^2(t)$	
Resolution	A	1.00E-05	3.464	1	8.33E-12	
Repeatability	A	1.95E-03	1	1	3.80E-06	
Drift	A	1.00E-05	1	1	1.60E-09	
u(I)					1.95E-03	
U(I)					K=2	0.0039008
Resistance						
Source	Units	Estimate	Divisor	Sensitivity Coefficient	$u^2(t)$	
Voltage	V	5.75E-05	1	3.33E+00	3.67E-08	
Intensity	A	1.95E-03	1	-1.67E+01	1.06E-03	
Temperature	1/K	9.00E-04	1	4.75E-03	1.83E-11	
u(R)					3.25E-02	

Appendix B

U(R)					K=2	0.0650149
Heat Generation (q)						
Source	Units	Estimate	Divisor	Sensitivity Coefficient	u ² (t)	
Intensity	A	1.95E-03	1	3.12E+00	3.71E-05	
Resistance	Ohm	3.25E-02	1	9.37E-02	9.27E-06	
Length	m	5.36E-03	1	4.87E-01	6.82E-06	
u(q)					7.29E-03	
U(q)					K=2	0.0145821

U(q)	0.015
-------------	--------------

In this case the sensitivity coefficient for the length is:

$$L = \frac{I^2 \cdot R}{k \cdot 4 \cdot \pi \cdot m}$$

$$\frac{\partial L}{\partial I} = \frac{2 \cdot I \cdot R}{k \cdot 4 \cdot \pi \cdot m}$$

$$\frac{\partial L}{\partial R} = \frac{I^2 \cdot 1}{k \cdot 4 \cdot \pi \cdot m}$$

$$\frac{\partial L}{\partial k} = \frac{-I^2 \cdot R}{k^2 \cdot 4 \cdot \pi \cdot m}$$

$$\frac{\partial L}{\partial m} = \frac{-I^2 \cdot R}{k \cdot 4 \cdot \pi \cdot m^2}$$

The estimate value of uncertainty for the thermal conductivity of water is from Nieto de Castro [29].

Slope Uncertainty for the platinum wire device

ΔT					
Source	Units	Estimate	Divisor	Sensitivity Coefficient	$u^2(t)$
Calibration	K	4.83E-03	1	1	2.33E-05
T	K	1.75E-02	1	1	3.06E-04
R	Ohm	3.83E-02	1	11.9	2.07E-01
$u(\Delta T)$					4.55E-01
$U(\Delta T)$				K=2	0.9106
time					
Source	Units	Estimate	Divisor	Sensitivity Coefficient	$u^2(t)$
Resolution	s	0.016	3.46E+00	1	8.33E-08
$u(t)$					2.89E-04
$U(t)$				K=2	0.001
slope (m)					
Source	Units	Estimate	Divisor	Sensitivity Coefficient	$u^2(t)$
ΔT	K	4.55E-01	1	9.96E-01	2.06E-01
t	s	0.00029	1	-1.18E+00	2.24E-07
$u(m)$					4.53E-01
$U(m)$				K=2	0.9069

U(m)	0.91
-------------	-------------

Appendix B

Slope Uncertainty for the glass capillary device

ΔT					
Source	Units	Estimate	Divisor	Sensitivity Coefficient	$u^2(t)$
Calibration	°C	2.29E-01	1	1	5.23E-02
T	°C	1.75E-02	1	1	3.06E-04
R	Ohm	3.25E-02	1	210.40	4.68E+01
$u(\Delta T)$					6.84
$U(\Delta T)$				K=2	13.68
time					
Source	Units	Estimate	Divisor	Sensitivity Coefficient	$u^2(t)$
Resolution	s	0.001	3.46	1	8.33E-08
$u(\Delta t)$					2.89E-04
$U(t)$				K=2	0.001
slope (m)					
Source	Units	Estimate	Divisor	Sensitivity Coefficient	$u^2(t)$
DT	°C	6.84198	1	0.9957	46.41
t	s	0.00029	1	-1.6413	2.24E-07
$u(m)$					6.81
$U(m)$				K=2	13.63

U(m)	13.63
-------------	--------------

In this case the sensitivity coefficient for the slope is:

$$T = R \cdot a$$

$$\frac{\partial m}{\partial T} = \frac{1 \cdot \ln t - 0 \cdot T \cdot \frac{1}{t}}{\ln t^2} = \frac{1}{\ln t}$$

$$\frac{\partial m}{\partial t} = \frac{0 - T \cdot \frac{1}{t}}{\ln t^2} = \frac{-T}{\ln t^2}$$

Thermal Conductivity Uncertainty for the platinum wire device

Thermal Conductivity					
Source	Units	Estimate	Divisor	Sensitivity Coefficient	$u^2(t)$
q	W/m	1.05E-02	1	2.47E-02	6.69E-08
m	K/s	4.53E-01	1	-1.77E-02	6.44E-05
u(k)					8.03E-03
U(k)				K=2	0.01605

U(k)	0.017
-------------	--------------

Thermal Conductivity Uncertainty for the glass capillary device

Thermal Conductivity					
Source	Units	Estimate	Divisor	Sensitivity Coefficient	$u^2(t)$
q	W/m	7.29E-03	1	1.78E-02	1.68E-08
m	°C/s	6.81E+00	1	-1.86E-03	1.60E-04
u(k)					1.26E-02
U(k)				K=2	0.02529

U(k)	0.025
-------------	--------------

In this case the sensitivity coefficient for the thermal conductivity is:

$$\frac{\partial K}{\partial q} = \frac{1 \cdot 4 \cdot \pi \cdot m - q \cdot 0}{(4 \cdot \pi \cdot m)^2} = \frac{1}{4 \cdot \pi \cdot m}$$

$$\frac{\partial K}{\partial m} = \frac{0 - q \cdot 4 \cdot \pi}{(4 \cdot \pi \cdot m)^2} = \frac{-q}{4 \cdot \pi \cdot m^2}$$